UC San Diego

UC San Diego Electronic Theses and Dissertations

Title

Mitochondrial structure during apoptosis

Permalink

https://escholarship.org/uc/item/7xv4q68c

Author

Sun, Mei Guo

Publication Date

2007

Peer reviewed|Thesis/dissertation

eScholarship.org Powered by the California Digital Library
University of California

UNIVERSITY OF CALIFORNIA, SAN DIEGO

SAN DIEGO STATE UNIVERSITY

Mitochondrial Structure During Apoptosis

A Dissertation submitted in partial satisfaction of the requirements for the degree

Doctor of Philosophy

in

Biology

by

Mei Guo Sun

Committee in charge:

University of California, San Diego
- Professor Mark H. Ellisman
- Professor Immo E. Scheffler

San Diego State University
- Professor Terrence G. Frey, Chair
- Professor Christopher Glembotski
- Professor Roger A Sabbadini

2007

Copyright

Mei Guo Sun, 2007

All rights reserved.

The Dissertation of Mei Guo Sun is approved, and it is acceptable in quality and form for publication on microfilm:

Chair

University of California, San Diego

San Diego State University

2007

DEDICATION

To my loving parents, Xiu Jin Guo and Jian Rong Gu

献给我亲爱的父母

Thank you for your unconditional support with my study. I am honored to have you as my parents. Thank you for giving me a chance to prove and improve myself through all my walks of life. I love you!

EPIGRAPH

I am among those who think that science has great beauty. A scientist in his laboratory is not only a technician: he is also a child placed before natural phenomena which impress him like a fairy tale.

Marie Curie
(Physicist, twice winner of the Nobel Prize, 1867-1934)

TABLE OF CONTENTS

LIST OF FIGURES

Chapter I.

Chapter II

Supplementary Figures

Chapter III

Chapter IV

ACKNOWLEDGEMENT

I would like to express my deep and sincere gratitude to my supervisor, Professor Terrence Frey. His wide knowledge and his guidance have been of great value for me. His understanding, encouraging and personal guidance have provided a good basis for my research.

I wish to express my warm and sincere thanks to my committees, Professor Roger Sabbadini, Professor Christ Glembotski, Professor Immo Scheffler and Professor Mark Ellisman. Their wisdom and excellent advice have proved to be invaluable.

I also wish to thank Dr. Steve Barlow for his teaching and help with Electron Microscopy. His passion and skill of Microscopy Technology is admirable.

Chapter II, in full, is a reprint of a manuscript as it was originally submitted to *Nature Cell Biology*. This manuscript was subsequently accepted for publication in a shortened version as a Letter. Co-authors are James Williams, Cristina Munoz-Pinedo, Guy Perkins, Joshua Brown, Mark Ellisman, Douglas Green and Terrence Frey. The dissertation author designed the experiments under the direction of Dr. Frey and carried out all experimental work with the assistance of the co-authors and then collaborated with Dr. Frey in writing the manuscript subsequently incorporating suggestions of the co-authors. This project was supported by Blasker Science and Technology Grant from the San Diego Foundation to TGF, by the NIH National Center for Research Resources Grant No. P41 RR004050 (GAP and MHE), by NIH Roadmap Grant GM72033 (to Roger Y. Tsien and MHE), and by NIH Grants AI40646, AI52735, and CA69381 (to DRG). C.M-P. was supported by the Secretaria de Estado de Universidades Investigacion and the Fondo de InvestigacionesSanitarias of Spain. We thank Ying Jones (NCMIR / UCSD) for assistance with high pressure freezing/freeze substitution and James Nulton for suggesting the mechanism of transformation mitochondria in Figure II.7.

The project in Chapter III, in full, is being prepared for future publication. Co-authors are Phuong Tran, Tong Xu, Douglas Green and Terrence Frey. I would like to acknowledge Phuong (Kathy) Tran for her great assistance and Tong Xu for her excellent advice and assistance with flow cytometry. This project was supported by Blasker Science and Technology Grant from the San Diego Foundation to TGF, and by NIH Grants AI40646, AI52735, and CA69381 to DRG.

The project in Chapter IV was in collaboration with Dr. Jodi Nunnari and was also supported by Blasker Science and Technology Grant from the San Diego Foundation to TGF.

I owe my loving thanks to my husband Wade and my 1-year-old son Samuel. Without their love and support it would have been impossible for me to finish this work.

VITA

1998	Xiamen University, China
2001-2004	Teaching Assistant, Department of Biology
	San Diego State University, San Diego
2007	Doctor of Philosophy
	San Diego State University
	and University of California, San Diego

PUBLICATIONS

Sun Mei G., Tran Phuong, Xu Tong, Green Douglas R, and Frey Terrence G. Correlated Light and Electron Microscopy Reveals the Mechanisms of Cytochrome *c* Release During Apoptosis in Response to Hydrogen Peroxide. In preparation.

Sun MG, Williams J, Munoz-Pinedo C, Perkins GA, Brown JM, Ellisman MH, Green DR, Frey TG. Correlated Three-Dimensional Light and Electron Microscopy Reveals Extensive Transformation of the Mitochondrial Inner Membrane During Apoptosis. Nature Cell Biology (2007)

O'Brien NW, Gellings NM, Guo M, Barlow SB, Glembotski CC, Sabbadini RA. Factor associated with neutral sphingomyelinase activation and its role in cardiac cell death. Circulation Research Apr 4; 92(6):589-91 (2003)

ABSTRACT OF THE DISSERTATION

Mitochondrial Structure During Apoptosis

by

Mei Guo Sun

Doctor of Philosophy in Biology

University of California, San Diego, 2007

San Diego State University, 2007

Professor Terrence G. Frey, Chair

Mitochondria are described as “cellular power plants” because they provide most of the ATP for the cell. Recent biological discoveries also strongly link mitochondria to what is commonly known as programmed cell death (apoptosis). Cytochrome *c* was found to be released from mitochondria in cells undergoing apoptosis signal, after which it binds to Apaf-1, caspase9 and ATP to form an ogliomeric complex that initiates the dismantling of the cell in a highly controlled, non-inflammatory manner. The release of cytochrome *c* as well as other proteins from

mitochondria is a pivotal event in the apoptotic process, but the precise mechanism is still under debate.

We have used fluorescence microscopy in order to characterize the state of apoptosis in HeLa cells under different treatments followed by electron microscopy and three-dimensional electron microscope tomography of the identical cells in order to study the sequence of mitochondrial structural changes. Our studies reveal that different mechanisms are involved in release of cytochrome *c* depending upon treatment conditions.

When etoposide was used to cause DNA damage that induces apoptosis, we confirmed the observation that cytochrome *c* is released from mitochondria without matrix swelling and rupture of the outer membrane; release probably occurs through a large outer membrane pore formed by proapoptotic proteins of the Bcl-2 family. However, we have identified a remodeling of the inner mitochondrial membrane into many separate vesicular matrix compartments that accompanies release of proteins. However, this remodeling is not required for efficient release of cytochrome *c*. Our Electron Tomography study of mitochondria in the process of fusing provided evidence that this vesicular morphology may be the reverse process of inner membrane fusion, and causes excessive mitochondrial fragmentation during apoptosis. Swelling occurs only late in apoptosis following release of cytochrome *c* and loss of the mitochondrial membrane potential.

In contrast, when apoptosis was initiated by H_2O_2 that mimics the high local Reactive Oxygen Species (ROS) damage from Ischemia/Reperfusion Injury, we have

observed immediate loss of the inner membrane potential, $\Delta\Psi_m$, subsequent opening of the mitochondrial permeability transition pore (mPTP), and large amplitude swelling of the mitochondrial matrix that appears to be the cause of cytochrome *c* release. Cyclosporin A (CsA), an inhibitor of the mPTP, prevents the immediate loss of $\Delta\Psi_m$ but does not prevent the release of cytochrome *c*. Interestingly, CsA inhibits mitochondrial swelling and induces formation of the vesicular mitochondrial structure, suggesting the release of cytochrome *c* via the outer membrane pore mechanism observed with etoposide treatment occurs in cells treated with H_2O_2 when the mPTP is blocked.

I

Introduction

The Structure of Mitochondria

1. Mitochondrial Membranes

Knowledge of the structure of mitochondria has paralleled the development of techniques for the preparation of biological samples for electron microscopy and biochemical studies of mitochondrial function (Frey and Mannella 2000). Palade and Sjostrand published the first pictures of mitochondria in 1952 and 1953 (Palade 1952; Sjostrand 1953). They both recognized that mitochondria contained more than one membrane system, but their interpretation of micrographs led to different models. Sjostrand's early model contained a double limiting membrane with internal membrane-bound compartments forming septa that divide the matrix into many compartments. The standard baffle model in old textbooks for cristae structure proposed by Palade showed the cristae with broad openings to the inter-membrane space on one side of the mitochondrion and protruding across the matrix to the other side (Nisoli, Clementi et al. 2004) (Figure I.1). Electron tomography by Mannella indicated that the mitochondrial inner membrane is not normally comprised of baffle-like folds (Mannella, Marko et al. 1994), and Perkins *et al.* subsequently showed that all cristae observed *in situ* connect to the inner boundary membrane via a tubular

structure they named crista junctions (Perkins, Renken et al. 1997). Therefore, a new model of mitochondrial internal structure replaced the old one in textbooks (Figure I. 2).

As shown in the new model, a mitochondrion contains an outer membrane (OM) and an inner membrane (IM) with different properties. The IM is composed of the cristae membrane and the inner boundary membrane. There are 3 distinct compartments defined by these two membranes: (1) The inter-membrane space between the outer and inner boundary membranes, (2) The intra-cristal space within cristae, and (3) The matrix space within the inner membrane. The inter-membrane and intra-cristal spaces are connected through crista junctions (CJ).

The OM, which encloses the entire organelle and separates the mitochondrion from the cytosol, has a protein-to-phospholipid ratio similar to the eukaryotic plasma membrane (approximately 1:1 by weight). It contains numerous voltage dependent anion selective channels (VDAC) also known as mitochondrial porins owing to their similarity to bacterial porins. Despite their name, VDAC channels are normally open to diffusion of virtually all ions and small molecules up to approximately 5000Da.

The IM contains more than 100 different polypeptides and has a very high protein-to-phospholipid ratio, more than 3:1 by weight, which is about 1 protein for every 15 phospholipids. Additionally, the IM is relatively rich in cardiolipin, bisphosphatidyl glycerol, which comprises approximately 10% of the total phospholipids and reduces the membrane's permeability to protons such that a proton-motive force can be established across it. Unlike the OM, the IM does not contain

porins and is highly impermeable to ions and polar molecules.

The inner mitochondrial membrane contains proteins with four types of functions: (1) Oxidation reactions of the respiratory chain; (2) ATP synthase; (3) Regulation of the passage of metabolites into and out of the matrix; (4) Protein import. The cristae expand the surface area of the inner mitochondrial membrane, enhancing its ability to generate ATP. For example, in typical liver mitochondria, it is about five times the area of the outer membrane. The cells with a greater demand for ATP, such as muscle cells, contain more mitochondrial cristae than others.

The inter-membrane and intra-cristal spaces are the compartments between the outer membrane and the inner membrane. In 1981, Bernardi and Azzone reported that only 15% to 20% of total cytochrome *c* is within the inter-membrane space with the remainder located within the intra-cristae space. Interest arose when it was shown by Liu in 1996 (Liu, Kim et al. 1996) that the release of cytochrome *c* from mitochondria was a critical event in apoptosis. Scorrano and co-workers suggested that inner membrane remodeling is required to release cytochrome *c* from the intra-cristae space (Scorrano, Ashiya et al. 2002) . The matrix is the compartment enclosed by the inner membrane and contains a high concentration of macromolecules including mitochondrial ribosomes, tRNA, multiple copies of the mitochondrial DNA genome and the mixture of enzymes that are involved in oxidation of pyruvate and fatty acids as well as the citric acid cycle.

2. Mitochondrial Morphology and Dynamics

Compared to Electron Microscopy, fluorescent light microscopy has a significantly lower resolution. However, the use of fluorescence microscopy offers a view of the entire cell and the complete distribution of mitochondria within it. Mitochondria are highly dynamic organelles. They frequently change size and shape through fusion and fission, and translocate constantly. The study of mitochondrial dynamics *in vivo* became possible with the advent of fluorescent labeling techniques in combination with live cell imaging microscopy (Jakobs 2006). Several innovative selective fluorescent probes have been developed to monitor mitochondrial morphology and organelle function. (1) The uptake of dyes such as TMRE, MitoTracker, and JC-1 into mitochondria can be performed with live cells in response to the $\Delta\Psi_m$. (2) Immuno-fluorescent techniques can be applied with a wide range of specific mitochondrial protein antibodies. (3) Fluorescent fusion proteins such as GFP and DsRed aid in visualizing mitochondria and the distribution of specific proteins in live cells.

An elegant assay for mitochondrial fusion in budding yeast cells was developed by Nunnari et al (Nunnari, Marshall et al. 1997). The mitochondria from opposite mating types of yeast were labeled with different markers: GFP and DsRed. During the mating of the yeast cells, the intermixing of the two mitochondrial labels is monitored by fluorescence microscopy. It was found that the mitochondrial markers were evenly redistributed throughout the fused cell, indicating mitochondria fuse together and mix contents. By employing this strategy, Meeusen, et al and Malka, et

al demonstrated that the fusion of the inner and outer membranes are separate events *in vitro* and *in vivo* (Meeusen, McCaffery et al. 2004; Malka, Guillery et al. 2005). I collaborated with Dr. Nunnari and examined the fusion of mitochondrial structure in different stages using electron microscopy/tomography. Additional introduction, results, and discussion of this topic will be covered in Chapter IV.

3. Study of Mitochondrial Structure Using Four Dimensional Correlated Light and Electron Microscopy

I performed correlated light, transmission electron microscopy (TEM), and three-dimensional EM tomography on cells growing in special Petri dishes containing a glass coverslip with an etched grid (MatTek Corp. Ashland, MA). The grid allowed me to locate, by confocal microscopy, a field of cells at defined time points, prepare the cells for TEM by conventional methods of chemical fixation, and subsequently re-locate the identical cells during sectioning for TEM and EM tomography. In Chapter II and III, by using this method, I identified cells at successive stages in the apoptotic program initiated in HeLa cells permanently transfected with fluorescent cytochrome *c* fusion proteins and stained with TMRE to monitor $\Delta\Psi_m$ (Goldstein, Waterhouse et al. 2000; Goldstein, Munoz-Pinedo et al. 2005). The cells were fixed and embedded for TEM, and their ultra-structure was characterized by both conventional thin section TEM and by three-dimensional EM tomography of semi-thick sections up to 0.5 μm thickness (Frey, Perkins et al. 2006). This is a form of virtual four-dimensional TEM (three spatial dimensions, and time expressed as the stage along the apoptotic

program) that reveals a remarkable structural transformation of mitochondria from the normal cristae junction paradigm through a form with in which the inner membrane forms multiple vesicular matrix compartments and then to a swollen form.

Mitochondrial Function

1. Mitochondrial Genome

Typically, a mammalian cell contains several hundred mitochondria. Each mitochondrion usually contains several copies of the circular DNA genome. Mitochondrial DNA (mtDNA) represents a separate and distinctive eukaryotic cellular genetic system (Clayton 1984) and encodes necessary ribosomal and transfer RNAs (rRNAs and tRNAs) for its own protein synthesizing machinery. The human mitochondrial genome is circular double-stranded DNA 16,569 base pairs (bp) in length (Anderson, Bankier et al. 1981). The genome encodes two rRNAs, 22 tRNAs and 13 of the 90 different proteins present in the respiratory chain (Asin-Cayuela and Gustafsson 2007). The remaining components of the respiratory chain such as the proteins for oxidative phosphorylation, enzymes, ribosomal proteins, and mtDNA regulatory factors are encoded by nuclear genes, synthesized in the cytosol and imported to the mitochondrion via "specialized import systems" (Wallace 1997; Asin-Cayuela and Gustafsson 2007). Human mtDNA doesn't have introns, and the control elements for mtDNA transcription and replication are in the non-coding region of the genome (Shadel and Clayton 1997). Transcription and replication of mtDNA are basic processes which are closely related to both the function of the organelle and its

biogenesis (Scheffler 1999). mtDNA has two strands, heavy (H) and light (L), based upon their different buoyant densities in a cesium chloride gradient. The transcription of the L-strand is initiated from a single promoter (LSP) while H-strand transcription is initiated from two specific and differentially regulated sites, HSP1 (H1) and HSP2 (H2) (Montoya, Christianson et al. 1982). HSP1 is located 100 bp upstream of HSP2, and HSP1 initiated transcription includes the two rRNA genes with a termination site at the end of the 16S rRNA-encoding gene (Christianson and Clayton 1988). HSP2 is located close to the 5' end of the 12S rRNA gene. It produces a "polycistronic molecule" that corresponds to almost the entire H strand, covering the two rRNA genes and 12 mRNA-encoding genes (Asin-Cayuela and Gustafsson 2007). These RNAs are then processed to the functional tRNA and mRNA molecules (Agsteribbe and Hartog 1987). All of the protein and rRNA genes are immediately flanked by at least one tRNA gene (Asin-Cayuela and Gustafsson 2007). This mode of RNA processing is known as the 'tRNA punctuation model'(Ojala, Montoya et al. 1981).

Mitochondrial translation machinery provides some peptides for the oxidative phosporylation system. Translation of mitochondrial mRNA is different from that of nuclear mRNA. Many details of mitochondrial protein biosynthesis are poorly understood maybe due to the lack of availability of an in vitro mitochondrial translation system. Only a limited number of the mammalian auxiliary factors involved in initiation and elongation of translation have been studied (Taanman 1999). Termination of the translation process still remains unknown.

It is well accepted that the mitochondrion developed from an α-

proteobacterium (Gray, Burger et al. 1999) via endosymbiosis of the bacterium residing within a eukaryotic cell. Evidence shows that the presence of orthologous genes in the mitochondrial genomes in some species and in the nuclear genomes of other species; this indicates "gene transfer" (Andersson, Karlberg et al. 2003) from the mitochondrion to the nucleus. Therefore, mitochondria from different species have different genomes. The mtDNA needs nuclear genes for carrying on replication, transcription and translation.

2. Mitochondrial Protein Import

Mitochondrial protein import requires a series of receptors, import channels, and molecular machines. All of these components are located in different mitochondrial locations: the outer and inner mitochondrial membranes, the intermembrane - intracristal spaces, and the matrix. Chaperon proteins in the cytoplasm maintain the targeted proteins in an import-competent state, and these proteins are specifically targeted to receptors at the mitochondrial surface. Many mitochondrial proteins contain a conserved targeting signal with an amphipathic α-helix containing positive charges (Pfanner and Geissler 2001). Proteins initially enter mitochondria via the protein translocase machinery of the outer membrane, the TOM complex (Rapaport 2005). This process does not depend on $\Delta\Psi_m$. From there, they are sorted to their final destination according to the targeting information encoded within the protein (MacKenzie and Payne 2007). Proteins enter the matrix via the TIM complex and the presequence translocase-associated motor (PAM). The TIM complex

forms the channel across the inner membrane, and this process requires $\Delta\Psi_m$ (Truscott, Kovermann et al. 2001). Matrix proteins undergo structural changes by mitochondrial processing peptidase (MPP) and matrix chaperons after crossing the inner membrane (Pfanner and Geissler 2001; Voos and Rottgers 2002). Some mitochondrial inner membrane proteins are re-exported by OXA from the matrix (Herrmann, Neupert et al. 1997).

TOM complex is short for translocase of the outer membrane complex. It consists of protein import receptors and the import channel (Koehler 2000). TOM22 (the number indicates the molecular weight in kDa) is the essential compartment of the protein import receptors. It together with TOM20, 37 and 70 localize on the mitochondrial surface as receptors to recognize the α-helix targeting sequence on mitochondrial precursors. TOM40 is the main component of the protein import channel. It coordinates with TOM5, 6, 7 and 38. The latter four proteins are believed to be regulators rather than major components (Scheffler 1999) of the channel.

Similar to TOM, TIM complex is short for translocase of the inner membrane. Generally, there are two different channels mediated by different TIMs for protein translocation into the matrix and for the protein insertion into the inner membrane (Koehler 2000). TIM17and 23 on the inner membrane and TIM 44 at the matrix side mediate the protein import into the matrix. TIM 11 is also believed to be associated with this channel. Different TIM complexes for the second channel that insert proteins into the inner membrane are located in the mitochondrial inner membrane and intermembrane space. Among them, TIM18, 22 and 54 are inner membrane proteins

and the family of small proteins called "Tiny TIMs" are in the intermembrane space, including TIM8, 9, 10, 12 and 13. Defects of mitochondrial protein import are one of the causes of severe mitochondrial disease.

3. Oxidative Phosphorylation

Oxidative phosphorylation is the oldest and best-known function of mitochondria. It forms the basis for mitochondrial ATP production. In most organisms it is composed of the ATP synthase complex (complex V) and four oxidoreductase complexes: the NADH dehydrogenase (complex I), the succinate dehydrogenase (complex II), the cytochrome *c* reductase (complex III), and the cytochrome *c* oxidase (complex IV) (Boekema and Braun 2007). All of these complexes reside within the inner mitochondrial membrane. The function of these complexes is the transfer of the electrons through a sequence of electron carrier molecules to create an electrochemical proton gradient across the membrane that is used to drive the ATP synthase. Complexes I and II transfer electrons from NADH or $FADH_2$ respectively to ubiquinone (Coenzyme Q) reducing it to ubiquinol (dihydroquinone). Complex III transfers electrons from ubiquinol to cytochrome *c*. Complex IV transfers electrons from cytochrome *c* to molecular oxygen, the terminal electron acceptor, reducing it to H_2O with the consumption of protons from the matrix. The electron transport is coupled with translocation of protons from the mitochondrial matrix into the intermembrane space creating the electrochemical proton gradient that comprises the protonmotive force. The protonmotive force contains two components, the proton

concentration gradient, ΔpH, and the membrane potential, $\Delta\Psi_m$, that gives protons in the intermembrane/ intracristal spaces a higher chemical potential than in the matrix. Complex V uses chemical potential energy from the protonmotive force to catalyze the formation of ATP by phosphorylation of ADP. The protonmotive force also provides energy for active transport of numerous chemical species into or out of the matrix.

Molecular oxygen is the terminal electron acceptor because of its high affinity for electrons. However, the reduction of molecular oxygen can yield potentially harmful intermediates (Davies 1995). The transfer of four electrons normally results in the production of water, which is not harmful. However, the transfer of one or two electrons results in superoxide anion and peroxide. These compounds and their reaction products such as the hydroxyl radical are very harmful to cellular components. During mitochondrial oxidative phophorylation, small amounts of superoxide anion and peroxide are produced as well as some unstable intermediate forms. On example is the reduction of coenzyme Q (ubiquinone) in complex III forming an unstable intermediate ($Q^{\bullet -}$), which can interfere with the well-controlled reactions and form the superoxide anion by leading the electrons directly to the oxygen (Finkel and Holbrook 2000). Species that can be produced from these such as Hydrogen peroxide (H_2O_2) and the hydroxyl radical (•OH) are called reactive oxygen species (ROS). I will discuss the cell damage caused by ROS in Chapter III.

There are many enzymes such as superoxide dismutase to convert ROS into less reactive species (Sies 1997). Superoxide dismutase converts superoxide radicals

into molecular oxygen and hydrogen peroxide. Catalase found in peroxisomes converts hydrogen peroxide into molecular oxygen and water. Antioxidants such as vitamins C and E can also convert ROS to less harmful compounds (Finkel and Holbrook 2000). Vitamin E in the mitochondrial inner membrane protects the membrane from being harmed by ROS while Vitamin C has the same function in the mitochondrial matrix.

4. Mitochondrial Mutations and Disease

Mitochondria host several metabolic pathways, including the Krebs cycle, β-oxidation of fatty acids, and lipid and cholesterol synthesis (Stark and Roden 2007). Since mitochondria play a fundamental role in so many pathways, defects of mitochondrial function in human body can lead to serious disease. Less and less energy generated within the cell results in cell injury and even cell death. Diseases of the mitochondria are related to the damage of the brain, heart, liver, skeletal muscles, kidney and the endocrine and respiratory systems. Depending on which cells are affected, symptoms may include loss of motor control, muscle weakness and pain, gastro-intestinal disorders and swallowing difficulties, poor growth, cardiac disease, liver disease, diabetes, respiratory complications, seizures, visual/hearing problems, lactic acidosis, developmental delays and susceptibility to infection (Schapira 2006). The effects of mitochondrial disease can be varied from organ to organ due to the distribution of defective mtDNA and/or the metabolic activity of different tissues. The same mutation can cause different diseases, such as liver disease or brain disorder. In

addition, the severity of the disease varies too. Some people with mitochondrial disease only show "exercise intolerance" while others have severe body-wide impacts. Mitochondrial diseases affect muscles or nerves more severely, because these organs need the most energy.

Human mitochondrial diseases encompass mutations of mtDNA and nuclear DNA, as well as toxin-induced defects (Schapira 2006). The mitochondrial genome mutation rate is 10 to 20 times higher than that of the nuclear genes in mammals, probably due to failure of proof-reading by mtDNA polymerases and to damage by free radicals (Lane 2006; Schapira 2006). mtDNA mutations include point mutations and rearrangements (deletions and duplications). Point mutations are commonly maternally inherited, but deletions and duplications are most often sporadic (Schapira 2006). Other than mtDNA, mutations of nuclear genes are also be responsible for mitochondrial dysfunction, such as nuclear genes encoding oxidative phosphorylation subunits(Schapira 2006). Leber hereditary optic neuropathy (LHON) is the first well-understood mitochondrial disease. It is a form of blindness that caused by the mutations to the NADH-Q oxidoreductase component of Complex I (Wallace, Singh et al. 1988). Some of these mutations impair NADH utilization, whereas others block electron transfer to Coenzyme-Q. The accumulation of mutations in mitochondrial genes in the course of several decades may contribute to aging, degenerative disorders, and cancer (Berg, Tymoczko et al.). At present there is no cure for mitochondrial disease.

Apoptosis & Mitochondria

1. Apoptotic Pathways

Apoptosis, also known as "Programmed Cell Death," is defined as " the physiological process by which unwanted or useless cells are eliminated during development and other normal biological processes". Kerr et al was the first to use this term in 1972 to describe "a structurally-distinctive mode of cell death responsible for cell loss within living tissues" (Kerr, Wyllie et al. 1972). Apoptosis is most often found during normal cell turnover and tissue homeostasis, embryogenesis, induction and maintenance of immune tolerance, and the development of the nervous system and endocrine-dependent tissue atrophy (Aktas, Prozorovski et al. 2006). Apoptotic cells show distinct morphological and biochemical features. These features include chromatin aggregation, nuclear and cytoplasm condensation, formation of apoptotic bodies, and fragmented mitochondria and nuclear material. Unlike necrosis, apoptosis is a regulated and non-inflammatory form of cell death. During necrosis, the cell swells, the cell membrane is disrupted, and the nuclear and cytosolic structures are released causing an inflammatory reaction in the neighboring cells.

Apoptosis is a genetically pre-determined mechanism that involves several molecular pathways. The best characterized and most prominent ones are called the extrinsic and intrinsic pathways. In the extrinsic pathway (also known as the 'death receptor pathway'), apoptosis is triggered by the ligand-induced activation of death receptors at the cell surface. Such death receptors include the tumor necrosis factor (TNF) receptor-1, CD95/Fas receptor, as well as the TNF-related apoptosis inducing

ligand (TRAIL) receptor-1 and 2 (Itoh and Nagata 1993; Tartaglia, Ayres et al. 1993; Zou, Li et al. 1999; Algeciras-Schimnich, Shen et al. 2002). After ligand binding, death receptors form a complex that leads to the recruitment of adaptor proteins that interact through the death domain. For Fas and TNF receptors, these adaptor proteins are the Fas-associated death domain (FADD) and the TNFR-associated death domain (TRADD), respectively (Chinnaiyan, O'Rourke et al. 1995; Hsu, Xiong et al. 1995). Activation leads to the recruitment and subsequent activation of caspase 8 (Boldin, Goncharov et al. 1996; Muzio, Chinnaiyan et al. 1996). The activation of caspase 8 further activates downstream effecter caspases, culminating in cell death by apoptosis (Hirata, Takahashi et al. 1998; Slee, Harte et al. 1999).

In the intrinsic pathway (also known as 'mitochondrial dependant pathway'), the mitochondria integrate various cellular stress signals, including DNA damage and endoplasmic reticulum (ER) stress. In response to these stimuli, the mitochondria release pro-apoptotic factors such as cytochrome *c*, apoptosis-inducing factor (AIF), Smac/Diablo, endonuclease G (endoG), and Htra2/Omi (Liu, Kim et al. 1996; Susin, Lorenzo et al. 1999; Chai, Du et al. 2000; Li, Luo et al. 2001; Hegde, Srinivasula et al. 2002). The release of cytochrome *c* is a critical step in the execution of apoptosis (Green and Evan 2002). When cytochrome c is released into the cytosol, it forms the apoptosome along with Apaf-1, dATP and caspase 9. The apoptosome then triggers the activation of caspase 3 and apoptosis (Zou, Li et al. 1999). Caspase activation is further increased by the release of mitochondrial Smac/Diablo (Du, Fang et al. 2000), which bind and sequester the inhibitors of apoptosis proteins (IAP) (Verhagen, Ekert

et al. 2000). AIF translocates from the mitochondria to the nucleus and causes chromatin condensation and large scale DNA fragmentation (Susin, Lorenzo et al. 1999). Similar to AIF, the mitochondrion specific nuclease, endoG also translocates to the nucleus and induces nucleosomal DNA fragmentation during apoptosis (Li, Luo et al. 2001).

The extrinsic and intrinsic pathways overlap in the activation of Caspase-3 through the pro-apoptotic Bcl-2 family member Bid. Bid is truncated by the activated caspase 8 from the extrinsic pathway, translocated to mitochondria, and then activates the intrinsic pathway by promoting cytochrome *c* release (Li, Zhu et al. 1998; Luo, Budihardjo et al. 1998).

2. Mechanisms for Releasing Mitochondrial Pro-Apoptotic Proteins

The mechanisms responsible for the release of mitochondrial pro-apoptotic proteins are still under debate. Skulachev first hypothesized that the opening of the permeability transition pore (mPTP) of the inner membrane would cause swelling of the matrix space rupturing the outer membrane releasing cytochrome *c* and other pro-apoptotic proteins into the cytosol (Skulachev 1996). The mPTP is a high conductance channel in the inner membrane that opens leading to an increase in mitochondrial inner membrane permeability to solutes with molecular masses up to approximately 1500 Da. It has been hypothesized to minimally consist of the voltage-dependent anion channel (VDAC) in the outer membrane, the adenine-nucleotide translocase (ANT) in the inner membrane and cyclophilin D in the matrix

(Brustovetsky and Klingenberg 1996) (Crompton, Virji et al. 1998). However recent genetic knockout experiments by different groups suggest that neither VDAC nor ANT are essential pore components (Kokoszka, Waymire et al. 2004; Baines, Kaiser et al. 2005; Baines, Kaiser et al. 2007). Genetic knockout of cyclophilin D confirms its important role for the mPTP, but more likely as a regulator and not part the pore itself (Baines, Kaiser et al. 2005; Basso, Fante et al. 2005; Nakagawa, Shimizu et al. 2005; Schinzel, Takeuchi et al. 2005). The structure of mPTP still remains a mystery (Bernardi, Krauskopf et al. 2006).

It was also shown that sustained mPTP opening is primarily involved in necrosis and ischemia reperfusion injury (Baines, Kaiser et al. 2005; Basso, Fante et al. 2005; Nakagawa, Shimizu et al. 2005). Cyclophilin-D deficient cells showed resistance to cell death induced by reactive oxygen species and Ca^{2+} overload but died by apoptosis in response to both the extrinsic and intrinsic pathways (Nakagawa, Shimizu et al. 2005). These observations suggest that, instead of outer membrane rupture, a more selective mechanism may be involved, such as the formation of a regulated pore in the outer membrane by proapoptotic proteins of the Bcl-2 family and the subsequent release of proteins from mitochondria that commit the cell to die (Pavlov, Priault et al. 2001). Kuwana et al have shown that in reconstitution experiments Bax oligomers can release macromolecules from vesicles that contain mitochondrial lipids. Chapter III focuses on discussing these different mechanisms and hypothesizes a combination of pathways from both, depending on death stimulus.

FIGURES & LEGENDS

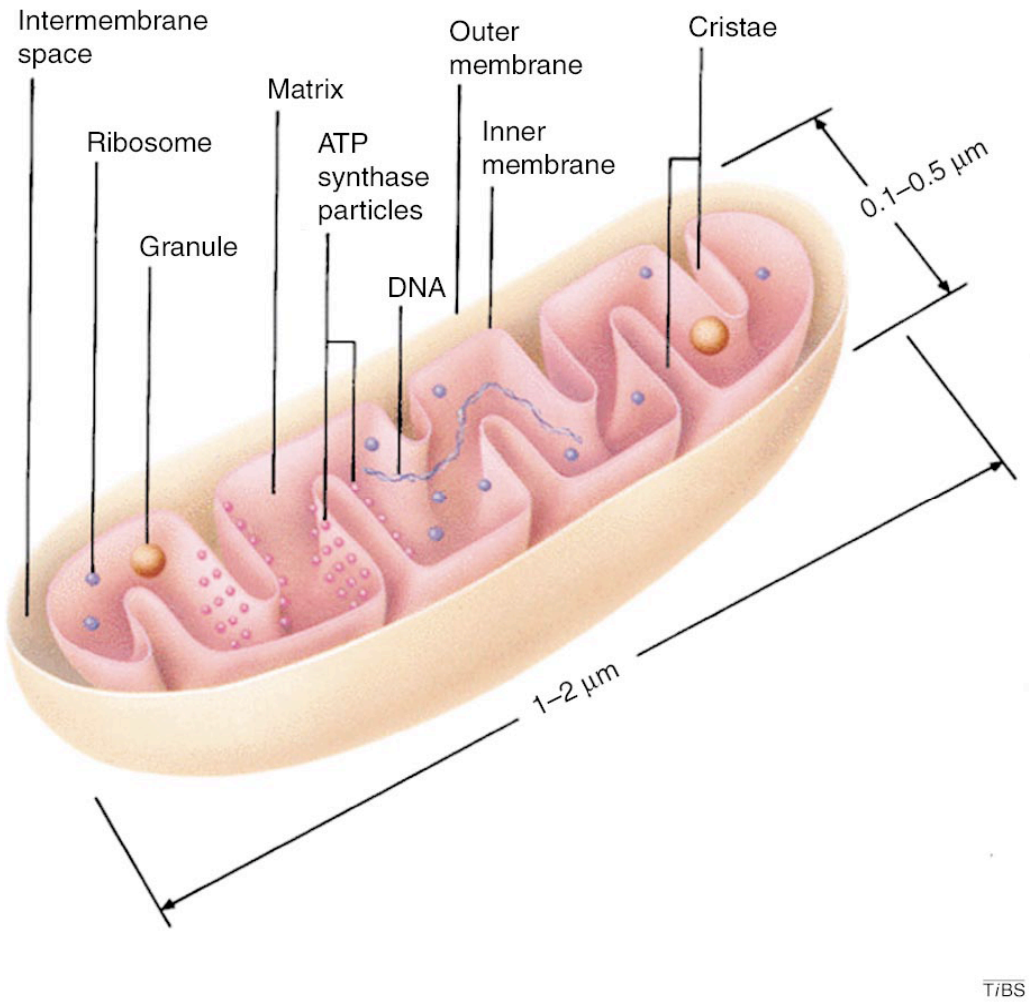

Figure I.1 Baffle Model

From Lodish, H. et al. eds (1999) Molecular Cell Biology (3rd ed)

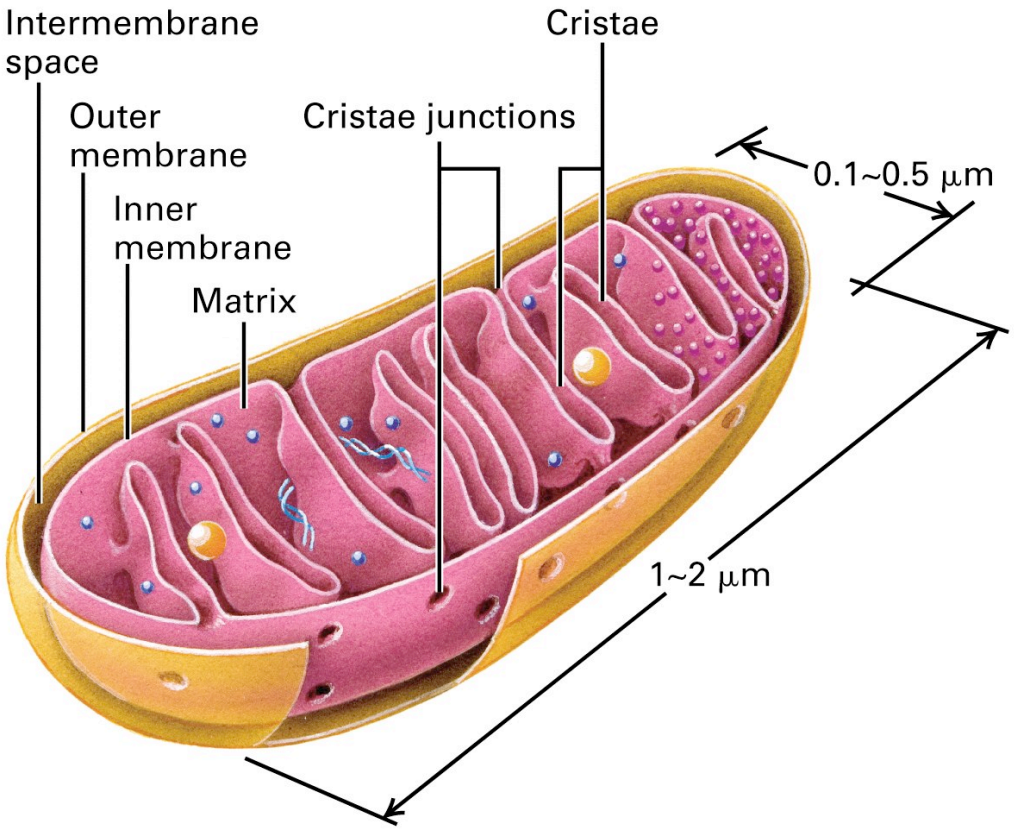

Figure I.2 New Model of Mitochondrial Internal Structure

From Lodish, H. et al. eds (2004) Molecular Cell Biology (5th ed)

II.

Mitochondrial Inner Membrane Transformation During Apoptosis

ABSTRACT

We have monitored apoptosis initiated in HeLa cells containing a cytochrome *c* fusion protein, Cyt. *c*-4CYS, that binds the biarsenical fluorophores, FlAsH and ReAsH. By staining the cells with FlAsH to monitor Cyt. *c*-4CYS and with TMRE to monitor the mitochondrial membrane potential ($\Delta\Psi_m$) we determined the timing of cytochrome *c* release and the loss of $\Delta\Psi_m$ during apoptosis. By growing the cells in Petri dishes containing a glass coverslip with an etched grid, we prepared and examined the same cells by electron microscopy and by three-dimensional electron microscope tomography. During and/or after the release of cytochrome *c* the inner membranes of mitochondria transform (remodel) from the normal conformation with lamellar cristae connected to the inner boundary membrane via discrete tubular crista junctions into a form we call vesicular mitochondria in which the inner membrane forms many separate vesicular matrix compartments that are vesicles of various size containing the fragmented matrix. The vesicular mitochondria subsequently swell

during and/or following the loss of $\Delta\Psi_m$. Forms intermediate between normal and vesicular mitochondria and between vesicular and swollen mitochondria were also observed. Inhibition of the mitochondrial permeability transition with Cyclosporin-A does not prevent release of cytochrome *c* nor prevent the formation of vesicular mitochondria. Significantly, inhibition of caspases by zVAD-fmk inhibits the formation of vesicular mitochondria but does not prevent release of cytochrome *c*. Thus, inner membrane remodeling is not required for efficient release of cytochrome *c* from intracristal spaces. The formation of vesicular mitochondria may be related to mitochondrial fragmentation observed during apoptosis.

INTRODUCTION

Release of cytochrome *c* and other proteins (AIF, endo-G, smac, Diablo *etc*.) from mitochondria initiates apoptosis in the intrinsic mitochondrial pathway and regulates apoptosis initiated by cell surface receptors in the extrinsic pathway (Shiozaki and Shi 2004), (Arnoult, Petit et al. 2003). Recognition of this critical function of mitochondria approximately a decade ago immediately stimulated suggestions for the mechanism by which these proteins could be released from the intermembrane and intracristal spaces across the outer mitochondrial membrane (Green and Reed 1998). One mechanism postulated mitochondrial swelling to the point that the outer membrane is ruptured releasing the contents of the intermembrane and intracristal spaces. The swelling is thought to be caused either by opening of the mitochondrial permeability transition pore (mPTP), a high conductance channel in the inner mitochondrial membrane, or by hyperpolarization of the mitochondrial inner membrane. An alternate mechanism postulated the formation of a large pore in the outer membrane through which the proteins could exit (Green and Reed 1998). Pro-apoptotic proteins (Bax, Bak, and Bid) of the BCl-2 family are believed to promote apoptosis either by regulating the MPTP or by participating in the formation of a large pore in the outer membrane, and Kuwana *et al.* have demonstrated that oligomeric Bax can form such pores in the context of appropriate mitochondrial lipids (Kuwana, Mackey et al. 2002).

Concurrent with the recognition of the importance of mitochondria in apoptosis has been the application of electron microscope tomography (EM

tomography), a form of three-dimensional transmission electron microscopy (TEM), to mitochondrial ultrastructure leading to a new paradigm of mitochondrial structure revealing that the inner membrane structure is much more complex than previously believed (Frey and Mannella 2000; Frey, Renken et al. 2002). In normal orthodox mitochondria the inner membrane has two topologically distinct components. The inner boundary membrane lies closely apposed to the outer membrane with a small space, the intermembrane space *ca.* 8 nm thick, between the two. At various loci the inner membrane projects into the matrix via tubular structures of uniform diameter called crista junctions that form the cristae enclosing the intracristal space. The tubular components are of various lengths in some cell types but are often very short and merge with large lamellar crista compartments (Perkins, Renken et al. 1997; Perkins, Song et al. 1998; Perkins, Renken et al. 2001). The inner membrane functions appear to be somewhat compartmentalized with a greater concentration of the ATP generating proteins of the electron transport complexes and the ATP Synthase in the cristae membranes (Frey, Renken et al. 2002; Gilkerson, Selker et al. 2003). Modeling studies suggest that the relatively small crista junctions may create concentration gradients between the intracristal spaces and the intermembrane space in actively respiring mitochondria (Mannella, Pfeiffer et al. 2001). Furthermore, Scorrano *et al.* suggested that crista junctions may inhibit release of the majority of cytochrome *c* that is found in the intracristal spaces, and postulated that inner membrane remodeling to increase the diameters of crista junctions is required for effective release of cytochrome *c* (Scorrano, Ashiya et al. 2002).

Fluorescence light microscopy is the most commonly used microscopic technique in studying apoptosis, owing to the ability to image live cells and the availability of fluorescent probes that are either: (1) Diagnostic of mitochondrial physiology such as those of the rhodamine family, TMRE and TMRM, that partition into the mitochondrial matrix in response to the creation of $\Delta\Psi_m$ (Loew 1996) or (2) Fusion proteins such as cytochrome *c*-GFP that display the intracellular distribution of critical proteins (Goldstein, Waterhouse et al. 2000; Goldstein, Munoz-Pinedo et al. 2005).

The ability to label different aspects of mitochondrial structure and function makes fluorescence confocal light microscopy a very powerful tool to study the time course of mitochondrial events such as release of proteins and loss of $\Delta\Psi_m$. However, the resolution of fluorescence microscopy is too poor to assess changes in fine structure such as swelling and rupture of the outer membrane and inner membrane remodeling. In contrast, TEM and EM tomography, are well suited to study the changes of the internal structure of mitochondria accompanying release of cytochrome *c* during apoptosis (Frey, Perkins et al. 2006). Unfortunately, application of TEM requires that biological samples be suitable for insertion into a high vacuum, thus this technique does not allow the continuous observation of fine structural changes of an individual organelle within a living cell. This problem is compounded by the fact that in most of the cell culture models of apoptosis the relevant events, release of cytochrome *c* and loss of $\Delta\Psi_m$, occur within minutes, while the onset of these changes occurs asynchronously among a population of cells over periods of several hours

(Goldstein, Waterhouse et al. 2000; Goldstein, Munoz-Pinedo et al. 2005). Thus, one cannot determine the sequence of structural changes within mitochondria simply by taking samples at different time points following the initiation of apoptosis, because cells at intermediate times will be at various stages of the process. Thus, previous studies by TEM could not characterize the exact stage of the cells imaged with respect to release of cytochrome *c* and $\Delta\Psi_m$.

In order to overcome the problem of an asynchronous cellular process, we performed correlated light and electron microscopy, (TEM) and EM tomography, on cells growing in special Petri dishes that contain a glass coverslip with an etched grid (MatTek Corp. Ashland, MA). The grid allowed us to identify by confocal microscopy a field of cells at defined stages of apoptosis, prepare the cells for TEM by conventional methods of chemical fixation, and then locate the identical cells during sectioning for TEM and EM tomography. We identified cells at successive stages in the apoptotic program initiated in HeLa cells permanently transfected with fluorescent cytochrome *c* fusion proteins and stained with TMRE to monitor $\Delta\Psi_m$ (Goldstein, Waterhouse et al. 2000; Goldstein, Munoz-Pinedo et al. 2005). The cells were fixed and embedded for TEM, and their ultrastructure was characterized by both conventional thin section TEM and by three-dimensional EM tomography of semi-thick sections up to 0.5 μm thickness (Frey, Perkins et al. 2006). This is a form of virtual four-dimensional TEM (three spatial dimensions plus time) that reveals a remarkable structural transformation of mitochondria from the normal crista junction paradigm through a form with in which the inner membrane forms multiple vesicular

matrix compartments to a swollen form. Inhibition of either caspases or the MPTP don't inhibit release of cytochrome *c,* but inhibition of caspases inhibits the transformation to the vesicular structure. Thus, inner membrane remodeling forming vesicular matrix compartments is not required for release of cytochrome *c* from the intracristal spaces but must have another function that may be related to the mitochondrial fragmentation that occurs during apoptosis.

RESULTS

1. Correlated light and electron microscopy of single cells reveals significant ultrastructural changes within mitochondria during and after release of cytochrome *c*.

As described previously, the principal mitochondrial events of apoptosis in HeLa cells, release of cytochrome *c* and loss of $\Delta\Psi_m$, occur asynchronously, and the release of cytochrome *c* precedes the loss of $\Delta\Psi_m$ (Goldstein, Waterhouse et al. 2000; Goldstein, Munoz-Pinedo et al. 2005). This is demonstrated in Figure II.1 in which HeLa cells permanently transfected with a 13.3 kD cytochrome *c* fusion protein containing a short tetracysteine motif (Cyt. *c*-4CYS) that binds the membrane permeable biarsenical fluorophore, FlAsH (Gaietta, Deerinck et al. 2002; Goldstein, Munoz-Pinedo et al. 2005), have been treated with etoposide to induce apoptosis, stained with FlAsH to reveal the distribution of Cyt. *c*-4CYS, and stained with TMRE to reveal mitochondria that maintain $\Delta\Psi_m$. Figures II.1a-c were recorded at the start of the experiment with the distribution of Cyt. *c*-4CYS in Figure II.1a and mitochondria maintaining a membrane potential revealed by the TMRE staining in Figure II.1b; Figure II.1c is an overlay of Figures II.1a and II.1b showing the near perfect correspondence between the two indicating the localization of Cyt. *c*-4CYS within healthy mitochondria. Figures II.1d-f image the same field of cells 16 hrs after addition of etoposide, and we identify two cells outlined by a circle and a square in all figure components that represent two successive stages in the apoptotic program. The circled cell has released cytochrome *c* as indicated by diffuse FlAsH staining in Figure

II.1d while the mitochondria maintain $\Delta\Psi_m$ indicated by punctate TMRE staining in Figure II.1e. The cell outlined in the square has also released cytochrome *c*, and the presence of greater FlAsH staining within the nucleus may indicate that it has released cytochrome *c* earlier than the circled cell (Figure II.1d). All of the mitochondria within this cell have, however, lost their $\Delta\Psi_m$ shown by the absence of TMRE staining. This same field of cells was chemically fixed, dehydrated, and embedded in plastic prior to cutting sections for examination by TEM, and a thin section of this area is shown at low magnification in Figure II.1f with the same cells outlined. We have observed the same results with a cytochrome *c*-GFP fusion protein in this system (Supplementary Figure II.3). Western blot analysis confirms that within a population of HeLa cells, release of native cytochrome *c* is 50% complete within 16-18 hours and nearly complete for all cells at 20 hours following treatment with etoposide (Figure II.1g). The amount of cytochrome *c* remaining in the mitochondrial fraction at 20 hours is consistent with the fraction of cellular volume occupied by mitochondria and the fact that the mitochondrial inner membrane contains high affinity cytochrome *c* binding sites. It also indicates that no appreciable fraction of cytochrome *c* is trapped within the mitochondrial fractions as was observed by Parone *et al.* and by Estaquier and Arnoult upon inhibition of mitochondrial fission.(Parone, James et al. 2006; Estaquier and Arnoult 2007) The maintenance of $\Delta\Psi_m$ for a short time following release of cytochrome *c* appears to be a function of the electron transport chain rather than reversal of the ATP Synthase reaction, since inhibition of the ATP Synthase by oligomycin had no effect on this phenomenon (Supplementary Figure II.5) as

previously reported by Goldstein *et al.* for this system (Goldstein, Waterhouse et al. 2000). Furthermore, we have not observed cells that have lost $\Delta\Psi_m$ but maintain punctate FlAsH – Cyt. c-4CYS staining confirming that in all cases that we have observed, release of cytochrome *c* precedes loss of $\Delta\Psi_m$. These changes are consistent with the earlier observations of Goldstein *et al.* that the release of cytochrome *c* from all mitochondria within a cell is complete within five minutes and precedes the loss of $\Delta\Psi_m$ and that the release of fluorescent cytochrome c fusion proteins, cytochrome c-GFP and cytochrome c-4CYS, closely follows the release of endogenous native cytochrome *c* (Goldstein, Waterhouse et al. 2000; Goldstein, Munoz-Pinedo et al. 2005).

Based upon the changes in fluorescence observed in HeLa cells expressing Cyt. *c*-4CYS labeled with FlAsH and TMRE, we identify three Stages during apoptosis initiated by etoposide:

- Stage 1 – Before release of cytochrome *c* and before loss of $\Delta\Psi_m$
- Stage 2 – After release of cytochrome *c* but before loss of $\Delta\Psi_m$
- Stage 3 – After both release of cytochrome *c* and loss of $\Delta\Psi_m$.

We then studied the ultrastructure of the mitochondria within representative cells in these three stages by TEM and by EM tomography of the identical cells that were characterized by fluorescence confocal microscopy. Figure II.2 shows fluorescent light and transmission electron micrographs of three different fields of cells at each of the three stages of the apoptotic program:

Stage 1—Figure II.2a contains a field of cells prior to release of cytochrome *c* and prior to loss of $\Delta\Psi_m$ as indicated by the punctate FlAsH and TMRE staining that match in the overlay of the two signals. The low magnification electron micrograph of this field of cells is shown in the inset at upper left in the higher magnification electron micrograph that reveals a number of mitochondria that all have the morphology of the normal orthodox conformation typically found in healthy cells.

Stage 2—in Figure II.2b the FlAsH staining is diffuse indicating that cytochrome *c* has been or is being released, while the TMRE staining remains punctate indicating the presence of $\Delta\Psi_m$. This characterization is also evident in the lack of correspondence between the green FlAsH signal overlaid on the red TMRE signal. The high magnification electron micrograph contains many normal mitochondria but also several mitochondria with an altered morphology that we refer to as "vesicular" (arrow) for reasons that will become apparent from the EM tomography described below.

Stage 3—in Figure II.2c the fluorescence microscopy again shows the diffuse FlAsH staining indicative of cytochrome *c* release and now the nearly complete absence of TMRE staining indicating that all of the mitochondria have lost $\Delta\Psi_m$. The higher magnification electron micrograph contains no normal mitochondria but does include several mitochondria that appear to be swollen (arrow), and some of these also display morphology similar to the vesicular mitochondria in Figure II.2b (arrowhead).

We have identified five characteristic mitochondrial morphologies based upon observation of electron micrographs of cells within the three stages, and these are

shown at higher magnification in Figure II.3: Normal—Figure II.3a; Normal/ Vesicular—Figure II.3b; Vesicular—Figure II.3c; Vesicular/Swollen—Figure II.3d; Swollen—Figure II.3e. Mitochondria exhibiting the vesicular ultrastructure are easily identified in electron micrographs of thin sections, but characterizing their structure required the third spatial dimension provided by EM tomography. Upon first inspection, thin section electron micrographs of vesicular mitochondria appear to display many of the "tripartite" cristae observed by Nicastro *et al.* in tomograms of purified frozen-hydrated *Neurospora crassa* mitochondria (Nicastro, Frangakis et al. 2000). However, the tomograms clearly show that in these vesicular mitochondria all of the inner membrane encloses vesicular matrix compartments, separate vesicles of various sizes whose lumen is topologically equivalent to the mitochondrial matrix (Figure II.4c). Furthermore, the change in morphology from normal to vesicular is progressive from one region of an extended mitochondrion to another, because intermediate forms designated normal/vesicular display normal cristae within an inner boundary membrane at one end and vesicular matrix compartments at the other (Figure II.4b). Note that the normal domain in the normal/vesicular mitochondrion in Figure II.4b contains an inner boundary membrane rendered in white that is absent in all vesicular domains in Figures II.4b-e. The absence of an inner boundary membrane in the regions of these mitochondria containing vesicular compartments confirms that these vesicles encapsulate fragmented matrix and are not simply detatched cristae within an inner boundary membrane as observed by Mannella et al (Mannella, Pfeiffer et al. 2001) and by Frezza et al (see Figure 6A) (Frezza, Cipolat et al. 2006).

Swollen mitochondria are identified by their expanded matrix space, fewer cristae, and less dense staining of the matrix. Examples are seen in Figure II.2c (arrow), Figure II.3e, and the tomogram in Figure II.4e in which the outer membrane appears to be ruptured by the expanded matrix. Again an intermediate form, vesicular/swollen, is observed in which one domain of a mitochondrion appears swollen, while another domain appears vesicular as in Figure II.2c (arrowhead), and Figure II.3d. The mitochondrion modeled in the tomogram in Figure II.4d contains two very large swollen vesicular compartments rendered in yellow and magenta with numerous smaller vesicular matrix compartments rendered in various colors.

These unusual mitochondrial inner membrane structures are unlikely to be the result of artifacts of either the specimen preparation procedure (chemical fixation followed by dehydration and plastic embedding) or illumination of cells containing multiple fluorophores. As a control for both possibilities we prepared nontransfected HeLa cells in the absence of fluorophores by high pressure cryofixation followed by freeze substitution and plastic embedding. Although this procedure is not immune from artifacts, it is widely regarded as providing superior preservation of native structure for most specimens when properly applied (see Frey *et al.* and references therein (Frey, Perkins et al. 2006)). Cryofixation/freeze substitution of untreated HeLa cells produced only normal mitochondrial structures while the same treatment applied to HeLa cells treated with Etoposide for 16 hours produced many cells containing mitochondria exhibiting the vesicular structure. (Figure II.8). We have also observed for extended periods of time by fluorescence confocal microscopy many

samples of cells with multiple fluorophores and subsequently prepared them for TEM but never observe the vesicular structure unless the cells have also been treated for several hours with Etoposide or other chemicals that stimulate the intrinsic apoptotic pathway (Supplementary Figures II.3, Figure II.4).

2. **Normal mitochondria transform progressively to the vesicular form during cytochrome *c* release; swelling occurs later during or after loss of membrane potential.**

In order to determine the sequence of ultrastructure changes during apoptosis induced by Etoposide, we recorded numerous electron micrographs of cells in each of the three stages as determined by fluorescence confocal microscopy and scored the numbers of mitochondrial profiles with each of the five morphologies: Normal, normal/vesicular, vesicular, vesicular/swollen, and swollen. The results are displayed graphically in Figure II.5 along with the number of cells and total number of mitochondria measured in each case. As expected, control cells that have not been treated with etoposide are defined as Stage 1 and display only normal mitochondrial profiles with a very low number of swollen mitochondria that may result from the specimen preparation procedure. Cells treated with Etoposide for 15 hrs and imaged before either the release of cytochrome *c* or loss of $\Delta\Psi_m$ are also defined as Stage 1, and they contain only normal mitochondrial profiles (Figure II.5b). Stage 2 mitochondria have released cytochrome *c* but maintain a normal $\Delta\Psi_m$, and although a small majority (62%) of Stage 2 cells still display a normal profile, there are a

significant number that exhibit vesicular morphology with a total of 32% falling into the normal/vesicular, vesicular, or vesicular/swollen morphologies and approximately 6% in the swollen category. Stage 3 mitochondria have released cytochrome *c*, have lost $\Delta\Psi_m$ and exhibit a further shift away from the normal structure (down to 35%) toward the vesicular and swollen structures (Figure II.5d). We interpret this to indicate that the progression of changes is from the normal structure to the vesicular during or after cytochrome *c* release then progressing to a swollen morphology following the loss of $\Delta\Psi_m$. Even Stage 3 cells still contain 35% normal mitochondria, thus we do not know whether all mitochondrial cristae convert to vesicular morphology prior to swelling. Indeed, the swollen mitochondrion in Figure II.4e contains two lamellar cristae (red and green) within a swollen matrix compartment surrounded by inner boundary membrane plus one swollen vesicular matrix compartment outside the inner boundary membrane.

3. Cytochrome *c* release does not require inner membrane remodeling to vesicular matrix compartments, but remodeling does require caspase activation.

In order to evaluate the importance of caspase activation we repeated the experiment in the presence of the general caspase inhibitor, zVAD-fmk, that inhibited caspases by more than 54% (Figure II.10). Caspase inhibited cells in Stage 3 maintained normal mitochondrial structure (84%) with a small number of swollen mitochondria (15%, Figure II.5e). Thus, transformation to the vesicular structure appears to require active caspases. We also tested the possible participation of the

mPTP by conducting the experiment in the presence of Cycloporin A (CsA). As expected CsA treatment inhibited the mPTP as it prevented the release of Calcein trapped within mitochondria (Figure II.9) (Petronilli, Miotto et al. 1999), but it did not inhibit cytochrome *c* release nor prevent the transformation to the vesicular structure as shown in Figure II.5f.

4. **The vesicular transformation is not an effect specific to etoposide treatment.**

We treated HeLa-Cyt. *c*-4CYS cells with Actinomycin-D, which also stimulates the intrinsic mitochondrial apoptosis pathway, and with Fas-Ligand that stimulates the extrinsic "death receptor" pathway in which mitochondria play a regulatory or amplification role. Both treatments produced vesicular mitochondria, however, in Fas-Ligand treated experiment, vesicular mitochondrial formation is not a major phenomena (Supplementary Figures II.3, II.4). Thus, the sequence of structural transformations reported here appears to be a general characteristic of mitochondria stimulated to release proteins.

DISCUSSION

We set out to answer the following two questions: **(1)** *Do mitochondrial swelling and/or inner mitochondrial membrane remodeling occur during apoptosis?* and **(2)** *Is either swelling or inner membrane remodeling required for release of cytochrome c?* The answers are *yes* and *no* respectively. By examination of the same cells by correlated light and electron microscopy and by EM tomography, we have been able to observe and characterize a remarkable structural transformation of the inner mitochondrial membrane from the normal crista junction paradigm to a vesicular form in which the cristae are transformed into numerous vesicles of various size enclosing separate matrix compartments. This remodeling occurs during or after release of cytochrome *c* from the intermembrane space and intracristal spaces. Later, as the apoptosis program progresses, mitochondria swell following loss of $\Delta\Psi_m$, and in at least some examples the outer membrane is ruptured.

Scorrano *et al.* suggested that since approximately 85% of cytochrome *c* resides within intracristal spaces separated from the intermembrane space by relatively narrow crista junctions, release of the cytochrome *c* in the intracristal spaces would require "remodeling" of the inner membrane to increase the crista junction diameter (Scorrano, Ashiya et al. 2002). They observed a remodeling of the inner membrane in purified rat liver mitochondria treated with the BH3-only proapoptotic protein, tBID, that appeared to fuse cristae together and significantly increased the diameter of crista junctions. The vesicular transformation that we have observed is fundamentally different from the "remodeling" reported by Scorrano *et al.*, but it would accomplish

the same purpose as the intracristal compartments are eliminated in the transformation to vesicular matrix compartments, and all cytochrome *c* has access to pores formed in the outer membrane for release into the cytosol. However, over 60% of mitochondria within Stage 2 cells that have released cytochrome *c* but maintain $\Delta\Psi_m$ are not remodeled and exhibit normal morphology (Figure II.5c). Furthermore, inhibiting caspases with zVAD-fmk has no effect on release of cytochrome *c*, but it does prevent transformation to the vesicular form, maintaining all cristae in the normal crista junction morphology (Figure II.5e) with normal crista junction sizes (Figure II.6a). Thus, inner membrane remodeling does not appear to be required for release of cytochrome *c* from the intracristal compartments. This is not surprising, since the normal crista junction inner diameter observed *in situ* in various cell types is approximately 14 nm or five times the diameter of a cytochrome *c* molecule (Perkins, Renken et al. 1997; Perkins, Renken et al. 2001) and should not present a physical barrier to diffusion of cytochrome *c*. Crista junctions of this size might present a kinetic barrier to rapid release of cytochrome *c*, however kinetic modeling studies (Manor, Frey et al. 2006) indicate that this would not prevent release of intracristal cytochrome *c* within the one to two minute time period measured by Goldstein *et al.* (Goldstein, Waterhouse et al. 2000; Goldstein, Munoz-Pinedo et al. 2005). Furthermore, Bernardi and Azzone(Bernardi and Azzone 1981) showed that essentially all cytochrome *c* within purified mitochondria is reduced by externally added NADH via NADH-cytochrome b_5 reductase in the outer mitochondrial membrane within 1-2 minutes demonstrating that cytochrome *c* is able to diffuse and

equilibrate between the intracristal spaces and the intermembrane space within the 1-2 minutes observed for release of cytochrome *c* during apoptosis.

If the mitochondrial transformation to the vesicular form is not required for release of cytochrome *c*, what is its function? Mitochondria in many cells are elongated often forming an extensive interconnected reticulum, and there are numerous studies showing extensive mitochondrial fragmentation during apoptosis (Karbowski, Arnoult et al. 2004; Lee, Jeong et al. 2004; Chan 2006; Heath-Engel and Shore 2006). The transformation of the inner membrane to the vesicular conformation effectively fragments the matrix compartment, and all that remains to complete fragmentation of the mitochondria is outer membrane fission. The beginning of fragmentation may be seen in the tomogram section of the vesicular mitochondrion shown in Figure II.4c where the arrows indicate a portion of the mitochondrion containing several vesicular matrix compartments that appears to be separating from the rest of the organelle.

An obvious question is how to effect the transformation of the inner mitochondrial membrane from the normal complex morphology with lamellar cristae connected to the inner boundary membrane via tubular crista junctions into individual vesicular matrix compartments without compromising the integrity of the matrix. An elegant and simple mechanism requires the elongation of crista junctions within individual lamellar cristae to a point where they meet and fuse. Once this occurs around the perimeter of a lamellar crista the two halves of the lamellar crista membrane are incorporated into the resulting vesicular matrix compartments. This

mechanism is diagrammed topologically with a sequence of schematic models in Figure II.7 showing the growth and fusion of crista junctions around the perimeter of lamellar cristae ultimately creating separate vesicular matrix compartments without exposing the matrix to the intermembrane space. This hypothetical mechanism is supported by EM tomography of Stage 1 mitochondria within cells treated with Etoposide for 16 hours. We measured the dimensions of crista junctions from: (1) Control cells that have not been treated with Etoposide, (2) Stage 1 mitochondria in cells treated with Etoposide for 16 hours that exhibit "normal" morphology in thin section TEM, and (3) Stage 3 mitochondria in cells treated with Etoposide and with zVAD-fmk to inhibit caspases. We measured length and width, which are the same for normal circular crista junctions but are expected to become progressively more elliptical during the transformation to the vesicular form by the model depicted in Figure II.7. As seen in Figure II.6, only Stage 1 mitochondria treated with etoposide exhibit significantly elliptical crista junctions, while both control and zVAD/Etoposide treated mitochondria contained predominantly circular crista junctions. The elliptical crista junctions are displayed in the tomogram of a Stage 1 mitochondrion in Figure II.6b and are also seen in the tomogram of a normal/vesicular mitochondrion in Figure II.4b (see arrows). It is noteworthy that in cells treated with Etoposide plus zVAD-fmk, cytochrome *c* is released without inner membrane remodeling or significant increase in crista junction size.

It is very significant that among the proteins released from mitochondria along with cytochrome *c* during apoptosis is OPA1, a dynamin-related GTPase whose yeast

homolog is called Mgm1p (Arnoult, Grodet et al. 2005). Mutations in OPA1 are the cause of autosomal dominant optic atrophy (ADOA) leading to progressive loss of vision (Alexander, Votruba et al. 2000; Delettre, Lenaers et al. 2000; Olichon, Guillou et al. 2006). Reducing the levels of OPA1 by siRNA in order to simulate the effects of ADOA results in disruption of the morphology of cristae and mitochondrial fragmentation (Olichon, Baricault et al. 2003; Griparic, van der Wel et al. 2004; Arnoult, Grodet et al. 2005). The exact changes in cristae morphology are difficult to discern from most published electron micrographs, but in at least one case they appear to be similar to our thin section electron micrographs of vesicular mitochondria (see Figure 6a of Griparic *et al.* (Griparic, van der Wel et al. 2004)). OPA1/mgm1p is bound to the inner mitochondrial membrane, is believed to regulate inner membrane conformation. (Shaw and Nunnari 2002), and is required for inner membrane fusion. (Meeusen, Devay et al. 2006) Thus, it is not surprising that lack of OPA1/mgm1p function leads to increased fission. Possibly the vesicular remodeling we observe during apoptosis is an extreme example of inner membrane fission that in normal cells occurs only at the sites of outer membrane fission. In this context it is interesting to note that Irwin et al observed mitochondria with a morphology identical in thin sections to our vesicular mitochondria within muscle tissue from mice deficient in Collagen VI created as a model for Bethlehem myopathy, a heritable human muscle disease (see their Figure 2d)(Irwin, Bergamin et al. 2003).

Frezza *et al.* recently published a study of the role of OPA1 in regulating the mitochondrial inner membrane conformation. Their results support the role of OPA1

in regulating crista junction diameter, as they found that loss of OPA1 function results in increased crista junction diameters, while increased OPA1 expression preserves normal crista morphology including maintenance of crista junction size in cells challenged with initiators of apoptosis. They come to the opposite conclusion, however, on the role of inner membrane remodeling in release of cytochrome *c* believing that inner membrane remodeling is required for release of cytochrome *c* from intracristal spaces. It is important to note, however, that they did not measure cytochrome *c* release in live cells nor did they monitor ultrastructural changes in the identical cells by TEM or EM tomography. Their studies by TEM and EM tomography were conducted on mitochondria purified from cells of different genetic lineages, and the purification procedure led to partial condensation of the matrix compartments. These mitochondria were subsequently challenged with tBid (cBid) to induce release of cytochrome *c*. Furthermore, the inner membrane remodeling that they observed in purified mitochondria involves fusion of cristae that appears to be fundamentally different from the changes that we observe by correlated light and electron microscopy and EM tomography of mitochondria *in situ* in live cells leading to individual vesicular matrix compartments (Frezza, Cipolat et al. 2006).

The role of caspase activation in the transformation from normal orthodox mitochondria to vesicular mitochondria is not obvious. It is important to know the timing of OPA1 release relative to release of cytochrome *c*, since active caspases are known to enter mitochondria following mitochondrial outer membrane permeabilization (MOMP) disrupting mitochondrial function by cleavage of inner

membrane proteins. (Ricci, Gottlieb et al. 2003; Ricci, Munoz-Pinedo et al. 2004) Thus, active caspases may be required for the release of OPA1 as has been reported for release of other proteins from mitochondria (Arnoult, Parone et al. 2002; Arnoult, Gaume et al. 2003; Arnoult, Karbowski et al. 2003; Munoz-Pinedo, Guio-Carrion et al. 2006). In this context we note that OPA1 function does appear to be regulated by proteolytic cleavage producing a soluble form that is released from mitochondria (Cipolat, Rudka et al. 2006; Frezza, Cipolat et al. 2006). Thus, inhibition of caspases could inhibit release of the soluble form of OPA1 preventing inner membrane remodeling to the vesicular form.

In summary, the release of cytochrome *c* from HeLa cells during apoptosis initiated by various agents including etoposide, actinomycin-D, and in some conditions by Fas-ligand appears to proceed through large outer membrane channels that are probably formed by the proapoptotic proteins Bax, Bak, and Bid. We observed a dramatic transformation of inner membrane structure to a vesicular form that fragments the matrix compartment and is probably related to inner membrane fission during mitochondrial fragmentation. Mitochondrial swelling occurs later in the apoptosis program, after release of cytochrome *c* and loss of $\Delta\Psi_m$. Complete release of cytochrome *c* does not appear to require remodeling of the inner membrane to the vesicular form, since zVAD-fmk prevented inner membrane remodeling but did not inhibit cytochrome *c* release. It is important to keep in mind that other stimuli of apoptosis may proceed by a different mechanism (Kroemer and Reed 2000). Indeed, in this same system initiation of apoptosis by addition of H_2O_2 results in immediate

loss of $\Delta\Psi_m$, subsequent opening of the mPTP, and large amplitude swelling of the mitochondrial matrix that appears in this case to be the immediate cause of cytochrome *c* release. (More result and discussion in Chapter III)

METHODS

1. Culture conditions and the induction of apoptosis

HeLa cells expressing cytochrome c-GFP or Cyt. *c*-4CYS are those previously described (Goldstein, Waterhouse et al. 2000; Goldstein, Munoz-Pinedo et al. 2005) and were grown and maintained at 37° C in Dulbecco's modified Eagles's medium (DMEM, Gibco) supplemented with 10% FBS, 2mM L-glutamine, 200 mg/ml penicillin, and 100 mg/ml streptomycin sulfate in a humidified atmosphere of 5% CO_2/95% air. Cells were subcultured 1:10 by incubating them in 0.25% trypsin (Gibco) when they were confluent and re-suspending cells in growth medium.

Apoptosis was induced with 100 μM etoposide for 12-18 hours. When indicated zVAD-fmk (100 μM, Sigma) was added hours before the apoptotic stimulus to inhibit caspase activity. TMRE (50 nM, Sigma) was added to monitor the $\Delta\Psi_m$, and when indicated Cyclosporin A (CsA, 0.1 μM, Sigma) was used to inhibit opening of the mitochondrial transition pore (MPTP).

2. Cytochrome *c* labeling with biarsenical ligands

The staining media were prepared by the addition of a premixed DMSO stock solution to give a final concentration of 2.5 μM of FlAsH-1,2-ethanedithiol $(EDT)_2$ and 10 μM EDT (Fluka) in DMEM. Cells were incubated at 37° C in an incubator for 1 hour and were then rinsed in glucose-containing Hanks' buffered saline solution (HBSS, Gibco) and incubated for 10 min at room temperature in HBSS containing

62.5 μM EDT. Cells were washed three times with HBSS and returned to the incubator for at least 12 hours before treatment.

3. Western blotting to detect cytochrome *c* release from HeLa cells

HeLa cells were incubated with etoposide (100 μM) and collected at the following time points: 0 hr, 14 hr, 16 hr, 18 hr, and 20 hr. Cells were then treated with lysis buffer (80 mM KCl, 250 mM sucrose, 500 μg/ml digitionin, 0.1 mM PMSF, 1 mM DTT, 1:800 protease inhibitors) for 5 min and centrifuged for 5 min at 10,000g at 4° C. The supernatant (cytosolic fractions) and pellets (mitochondrial fractions) were used for Western blot analysis of 13 μg of total protein aliquots subjected to SDS-PAGE. The proteins were transferred to PVDF membranes and subjected to immunoblotting with anti-cytochrome *c* (BD Biosciences). Film was developed after incubation of the PVDF with SuperSignal West Pico Chemiluminescent ECL Substrate (Pierce).

4. Calcein-AM to monitor mPTP

HeLa cells were incubated with calcein-AM (2 μM, Invitrogen) and $CoCl_2$ (1 mM) for 60 min at 37° C. The cytosolic and nuclear calcein signal is quenched by $CoCl_2$, and mPTP opening was detected by a rapid release of mitochondrial calcein fluorescence.

5. Confocal microscopy

For time-lapse analysis, cells were grown in 35 mm microwell dishes containing a glass coverslip with an etched grid (MatTek Corp. Ashland, MA). Images were acquired using a Leica TCS SP2 inverted confocal microscope. Cyt *c*-GFP, FlAsH, and Calcein were excited using the 488nm line from an Ar/Kr laser attenuated to 35%. TMRE was excited using a 543nm line from an Ar/Kr laser attenuated to 34%. The detector slits of the confocal microscope were adjusted to detect GFP emission between 497-553 nm, FlAsH emission between 497-553 nm, TMRE emission between 555-620 nm and Calcein emission between 497-553 nm.

6. Single cell analysis of mitochondrial structure by correlated confocal and electron microscopy/tomography.

By growing HeLa cells in special Petri dishes containing an etched grid (MatTek Corp. Ashland, MA), we can monitor cytochorome *c* release and $\Delta\Psi_m$ simultaneously by confocal microscopy and subsequently fix and embed the identical cells for examination by electron microscopy and by electron tomography. After confocal imaging, cells were fixed immediately by an 1 hour incubation on ice in a 2.5% paraformaldehyde – 2.5% glutaraldehyde – 0.1 M sodium cacodylate pH 7.4 buffer. After washing three times in ice-cold 0.1 M sodium cacodylate buffer containing 3 μM calcium chloride for 3 minutes, the primary fixed cells were then incubated with 1% osmium tetroxide – 0.8% potassium ferrocyanide – 3 μM calcium chloride in 0.1 M sodium cacodylate for 60 minutes on ice. After washing with

distilled water 3 times for 3 minutes, fixed cells were stained and stabilized in ice-cold 2% uranyl acetate for 30 min on ice and dehydrated in an ice-cold ethanol series of 20, 50, 70, 90% successively on ice for 3minutes each. The cells were then dehydrated at room temperature 3 times for 3 minutes each in 100% ethanol and infiltrated in well-mixed 50% ethanol, 50% Durcupan ACM resin (Fluka) for 60 minutes with agitation at room temperature followed by 100% Durcupan ACM twice for 1 hour with agitation after which the samples were placed in an oven and allowed to polymerize at 60-80° C for at least 48 hours. The glass coverslip was peeled away from the bottom using a razor blade and the selected area was cut out and glued to a block for sectioning. Thin sections (approximately 80nm) were collected and pre-stained with 2% uranyl acetate and Sato lead before examination in an FEI Tecnai 12 TEM

For EM tomography single-tilt series 3-D reconstructions were obtained from semi-thick samples (250 – 500 nm) in a tilt-series every 2° from -60° to +60° on a JOEL 4000EX electron microscope operated at 400 kV. The IMOD software suite was used to process the images in each tilt series (Boulder Laboratory for 3-Dimensional Electron Microscopy of Cells, University of Colorado, Boulder). X-Voxtrace software enabled volume segmentation of tomographic data using manual tracing followed by rendering using Synu (National Center for Microscopy and Imaging Resources, UCSD).

7. High Pressure Freezing

HeLa cell pellets were loaded into the 100 μm-deep well of a type A brass planchettes (Ted Pella, Inc.) and covered with the flat side of brass type B planchettes. The planchette A and B sandwiches were quickly loaded into the freezing holder and frozen in a Bal-Tec HPF 010 high pressure freezing machine. The sandwich was separated under liquid nitrogen and the type A planchette which held the cells was placed in a cryo-vial filled with 2% Osmium and 0.1 % Uranyl Acetate in acetone (EM grade from Fullam Inc.). Freeze substitution was carried out in a Leica EM AFS raising the temperature to −90 °C over 72 h, then to 0°C over 2 h, and finally to room temperature over 4 h. After substitution, the specimens were rinsed in pure acetone three times (10 min. at room temperature). The specimens were removed from planchettes after the last wash and infiltrated with 30% Durcupan in acetone for 2hrs, 50% Durcupan overnight, 70% Durcupan for 4hrs, 90% over 2hrs and 100% Durcupan overnight. The next day the 100% Durcupan was changed twice more, and the resin polymerized in the oven at 60° C overnight.

8. Caspase-3 assay

Caspase-3 activity was measured using its fluorogenic substrate, Ac-DEVD-AFC (Sigma). Cells were lysed on ice by lysis buffer (0.71% NP-40, 71 mM Tris pH 7.5, 0.71 mM EDTA, 212 mM NaCl). The protein concentration of the resulting supernatant was determined using the Bio-Rad DC protein Assay. Equal amounts of

total cell lysate protein (40 μg) were mixed with caspases-3 assay buffer (21 mM HEPES, 105 mM NaCl, 5.35 mM DTT) containing substrate Ac-DEVD-AFC (25 μM) in a black 96 well titer plate in triplicate. Caspase-3 mediated cleavage of Ac-DEVD-AFC into free AFC was measured using a Spectra Max Gemini XS flourimeter plate reader with an excitation wavelength of 400 nm and emission wavelength of 505 nm using Softmax Pro version 3.1.2 software. This experiment was replicated three times.

FIGURES & LEGENDS

Figure II.1: Cyt. *c*-4CYS staining with FlAsH co-localizes with TMRE staining of mitochondria maintaining $\Delta\Psi_m$, and Cyt. *c*-4CYS is released before loss of $\Delta\Psi_m$.

HeLa cells transfected with Cyt. *c*-4CYS were grown in Petri dishes with a glass coverslip containing an etched grid and then stained with FlAsH and TMRE. Apoptosis was initiated with 100 μM etoposide.

(a) – (**c)** show respectively Cyt. *c*-4CYS in green, TMRE in red, and the overlay showing overlap of the two signals in yellow of a field of cells at the start of the experiment (Stage 1).

(d) – (e) shows the same field of cells 16 hrs. after addition of Etoposide.

(f) is a low magnification electron micrograph of the same field of cells after chemical fixation, dehydration, and embedding in plastic at 16 hrs. The circle encloses a cell whose mitochondria have released Cyt. *c*-4CYS but maintain $\Delta\Psi_m$ after 16 hrs (Stage 2); the square encloses a cell whose mitochondria have both released Cyt. *c*-4CYS and lost $\Delta\Psi_m$ after 16 hrs. (Stage 3).

(g) Western blot of total cytochrome *c* in cytosolic and mitochondrial fractions of HeLa cells following treatment with Etoposide. 13μg protein aliquots from cytosolic fractions and mitochondrial fractions were prepared at 0, 14, 16, 18, and 20 hours after Etoposide addition and subjected to SDS-PAGE. The proteins were transferred to PVDF and subjected to immunoblotting with anti-cytochrome *c*, and visualized by chemiluminescent ECL substrate.

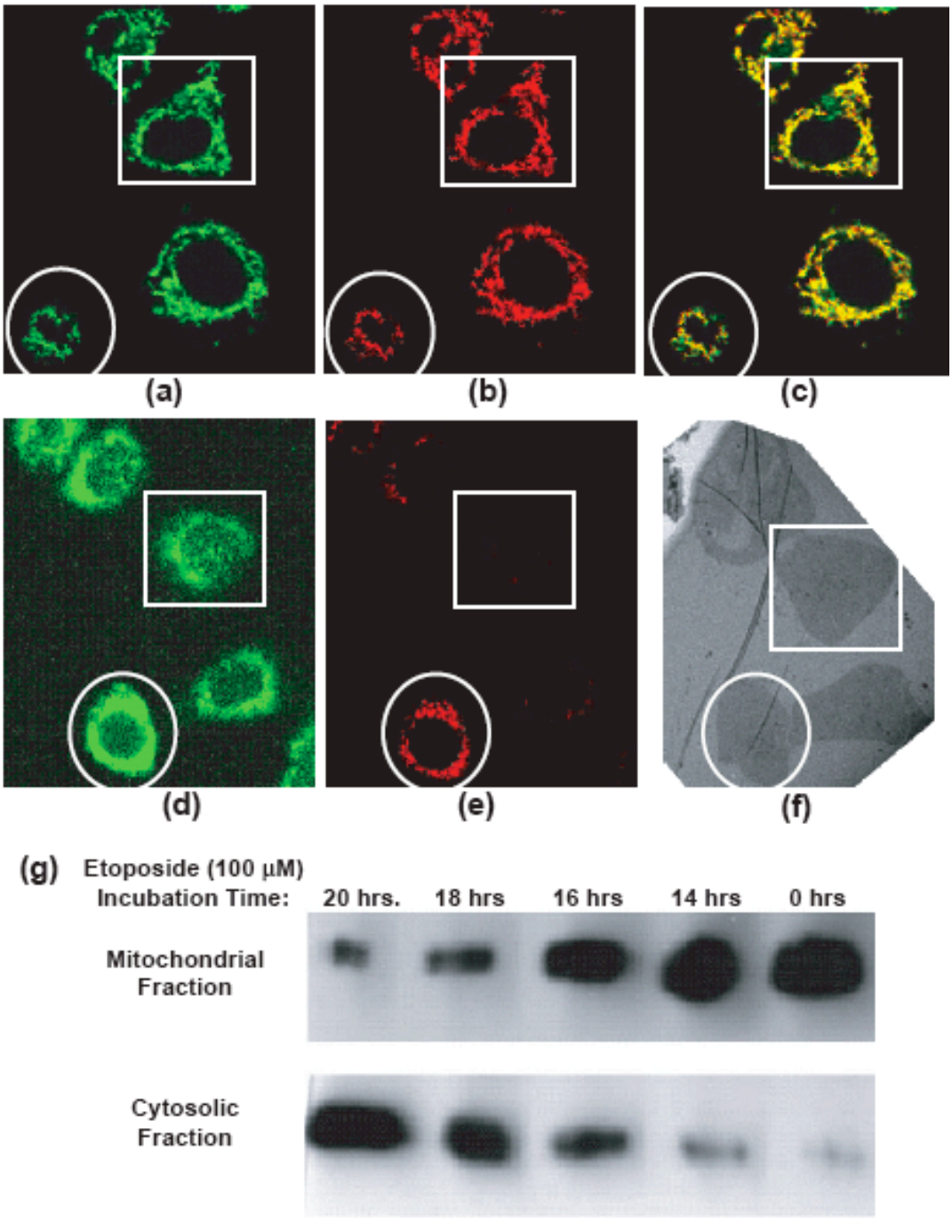
(a)
(b)
(c)
(d)
(e)
(f)
(g)
Etoposide (100 μM)
Incubation Time:
20 hrs.
18 hrs
16 hrs
14 hrs
0 hrs
Mitochondrial Fraction
Cytosolic Fraction

Figure II.1

Figure II.2: Mitochondrial inner membrane conformation changes to the vesicular form during cytochrome *c* release and the matrix swells during or after the loss of $\Delta\Psi_m$.

HeLa cells transfected with Cyt. *c*-4CYS and stained with FlAsH and TMRE were monitored by confocal microscopy before preparation for electron microscopy of the same fields of cells. Scale bars are 25 μm in the fluorescent micrographs and low magnification TEM's and 500 nm in the high magnification TEM's.

(a) Stage 1 cells have neither released Cyt. *c*-4CYS nor lost $\Delta\Psi$ as indicated by the co-localization of FlAsH staining of Cyt. *c*-4CYS (upper left) with TMRE staining (upper center) in the overlay image (upper right). The electron micrographs show only the normal mitochondrial morphology; the inset at upper left is a low magnification electron micrograph of the complete field of six cells.

(b) Stage 2 cells have released (or are releasing) Cyt. *c*-4CYS but maintain $\Delta\Psi_m$ as indicated by the diffuse FlAsH staining in the upper left that does not correlate with the punctate TMRE staining (upper center) in the overlay (upper right). These cells display both normal mitochondrial morphologies in electron micrographs but also many mitochondria with vesicular matrix compartments with one indicated by the arrow; the inset at lower right shows a low magnification electron micrograph of this field of four cells.

(c) Stage 3 cells that have released Cyt. *c*-4CYS and have lost $\Delta\Psi_m$ contain relatively few mitochondria with normal morphology with many swollen mitochondria (arrow) and vesicular/swollen mitochondria (arrowhead).

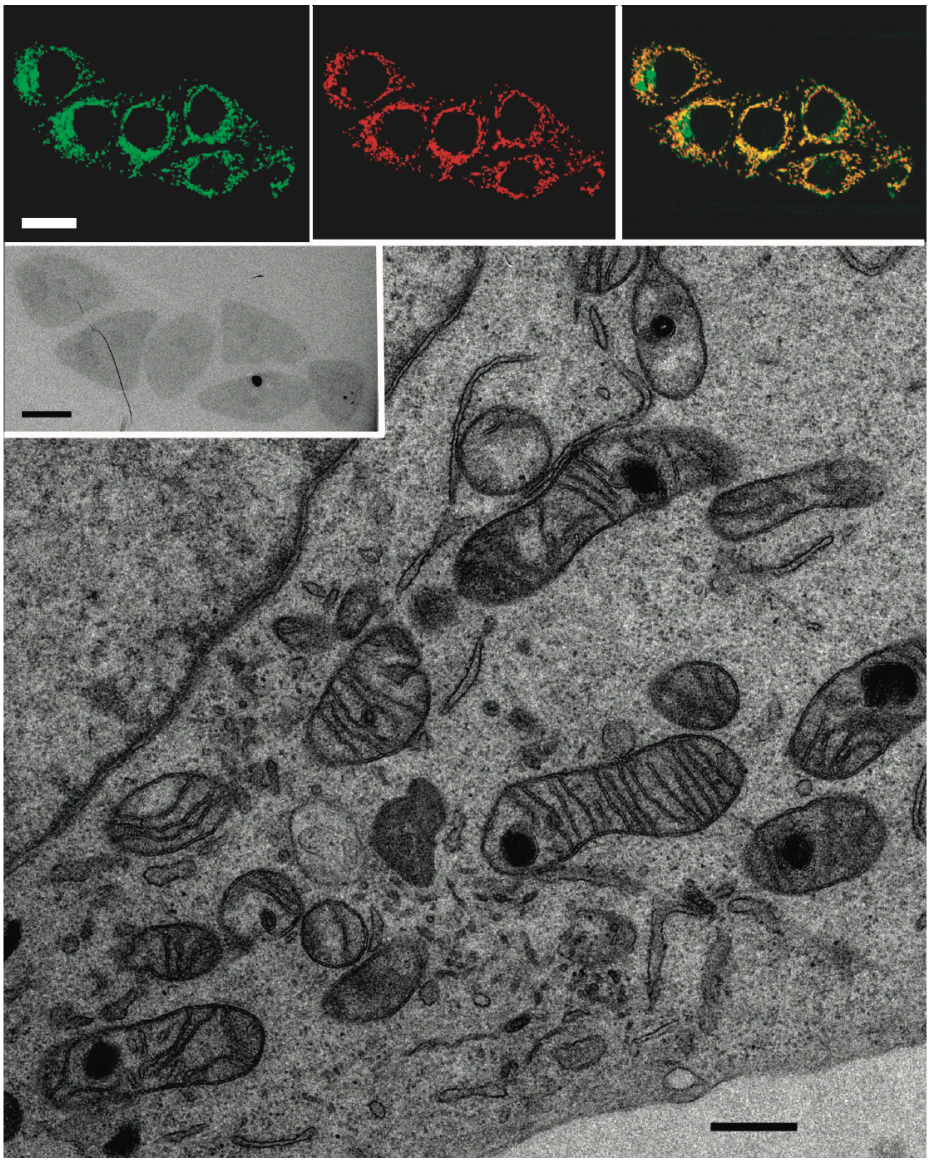

Figure II.2.a

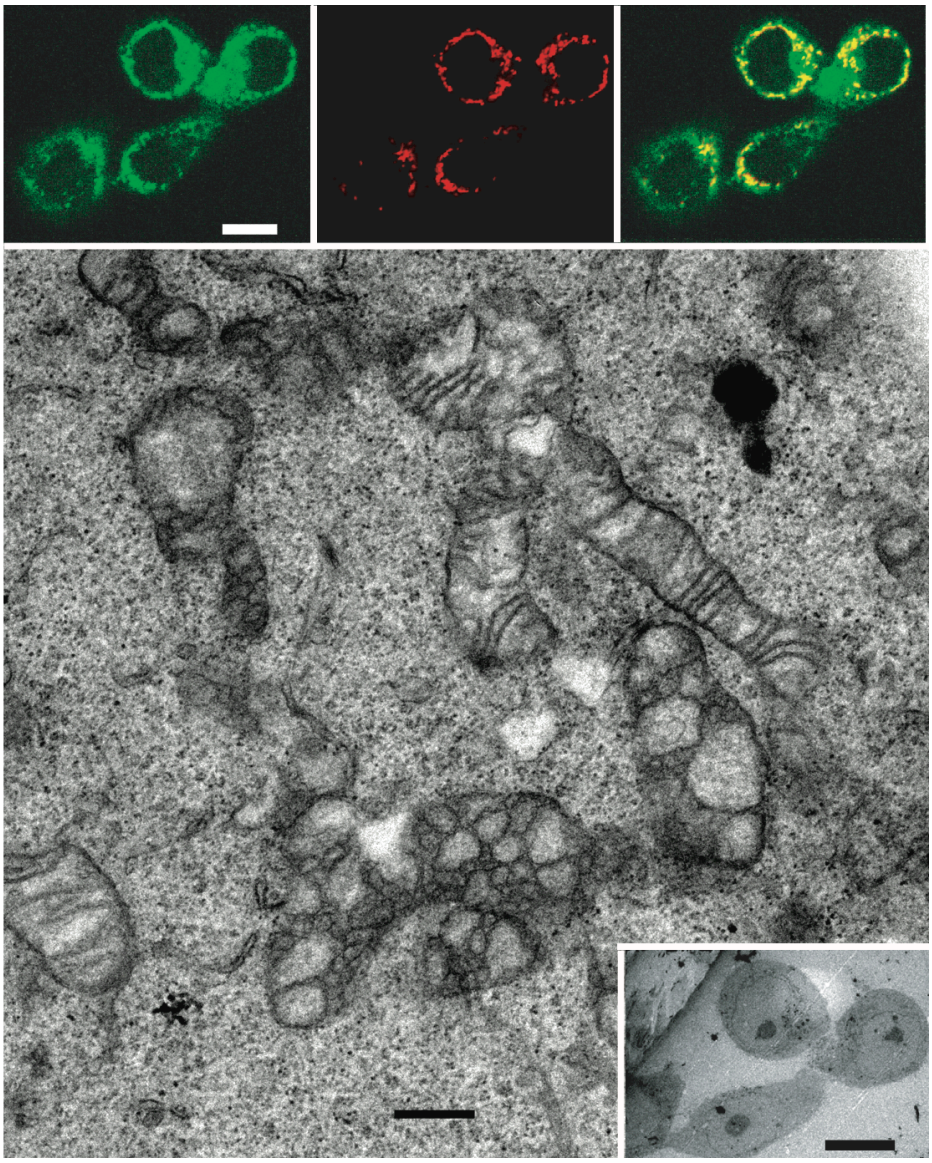

Figure II.2.b Continued

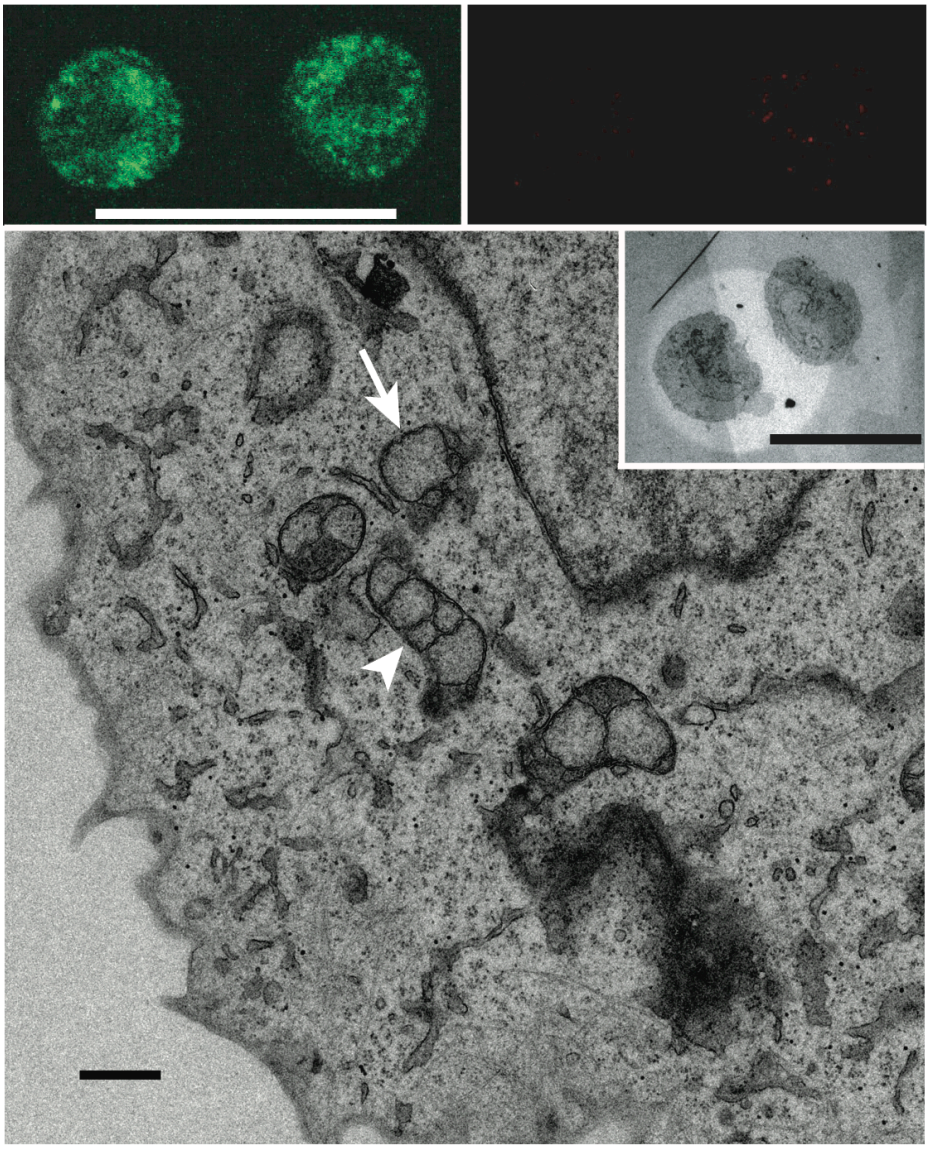

Figure II.2.c Continued

Figure II.3: Five mitochondrial morphologies are identified.

(a) Normal;
(b) Normal/Vesicular;
(c) Vesicular;
(d) Vesicular/Swollen;
(e) Swollen.

Scale bars are 200 nm in (a) – (d) and 100 nm in (e)

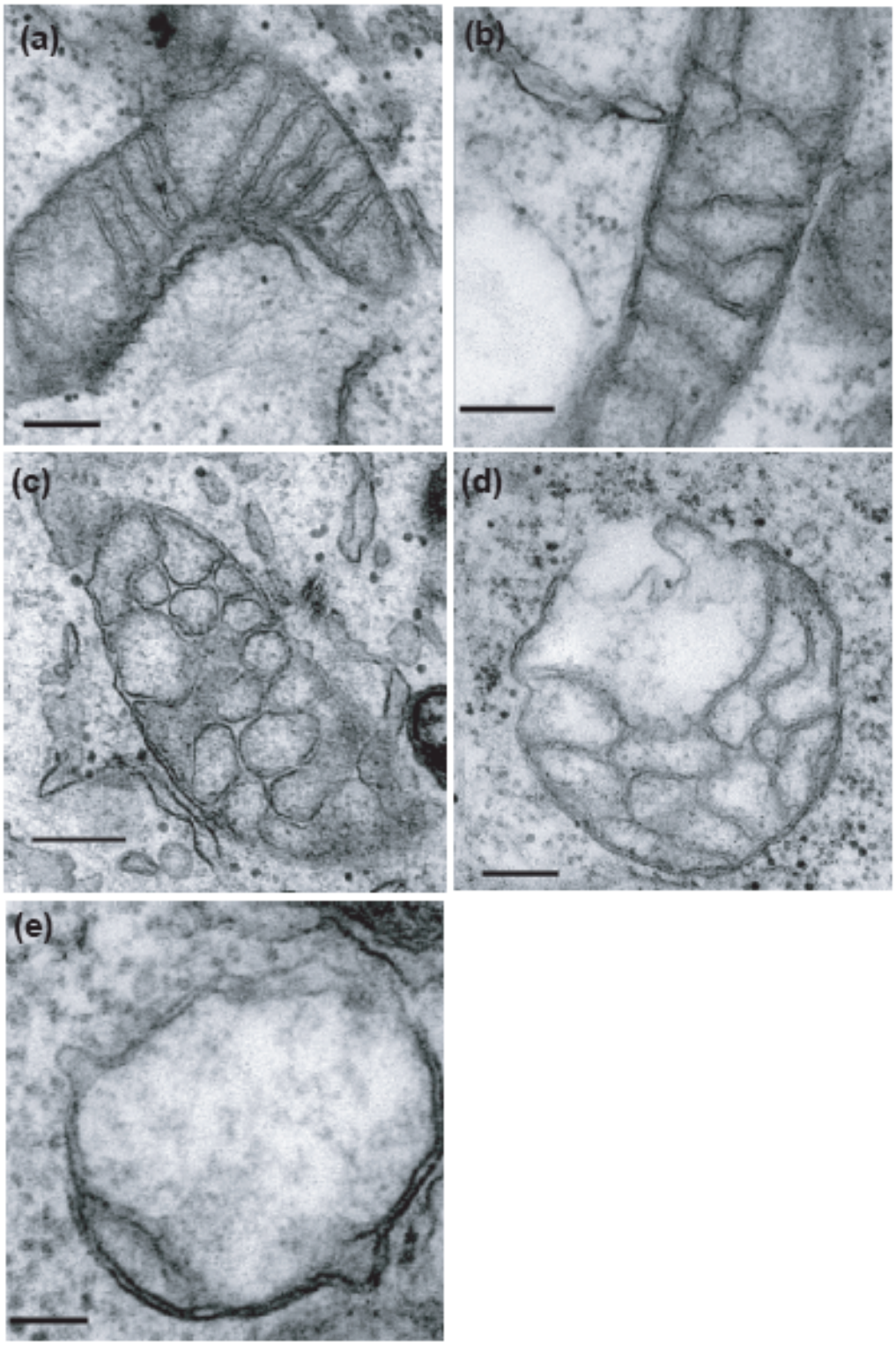

Figure II.3

Figure II.4: Electron microscope tomography of examples of the five mitochondrial morphologies.

On the left are sections of constant z through the electron tomograms and on the right are renderings of the models produced from the segmented tomograms: the outer membrane is rendered in translucent light blue, the inner boundary membrane is rendered in white, and the cristae are rendered in various colors. The successive views rotate about a vertical axis by varying amounts from left to right. Scale bars are 250 nm.

(a) Normal mitochondrion – rendering of the outer membrane in the leftmost and two rightmost views is reduced to reveal the small discrete crista junctions in red, green, and yellow.

(b) Normal/Vesicular mitochondrion – the vesicular portion is at the upper right with different vesicular matrix compartments rendered in various colors; the normal portion is below and the normal cristae are rendered in green and contained within the matrix compartment enclosed within the inner boundary membrane rendered in white; arrow in left most rendered view identifies an elongated crista junction.

(c) Vesicular mitochondrion – The vesicular matrix compartments containing the fragmented matrix are rendered in various colors; note there is no inner boundary membrane.

(d) Vesicular/Swollen mitochondrion – Two swollen vesicular matrix compartments are rendered in yellow (upper end) and in magenta (center) with small vesicular matrix compartments rendered in various colors surrounding the magenta swollen vesicular compartment; note again the absence of an inner boundary membrane.

(e) Swollen mitochondrion – One swollen vesicular matrix compartment is rendered in yellow with two lamellar crista rendered in red and green contained within a swollen matrix bounded by an inner boundary membrane rendered in white. Note that the outer membrane appears to be ruptured at the bottom

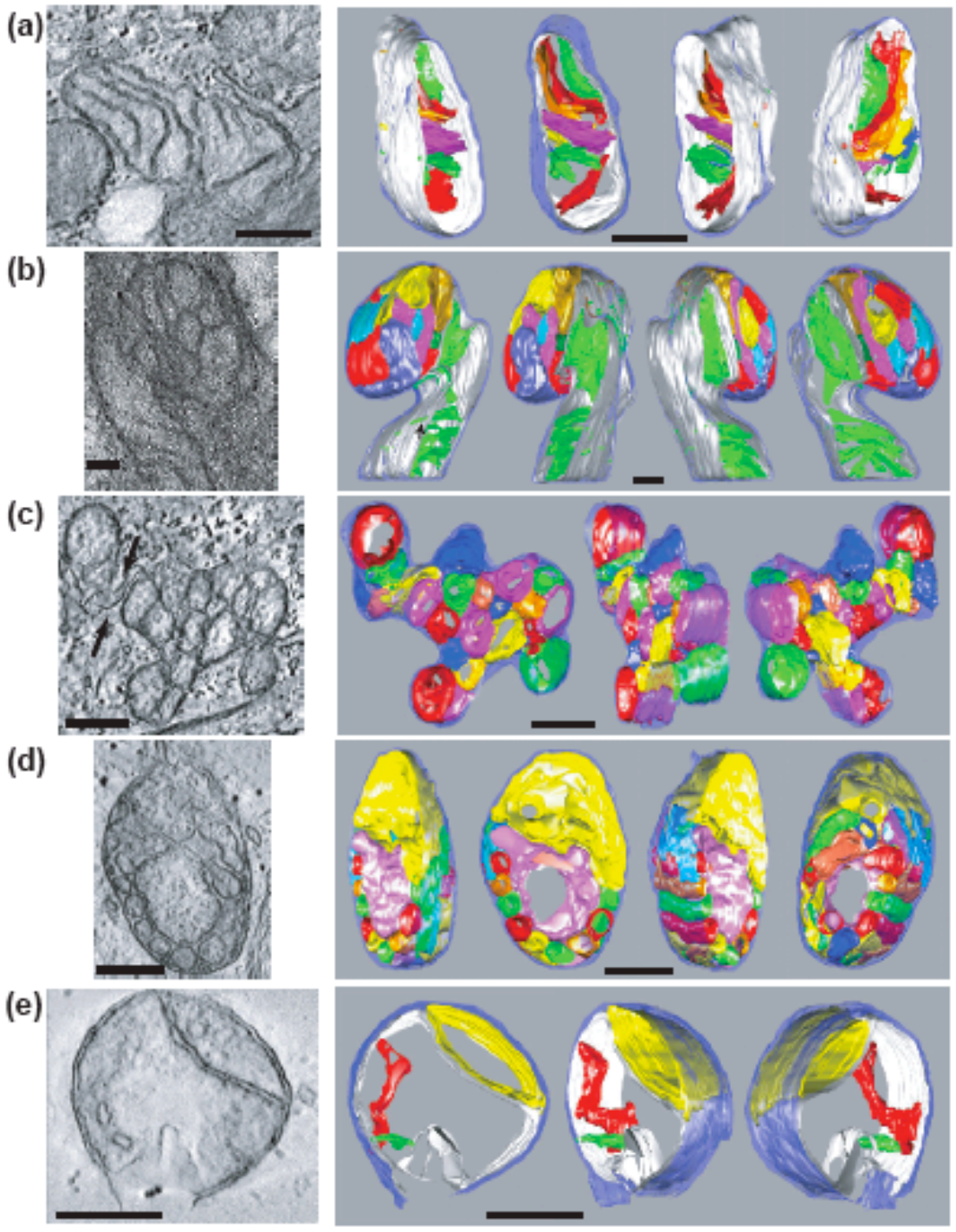

Figure II.4

Figure II.5: Mitochondria progress from normal to vesicular during release of cytochrome *c* and then swell during or after the loss of $\Delta\Psi_m$.

Bar graphs show the percentages of mitochondria observed within each of the five morphologies – Normal, Normal/Vesicular, Vesicular, Vesicular/Swollen, and Swollen – for cells in Stages 1 – 3. Cells were selected based upon FlAsH and TMRE staining of HeLa cells transfected with Cyt. *c*-4CYS (see Fig. 2 for examples). Following preparation for electron microscopy, electron micrographs of each cell were collected and all of the mitochondria within a thin section of each cell were classified in a double-blind fashion. The number of cells / number of mitochondria analyzed are indicated at the top of each graph.

(a) Stage 1 – Control cells; no treatment.

(b) Stage1 – Treatment with etoposide for 15 hrs; cells have not released Cyt. *c*-4CYS and maintain $\Delta\Psi_m$.

(c) Stage 2 – treatment with etoposide for 16 hrs; cells have released Cyt. *c*-4CYS but maintain $\Delta\Psi_m$.

(d) Stage 3 – treatment with etoposide for 16 hrs; cells have released Cyt. *c*-4CYS and have lost $\Delta\Psi_m$.
(e) Stage 3 with caspases inhibited – treatment with etoposide for 16 hrs. in the presence of zVAD-fmk; cells have released Cyt. *c*-4CYS and have lost $\Delta\Psi_m$.

(f) Stage 3 with MPTP inhibited – treatment with etoposide for 16 hrs in the presence of Cyclosporin A; cells have released Cyt. *c*-4CYS and have lost $\Delta\Psi_m$.

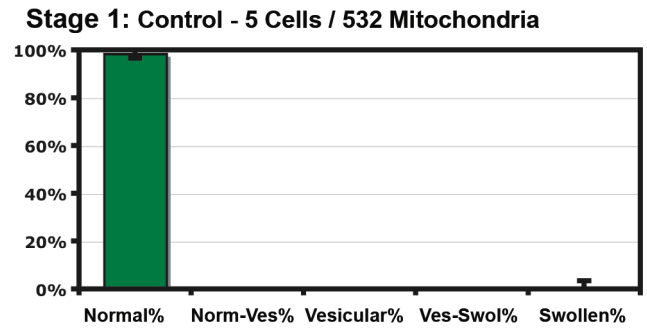

Figure II.5.a

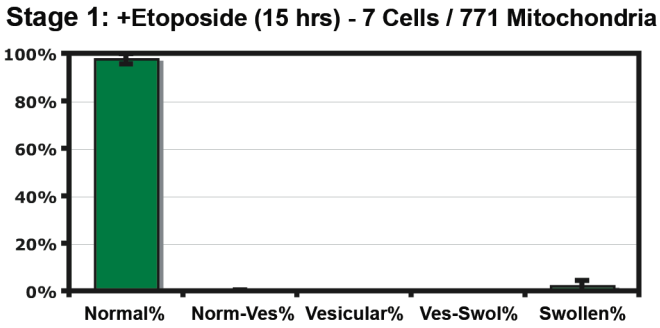

Figure II.5.b

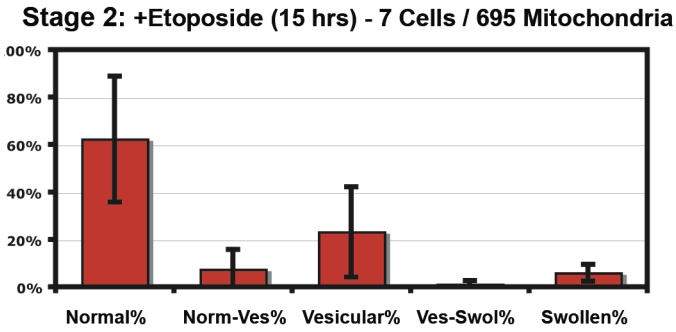

Figure II.5.c

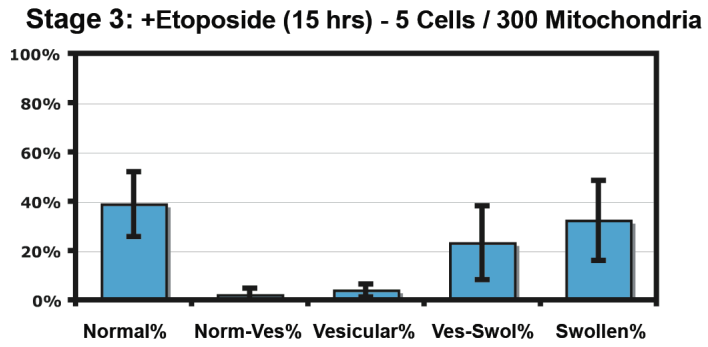

Figure II.5.d

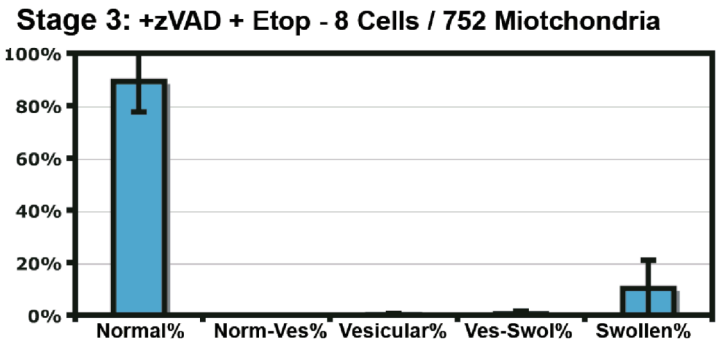

Figure II.5.e

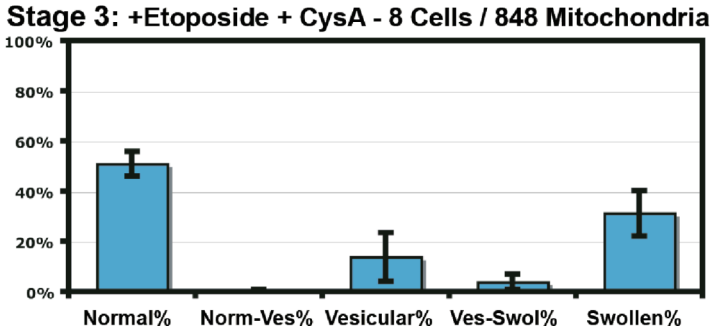

Figure II.5.f

Figure II.5 Continued

Figure II.6. z-VAD-fmk inhibits crista junction elongation.

(a) 50 Cristae Junctions from each of three groups of HeLa cells were measured by Image J. For each crista junction, length and width were measured from the three-dimensional tomogram.

Group 1: Normal is the untreated control (measured from 5 tomograms).

Group 2: Etop+zVAD are Stage 3 HeLa cells pretreated with zVAD and treated with Etoposide for 16 hours (measured from 3 tomograms); these have released Cyt. *c*-4CYS, have lost $\Delta\Psi_m$, and appear normal in TEM thin sections.**Group 3: Etop Stage 1** are cells treated with Etoposide for 15 hours (measured from 4 tomograms); these have not released Cyt. *c*-4CYS, maintain $\Delta\Psi_m$, and appear normal in TEM thin sections.

(b) Three-dimensional models from EM tomography of mitochondria representing each of the three groups described in (a). Arrows in the Group 3 tomogram identify elongated crista junctions.

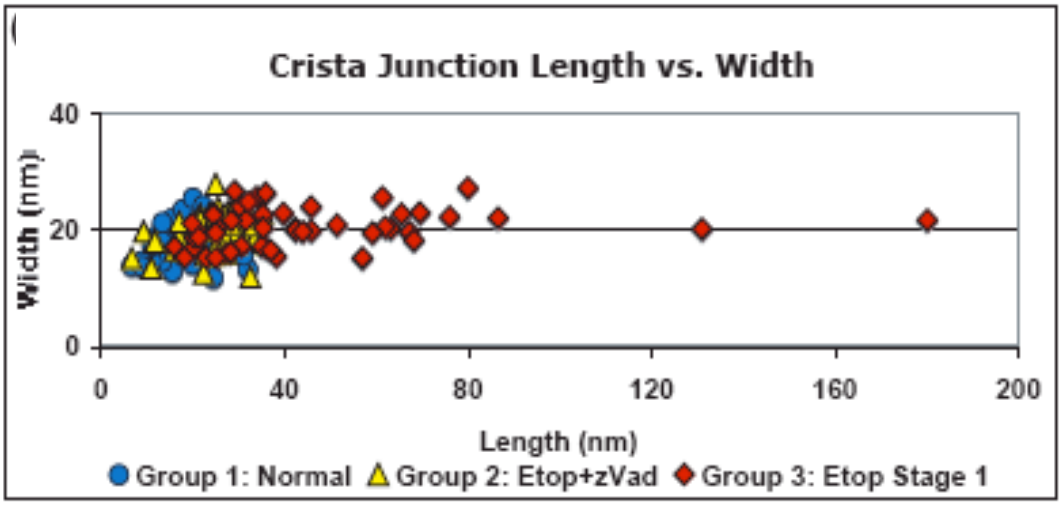

Figure II.6.a

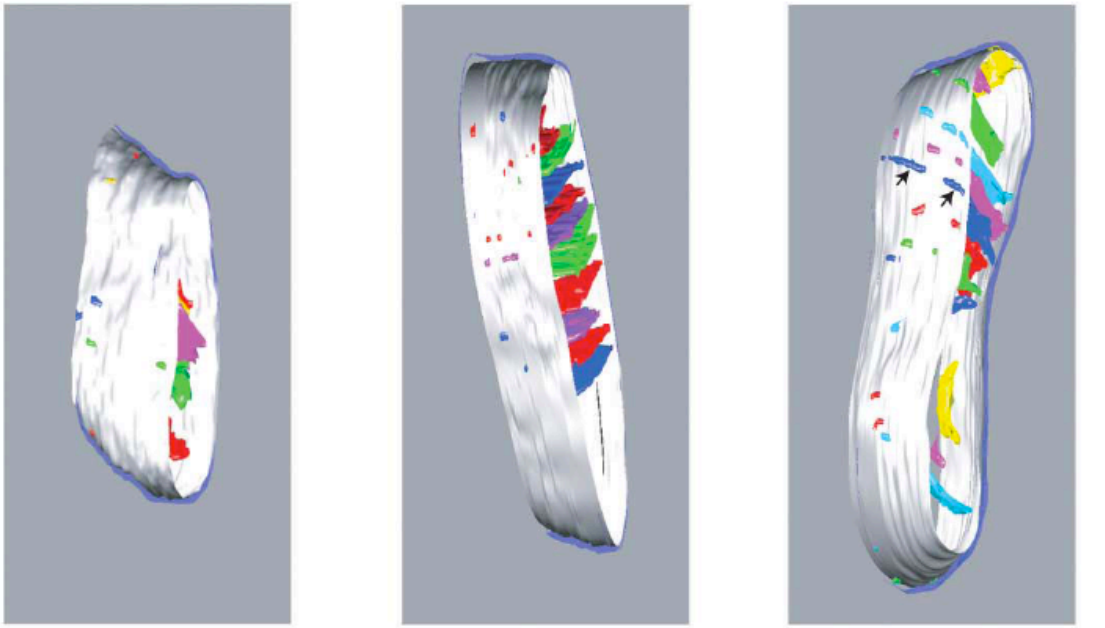

Figure II.6.b

Figure II.7: A schematic topological model by which normal mitochondria transform to vesicular mitochondria by elongation of crista junctions until nearest neighbors within each lammelar crista fuse followed by continued elongation of the fused crista junctions around the perimeter of the crista.

(a) Schematic model of the inner membrane of a normal orthodox mitochondrion; the outer membrane is not included. The two lamellar cristae in opaque yellow are connected to the inner boundary membrane in translucent blue that surrounds them through short tubular crista junctions, four in the upper crista and three in the lower crista. The cristae plus the inner boundary membrane are one complex two dimensional surface. The ends of the mitochondrion at the top and bottom are not modeled for simplification.

(b - d) The crista junctions in each lamellar crista elongate around the perimeter of the cristae and fuse to form slot like crista junctions.

(e) The crista junctions have elongated completely around the perimeter of what were previously lamellar cristae separating the matrix into three separate vesicular matrix compartments. The model continues to show the distinction between yellow opaque crista membrane and translucent light blue inner boundary membrane with the former crista membranes forming the upper and lower boundaries of the matrix compartments; however, in vesicular mitochondria this distinction is no longer relevant, and the shapes of the vesicular compartments would be round. Three-dimensional models were created with Google SketchUp 5 (www.sketchup.com).

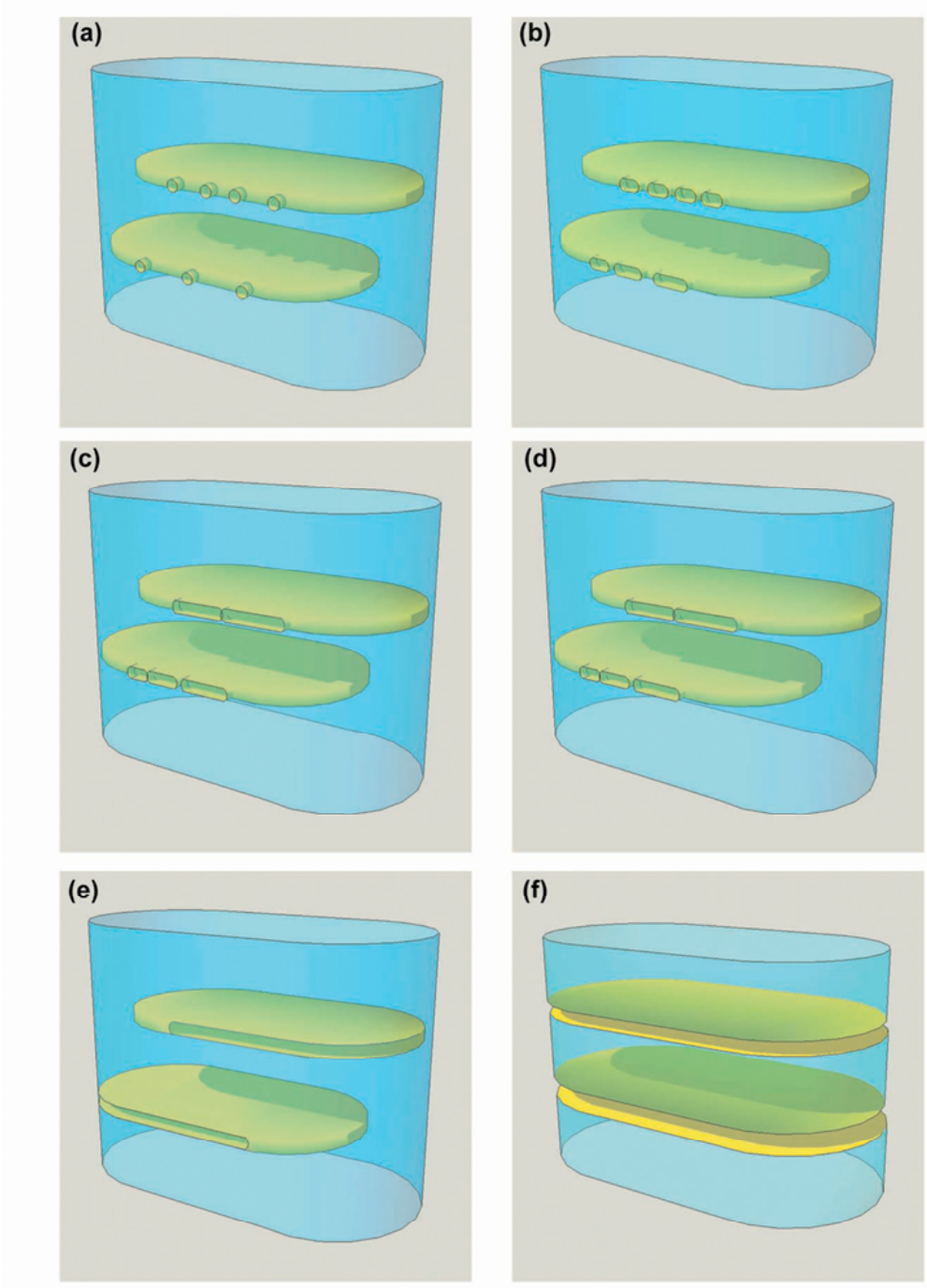

Figure II.7

Figure II.8. High Pressure Freezing Method confirms mitochondrial structure in Etoposide treated HeLa cells.

Wild Type HeLa cells were treated with Etoposide for 16 hours. Pellet sample was frozen by High Pressure Freezing. After freeze substitution, sample was embedded in Durcupan for sectioning. Scale bar is 500nm.

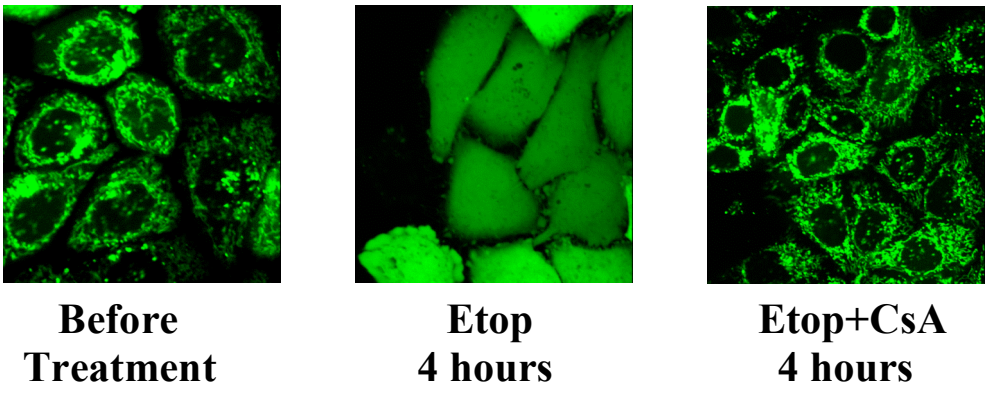

Figure II.9. Cyclosporin A (CsA, 0.1μM) inhibits mPTP opening

HeLa cells were treated with etoposide (1mM) for 4 hours. mPTP opening was determined by monitoring the fluorescence of calcein trapped in mitochondria. Confocal images revealed the mPTP opened within 4 hour while CsA inhibited mPTP opening after 4 hours treatment.

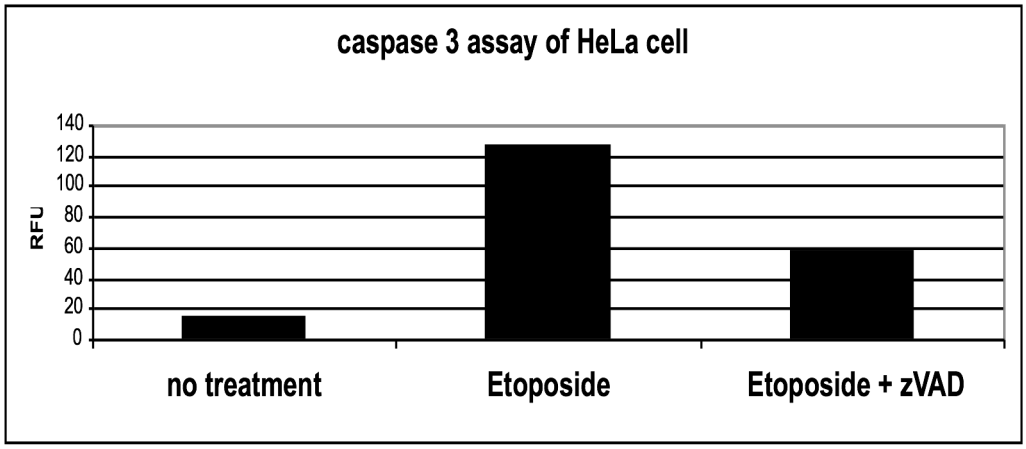

Figure II.10 z-VAD (100μM) inhibits caspase activity during etoposide induced apoptosis

Caspase-3 activity was measured using a caspase-3 fluorogenic substrate Ac-DEVD-AFC (Sigma). Cells were lysed and equal amounts of total cell lysate protein (40μg) were mixed with caspase-3 assay buffer containing substrate Ac-DEVD-AFC (25 μM) in a 96-well plate in triplicate. Caspase-3 mediated cleavage of Ac-DEVD-AFC into free AFC was measured using a plate reader flourimeter at an excitation wavelength of 400 nm and emission of 505 nm. This experiment was replicated three times.

Supplementary Figures

Supplementary Figure II.1: Cyt. *c*-GFP co-localizes with TMRE staining of mitochondria maintaining $\Delta\Psi_m$, and Cyt. *c*-GFP is released before loss of $\Delta\Psi_m$.

HeLa cells transfected with Cyt. *c*-GFP were grown in Petri dishes with a glass coverslip containing an etched grid and then stained with TMRE to monitor $\Delta\Psi_m$. Apoptosis was initiated with 100 μM etoposide.

(a) – (**b)** show respectively Cyt. *c*-4CYS in green, TMRE in red at the start of the experiment (before treatment).

(c) – (d) shows the same field of cells 16 hrs. after addition of Etoposide.

(e) is a low magnification electron micrograph of the same field of cells after chemical fixation, dehydration, and embedding in plastic at 16 hrs. The circle encloses a cell whose mitochondria have released Cyt. *c*-GFP but maintain $\Delta\Psi_m$ after 16 hrs (Stage 2); the square encloses a cell whose mitochondria have both released Cyt. *c*-GFP and lost $\Delta\Psi_m$ after 16 hrs. (Stage 3).

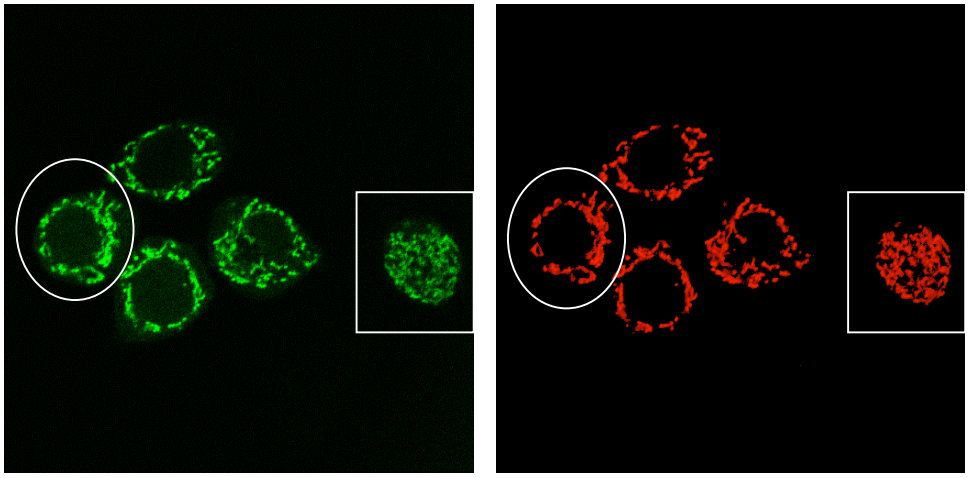

(a) **(b)**

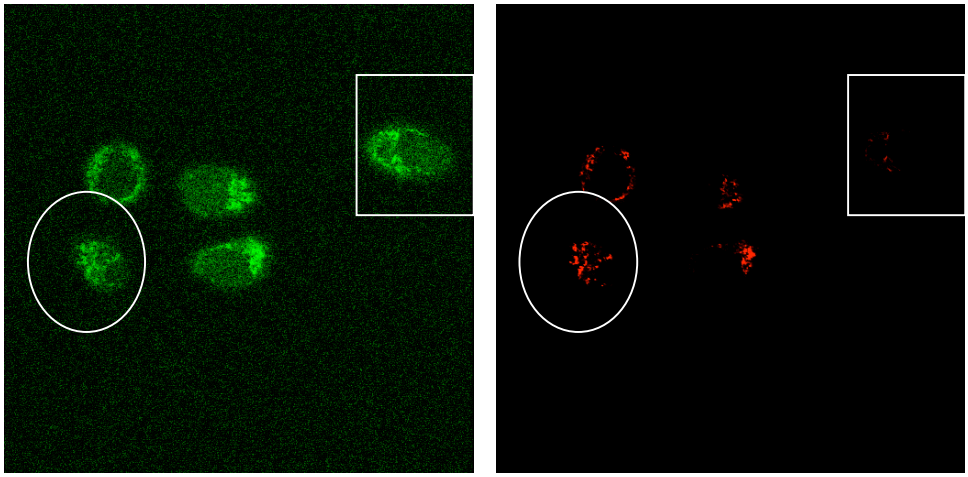

(c) **(d)**

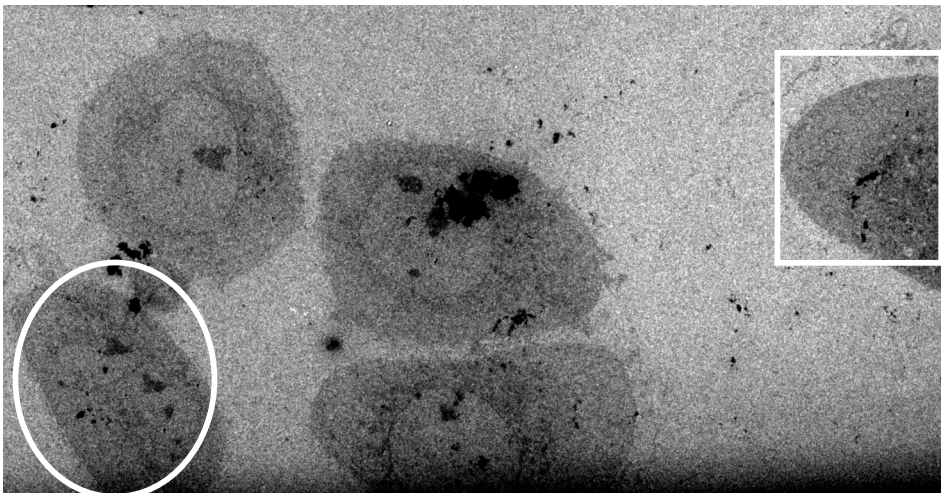

(e)

Supplementary Figure II.1

Supplementary Figure II.2: HeLa cell transfected with cyt c-GFP undergo the transformation of vesicular mitochondrial morphology during release of cytochrome *c* and this transformation is caspases sensitive.

Bar graphs show the percentages of mitochondria observed within each of the five morphologies – Normal, Normal/Vesicular, Vesicular, Vesicular/Swollen, and Swollen – for cells in Stages 1 – 2. Cells were selected based upon GFP and TMRE florescent. Following preparation for electron microscopy, electron micrographs of each cell were collected and all of the mitochondria within a thin section of each cell were classified in a double-blind fashion. The number of cells / number of mitochondria analyzed are indicated at the top of each graph.

(a) Stage1 – Treatment with etoposide for 15 hrs; cells have not released Cyt. *c*-GFP and maintain $\Delta\Psi_m$.

(b) Stage 2 – treatment with etoposide for 15 hrs; cells have released Cyt. *c*-GFP but maintain $\Delta\Psi_m$. Transformation of vesicular mitochondria were found in this group.

(c) Stage 2 with caspases inhibited – treatment with etoposide for 15 hrs. in the presence of zVAD-fmk; cells have released Cyt. *c*-GFP but maintain $\Delta\Psi_m$.

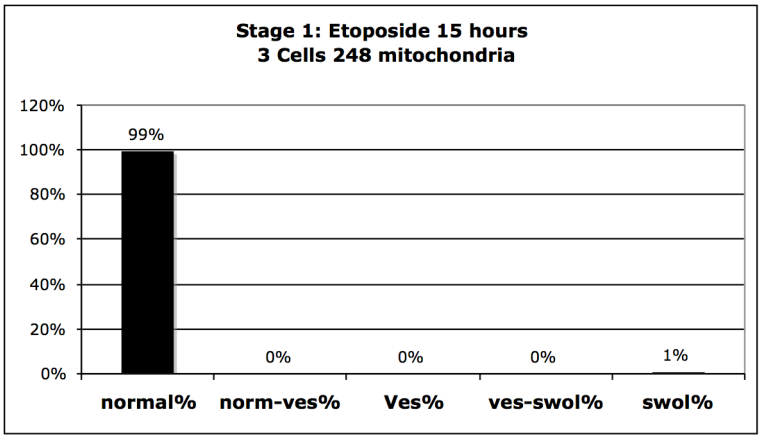

(a)

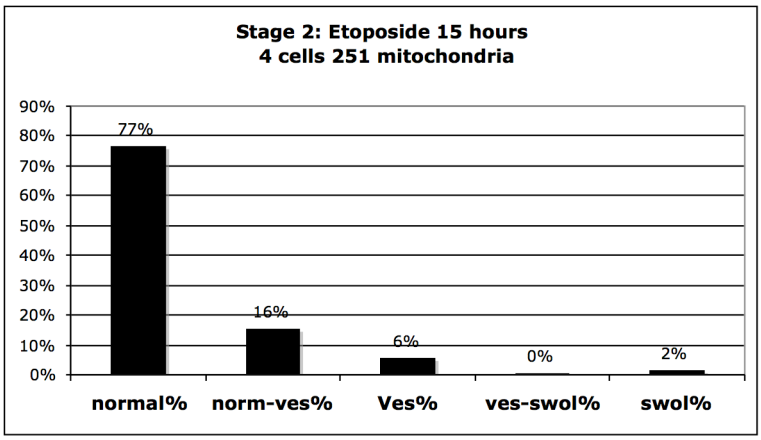

(b)

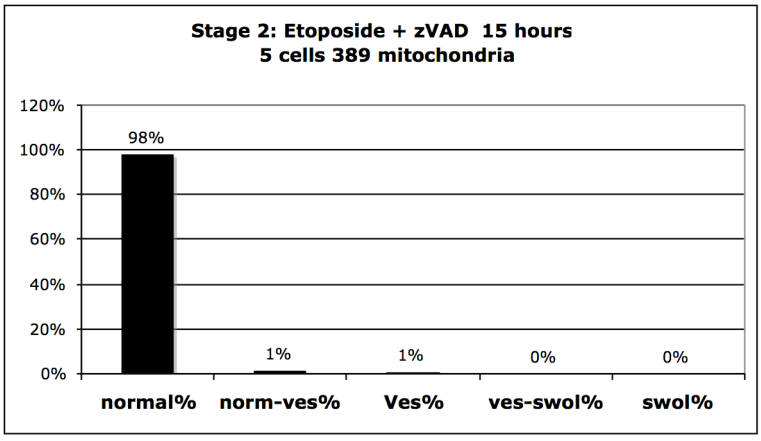

(c)

Supplementary Figure II.2

Supplementary Figure II.3: HeLa cells undergo transformation of vesicular mitochondria during Cyt. *c*-4CYS release upon Actinomycin D (Act D) induced apoptosis.

HeLa cells transfected with Cyt. *c*-4CYS were grown in Petri dishes with a glass coverslip containing an etched grid and then stained with TMRE to monitor $\Delta\Psi_m$. Apoptosis was initiated with 100 μM Act D.

(a) – (**b)** show respectively Cyt. *c*-4CYS in green, TMRE in red at the start of the experiment (before treatment).

(c) – (d) show the same field of cells 8 hrs. after addition of Act D. Diffuse green indicates Cyt.c-4CYS is released/releasing. Less bright red florescence indicates loss / or partial loss of $\Delta\Psi_m$.

(e) – (f) show the transmission light microscopy picture and the low magnification electron micrograph of the same field of cells after chemical fixation, dehydration, and embedding in plastic at 16 hrs.

(g) shows an example of the vesicular transformation of mitochondrion found in this group of cells. Scale bar is 500nm.

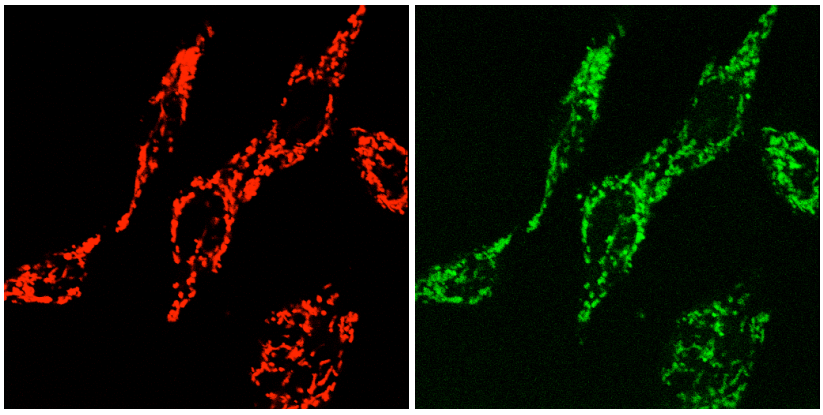

(a) (b)

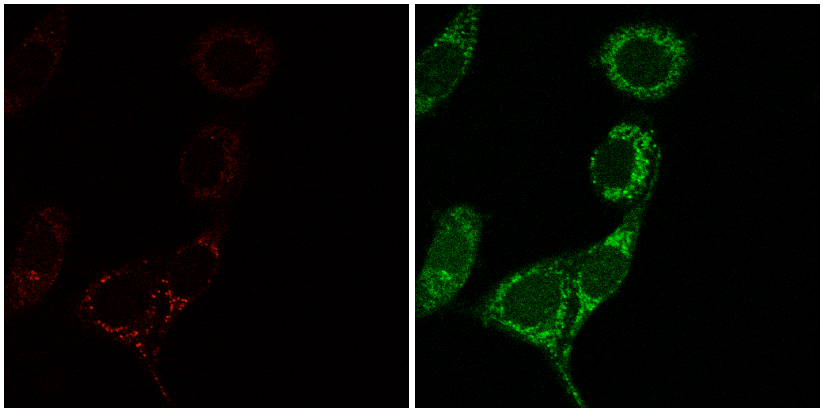

(c) (d)

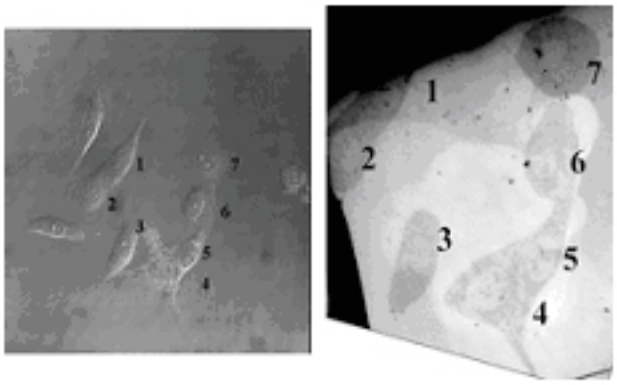

(e) (f)

Supplementary Figure II.3

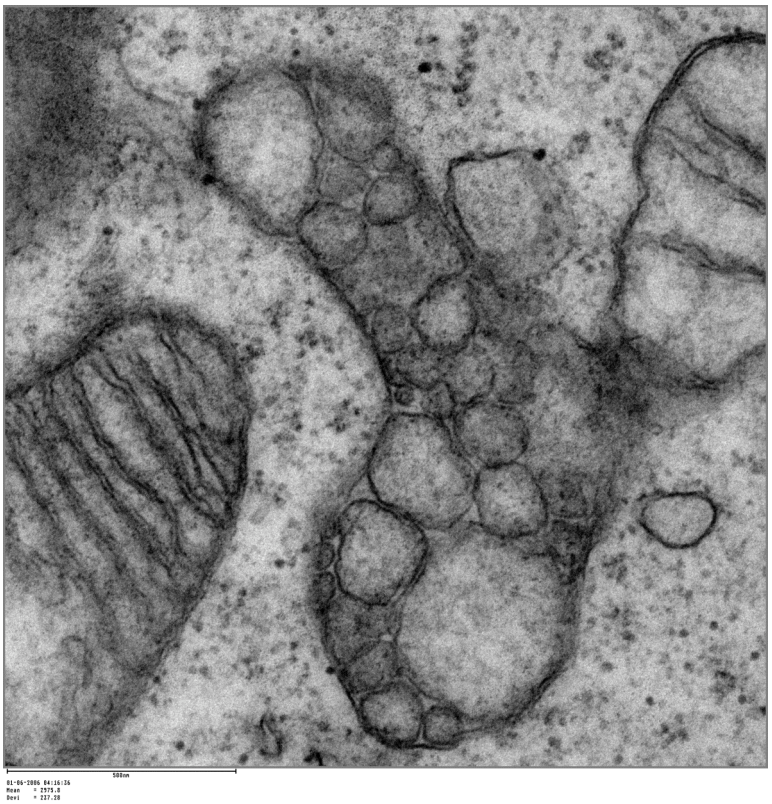

(g)

Supplementary Figure II.3 Continued

Supplementary Figure II.4: HeLa cells undergo transformation of vesicular mitochondria during Cyt. *c*-4CYS release upon Fas-Ligand induced apoptosis.

HeLa cells transfected with Cyt. *c*-4CYS were grown in Petri dishes with a glass coverslip containing an etched grid and then stained with TMRE to monitor $\Delta\Psi_m$. Apoptosis was initiated with 100 nM Fas L.

(a) show respectively Cyt. *c*-4CYS in green, TMRE in red after incubation with Fas L for 1 hour. Cyt.c-4CYS is not released from mitochondria which maintain $\Delta\Psi_m$. The low magnification of the electron microgram show these identical 4 cells. Scale bar is 10000nm.

(b) show respectively Cyt. *c*-4CYS in green, TMRE in red after incubation with Fas L for 2 hour. Cyt.c-4CYS is not released from mitochondria which still maintain $\Delta\Psi_m$. The low magnification of the electron microgram show these identical 8 cells. Scale bar is 20000nm.

(c) show respectively Cyt. *c*-4CYS in green, TMRE in red after incubation with Fas L for 3 hour. Cyt.c-4CYS is not released from mitochondria. Less TMRE staining indicates $\Delta\Psi_m$. loss. The low magnification of the electron microgram shows these identical 4 cells. Scale bar is 20000nm.

(d) Bar graphs show the percentages of mitochondria observed within each of the five morphologies – Normal, Normal/Vesicular, Vesicular, Vesicular/Swollen, and Swollen – for above cells after FasL treatment. The number of cells / number of mitochondria analyzed are indicated in the legend.

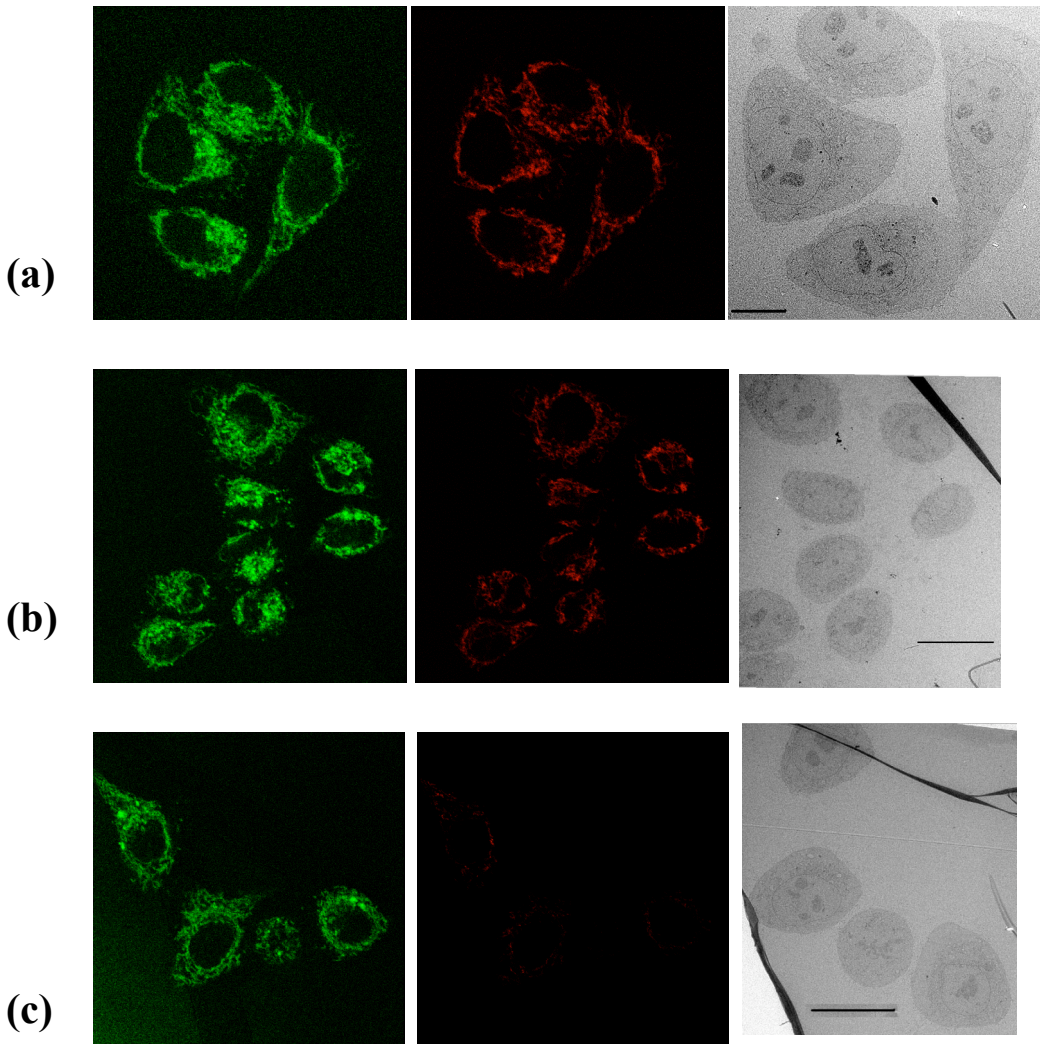

Supplementary Figure II.4

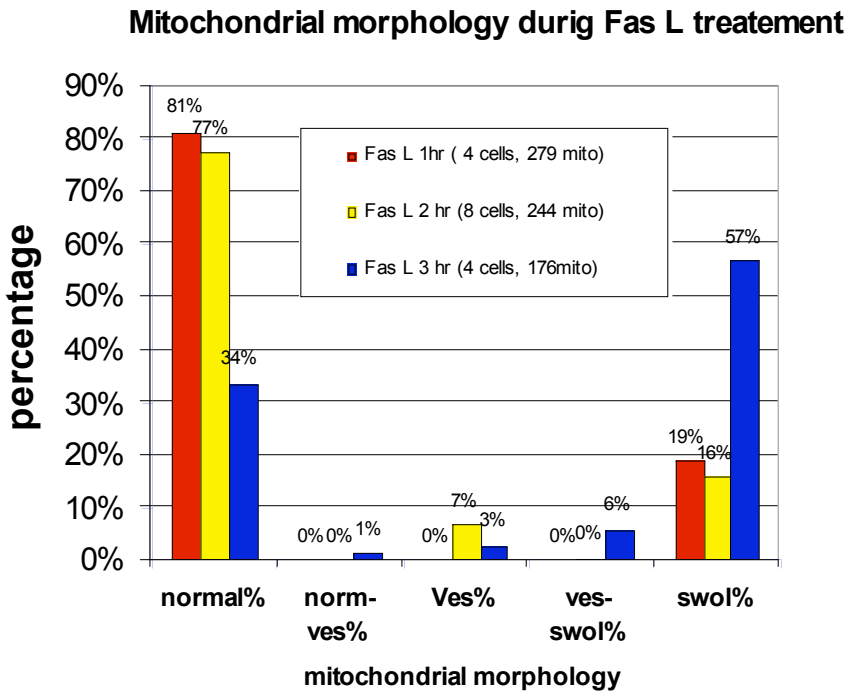

(d)

Supplementary Figure II.4 Continued

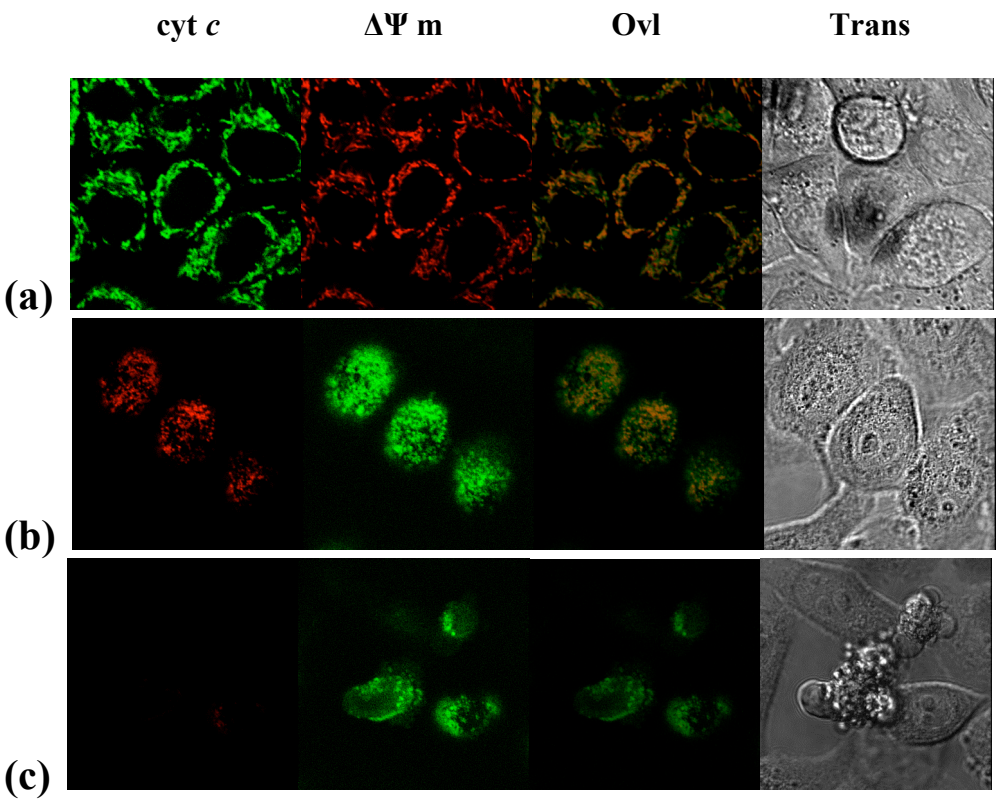

Supplementary Figure II.5. Release of cytochrome c occurs before the loss of $\Delta\Psi_m$ during etoposide induced apoptosis in HeLa cells with ATP sythases inhibitor oligomycin.

(a) Before treatment, HeLa cells expressing cyt *c*-4CYS (green) and mitochondria with $\Delta\Psi_m$ (red) co-localized as punctate yellow colors.

(b) Cells were treated with etoposide for 17 hours and oligomycin (10uM) for 1.5 hours. Confocal microscope detected that cytochrome c was released from mitochondria while mitochondria still maintained $\Delta\Psi_m$.

(c) Cells were treated with etoposide 18 hours and oligomycin (10μM) for 2.5 hours, mitochondria lost $\Delta\Psi_m$ were detected.

ACKNOWLEDGEMENTS

This work was done with the help of James Williams, Cristina Munoz-Pinedo, Guy Perkins, Joshua Brown, Mark Ellisman and Terrence Frey, who were also co-authors on the paper that was accepted for publication; Correlated Three-Dimensional Light and Electron Microscopy Reveals Extensive Transformation of the Mitochondrial Inner Membrane During Apoptosis. *Nature Cell Biology* 2007

This chapter in full, is a reprint of a manuscript as it was originally submitted to *Nature Cell Biology*. This manuscript was subsequently accepted for publication in a shortened version as a Letter. The dissertation author designed the experiments under the direction of Dr. Frey and carried out all experimental work with the assistance of the co-authors and then collaborated with Dr. Frey in writing the manuscript subsequently incorporating suggestions of the co-authors. This project was supported by Blasker Science and Technology Grant from the San Diego Foundation to TGF, by the NIH National Center for Research Resources Grant No. P41 RR004050 (GAP and MHE), by NIH Roadmap Grant GM72033 (to Roger Y. Tsien and MHE), and by NIH Grants AI40646, AI52735, and CA69381 (to DRG). C.M-P. was supported by the Secretaria de Estado de Universidades Investigacion and the Fondo de InvestigacionesSanitarias of Spain. We thank Ying Jones (NCMIR / UCSD) for assistance with high pressure freezing/freeze substitution and James Nulton for suggesting the mechanism of transformation mitochondria in Figure II.7.

III

Correlated Light and Electron Microscopy Reveals the Mechanisms of Cytochrome c Release During Apoptosis in Response to Hydrogen Peroxide.

ABSTRACT

Mitochondria initiate and/or regulate apoptosis through the release of cytochrome *c* and other proteins from the intermembrane and intracristal compartments. Two principal mechanisms have been proposed by which cytochrome *c* can cross the outer membrane: (1) the opening of the mitochondrial permeability transition pore (mPTP), producing large amplitude swelling of the mitochondrial matrix rupturing the outer membrane, or (2) the formation of a large pore in the outer membrane through which proteins can exit. We have studied this process in HeLa cells in which apoptosis was initiated by various agents using correlated light and electron microscopy to monitor the release of cytochrome *c* in cells transfected with fluorescent cytochrome *c* fusion proteins and stained with TMRE to monitor

mitochondrial membrane potential ($\Delta\Psi_m$). Calcein staining was used to monitor the opening of the mPTP. Previously we observed that apoptosis initiated by etoposide and actinomycin, induced a dramatic transformation of the mitochondrial inner membrane during the release of cytochrome *c* into a form in which the matrix was fragmented into individual vesicular matrix compartments. Although this transformation is not required for the release of cytochrome *c*, the swelling that occurred after the loss of $\Delta\Psi_m$ indicates that cytochorme *c* is released through an outer membrane pore prior to mitochondrial swelling. In this study, we used H_2O_2 to induce apoptosis in HeLa cells as a model for ischemia/reperfusion injury. Initiation of apoptosis by H_2O_2 results in immediate loss of $\Delta\Psi_m$, subsequent opening of the mPTP, and large amplitude swelling of the mitochondrial matrix that appears to be the cause of cytochrome *c* release. Cyclosporin A (CsA), an inhibitor of the mPTP, prevents the immediate loss of $\Delta\Psi_m$, but does not prevent the release of cytochrome *c*. Interestingly, CsA inhibits mitochondrial swelling and induces formation of the vesicular mitochondrial structure, suggesting the release of cytochrome *c* via the formation of an outer membrane pore when the mPTP is blocked. Thus, our results indicate that H_2O_2 can initiate either mechanism for cytochrome *c* release depending upon certain factors.

INTRODUCTION

The mitochondrion is a dynamic organelle comprised of two membranes, the inner boundary membrane (IM) and the outer membrane (OM). These two membranes define two compartments: the matrix, surrounded by the inner boundary membrane and the intermembrane and intracristal spaces, which are between the inner and outer membranes (Frey and Mannella 2000; Frey, Renken et al. 2002). Release of apoptotic signaling proteins such as cytochrome *c*, AIF, endo-G, smac, and Diablo from the intermembrane and intercristae spaces promotes cell death (Joza, Susin et al. 2001; Shiozaki and Shi 2004; Munoz-Pinedo, Guio-Carrion et al. 2006). Recent studies suggest that there are two principal mechanisms for cytochrome *c* release through mitochondrial outer membrane permeabilization (MOMP) (Kroemer, Galluzzi et al. 2007): (1) IM permeabilization caused by opening of the mitochondrial permeability transition pore (mPTP), a high conductance channel in the inner mitochondrial membrane, or by hyperpolarization of the mitochondrial inner membrane, followed by osmotic matrix swelling and consequent outer membrane rupture to release cytochorme *c*, and (2) OM permeabilization regulated by pro-apoptotic proteins (Bax, Bak, and Bid) of the BCl-2 family (Green and Kroemer 2004). Kuwana, *et al.* have demonstrated that oligomeric Bax can form pores large enough to release macromolecules in the context of appropriate mitochondrial lipids (Kuwana, Mackey et al. 2002). These channels are inhibited by Bcl-$_{XL}$ and do not require any IM constituents. Therefore they are independent of mPTP opening (Green and Kroemer 2004).

Using confocal microscopy, cells were identified at successive stages in the apoptotic program initiated by H_2O_2 in HeLa cells permanently transfected with fluorescent cytochrome *c* fusion proteins and stained with TMRE to monitor $\Delta\Psi_m$ (Loew 1996; Goldstein, Waterhouse et al. 2000; Goldstein, Munoz-Pinedo et al. 2005). Calcein staining was used to monitor mPTP opening (Petronilli, Miotto et al. 1999). These cells were grown in special Petri dishes that contain a glass coverslip with an etched grid (MatTek Corp. Ashland, MA). The grid allowed precise identification of a field of cells at defined stages of apoptosis. After preparing the cells by conventional methods of chemical fixation, the grid allowed us to find the same cells during sectioning for TEM.

The release of cytochrome *c* from HeLa cells during apoptosis has been shown to be initiated by various agents including etoposide, actinomycin-D, and Fas-ligand, and in these cases appears to proceed through large OM channels formed by the proapoptotic proteins Bax, Bak, and Bid. During and/or after the release of cytochrome *c*, the IM of some mitochondria transforms (remodels) from the normal conformtion with lamellar cristae connected to the inner boundary membrane via discrete tubular crista junctions into a vesicular form that fragments the matrix compartment. Mitochondrial swelling occurs later in the apoptosis program, after the release of cytochrome *c* and loss of $\Delta\Psi_m$. Inhibition of mPTP by Cyclosporine A (CsA) does not prevent release of cytochrome *c* nor prevent the formation of vesicular mitochondria, indicating that the transformation is mPTP independent. Notably, the inhibition of caspases by zVAD-fmk inhibits the formation of vesicular mitochondria,

but does not prevent the release of cytochrome *c*. Thus, inner membrane remodeling is not required for efficient release of cytochrome *c* from intracristal spaces, but may be related to inner membrane fission during mitochondrial fragmentation.

In this study, H_2O_2 was used to induce apoptosis in HeLa cells as a model for apoptosis induced by high concentrations of reactive oxygen species (ROS) as would occur during ischemia/reperfusion injury (Akao, O'Rourke et al. 2003). Initiation of apoptosis by H_2O_2 results in the immediate loss of $\Delta\Psi_m$, subsequent activation of mPTP, and large amplitude swelling of the mitochondrial matrix, which appears to be the cause of cytochrome *c* release. Therefore, different stimuli of apoptosis may be followed by different mechanisms for the release of cytochrome *c*. Cyclosporine A (CsA), an inhibitor of the mPTP in this system, prevents the immediate loss of $\Delta\Psi_m$ but does not prevent the release of cytochrome *c*. Interestingly, CsA inhibits early mitochondrial swelling and induces formation of the vesicular mitochondrial structure, suggesting the release of cytochrome *c* through a secondary mPTP independent mechanism. The results indicate that H_2O_2 can initiate either mechanism for cytochrome c release, depending upon certain factors conditions.

RESULTS

1. H_2O_2 causes $\Delta\Psi_m$ to drop immediately and induces mPTP opening and mitochondrial swelling. The mitochondrial matrix continues to swell until the outer membrane ruptures releasing cytochrome *c*.

Our first goal was to study the process of $\Delta\Psi_m$ change and determine whether mPTP opening is involved in H_2O_2 induced apoptosis. This is shown in Figure III.1a, in which HeLa cells permanently transfected with a 13.3 kD cytochrome *c* fusion protein containing a short tetracysteine motif (Cyt. *c*-4CYS) were stained with the membrane permeable biarsenical fluorophore, ReAsH (red) (Gaietta, Deerinck et al. 2002; Goldstein, Munoz-Pinedo et al. 2005) that binds to the 4CYS motif, with TMRE (displayed in yellow) to reveal mitochondria that maintain $\Delta\Psi_m$, and with calcein (green) to reveal the opening of mPTP. Figures III.1b were automatically recorded by confocal microscopy every four minutes after H_2O_2 was added. Mitochondrial loss of $\Delta\Psi_m$ was revealed by the disappearance of TMRE staining within the first 2 minutes, while the diffuse green calcein staining indicating opening of the mPTP became noticeable after 10 minutes. The interpretation of the sudden drop of $\Delta\Psi_m$ (Figure III.1b) is termed as "ROS-induced ROS release" (RIRR) by Zorov et al., which is caused by a local high ROS concentration and results in mitochondrial depolarization followed by mitochondrial ROS production and activation of the mPTP opening (Zorov, Filburn et al. 2000; Brady, Elmore et al. 2004). Note that this mitochondrial depolarization is reversible if the mPTP opening is temporary. The permanent loss of mitochondrial membrane potential is due to the persistent opening of mPTP (Huser

and Blatter 1999; Weiss, Korge et al. 2003). Our research confirms Akao's report of the abrupt loss of $\Delta\Psi_m$ being mediated by mPTP opening (Akao, Teshima et al. 2002). Figure III.1b also shows that cytochorme *c* wasn't released within the first 34 minutes, illustrated by the persistence of punctate red ReAsH staining. Thus, $\Delta\Psi_m$ loss and mPTP opening occurred prior to cytochrome *c* release.

Based on the knowledge that H_2O_2 induced apoptosis is dose dependent (Tang, Feng et al. 2005), we incubated our cells with different H_2O_2 concentrations. Resulting data confirms Tang et al's report that low doses of H_2O_2 (5 to 20 μM) protects cells against apoptosis, moderate doses (30 μ) have no effect, and higher doses (above 50 μM) induce apoptosis Figure III.1c shows mitochondrial swelling with three different concentrations starting from the minimum lethal dose of 50 μM. From our observation, cell death was not detectable under 25 μM H_2O_2 treatment for over 24 hours.

Cells treated with different H_2O_2 incubation times (from 2 to 32 minutes) were fixed and observed by TEM. Figure III.1d shows morphology analysis of the electron micrographs, with gradual mitochondrial swelling occurring with the opening of mPTP indicated by the gradual release of calcein from mitochondria into the cytosol. This result is consistent with many reports that the opening of mPTP causes mitochondrial matrix swelling (Kroemer, Galluzzi et al. 2007). Because the surface area of the mitochondrial inner membrane exceeds that of the outer membrane, extensive matrix swelling with persistent mPTP opening can lead to the unfolding of

cristae, causing the outer membrane to rupture irreversibly damaging mitochondria (Weiss, Korge et al. 2003).

Since the drop of $\Delta\Psi_m$ happens immediately after H_2O_2 treatment and is followed quickly by the opening of the mPTP, we observed the changes in fluorescence in HeLa cells expressing Cyt. *c*-4CYS labeled with ReAsH , TMRE and Calcein, and have separated the H_2O_2 initiated apoptosis program into 2 different stages based on whether cytochorme *c* is released. We then studied the ultrastructure of the mitochondria within representative cells in these 2 stages by TEM of the identical cells that were characterized by fluorescence confocal microscopy. Figure III.2 shows fluorescent light and transmission electron micrographs of different fields of cells at each stage of the apoptotic program:

Pre-cytochrome *c* release stage—Figure III.2a contains a field of cells treated with 200 μM H_2O_2 for 2 minutes; this is prior to the release of cytochrome *c* but follows loss of $\Delta\Psi_m$ with an open mPTP. These events were indicated by the punctate Cyt.c-4CYS-ReAsH staining localized to mitochondria, the loss of the TMRE staining correlated with loss of $\Delta\Psi_m$, and the diffused calcein staining in the cytosol respectively. The low magnification electron micrograph of this field of cells is shown in the insert at the lower left. At higher magnification, the electron micrograph reveals a number of mitochondria that have begun to swell (noted by the arrow) while others have the morphology of the normal orthodox mitochondria typically found in healthy cells. Swollen mitochondria are identified by their expanded matrix space, fewer cristae, and less dense staining of the matrix.

Post-cytochrome *c* release stage—in Figure III.2b, the Cyt.*c*-4CYS-ReAsH staining is diffuse indicating that cytochrome *c* has been released, while the TMRE staining is gone indicating non-recovery of $\Delta\Psi_m$ loss. Diffuse calcein staining indicates opening of the mPTP. The high magnification electron micrograph contains only swollen mitochondria and also several mitochondria with ruptured outer membranes (noted by the arrow). This data suggests the release of cytochorme *c* and other inter-membrane space proteins by a passive mechanism through the rupturing of the OM. Thus, mPTP dependent mitochondrial swelling appears to be the direct cause of the OM rupture and cytochrome *c* release.

2. Inhibition of mPTP opening inhibits the immediate loss of $\Delta\Psi_m$, but doesn't inhibit cytochrome *c* release. When mPTP opening is inhibited, cytochrome *c* may be released through OM pores, which is an mPTP independent mechanism.

The next step was to determine the involvement of mPTP in cell death by using the immunosuppressive cyclic oligopeptide, Cyclosporin A (CsA), which is a specific inhibitor of the mPTP (Bernardi, Broekemeier et al. 1994). As expected, CsA treatment inhibited the mPTP, as it prevented the release of Calcein trapped within the mitochondria (Figure III.5) (Petronilli, Miotto et al. 1999). An obvious question is whether the inhibition of mPTP with CysA would affect the apoptosis program we observed upon treatment of H_2O_2 in the absence of CysA. To examine a large populations of cells, we measured the $\Delta\Psi_m$ by TMRE intensity using flow cytometry with the results shown in Figure III.3A. The TMRE intensity indicates a loss of $\Delta\Psi_m$.

Carbonylcyanide *p*-(trifluoromethoxy) phenylhydrazone (FCCP) is a mitochondrial uncoupler that induces immediate and complete dissipation of $\Delta\Psi_m$. Due to the loss of $\Delta\Psi_m$, cells treated with FCCP show significant decrease in TMRE florescence intensity. H_2O_2 treated cells lost TMRE intensity indicating a loss of $\Delta\Psi_m$, but in a less robust way compared to FCCP treated cells. CsA pre-treatment protected the cells from loss of $\Delta\Psi_m$ following treatment with H_2O_2, resulting in higher TMRE intensity. This result clearly indicates that inhibition of mPTP prevents $\Delta\Psi_m$ loss. Cell images by confocal microscopy are shown in Figure III.3b. HeLa cells expressing Cyt.*c*-4CYS were stained with FlAsH (green) to reveal the distribution of Cyt.*c*-4CYS, and with TMRE (red) to reveal mitochondria that maintain $\Delta\Psi_m$. In the control group (no treatment), cells contained cytochrome *c* within mitochondria and maintained $\Delta\Psi_m$ as indicated by the punctate FlAsH and TMRE staining. The H_2O_2 treated group shows the diffuse FlAsH staining, indicating that cytochrome *c* was released, and the complete absence of TMRE staining indicates that all of the mitochondria have lost $\Delta\Psi_m$. In the CysA pre-treated group, after the H_2O_2 treatment, the FlAsH staining is diffuse, indicating that cytochrome *c* has been released while the TMRE staining remains punctate although reduced in intensity, indicating the presence of $\Delta\Psi_m$. Our results suggest that there may be an mPTP independent mechanism that exists in the same system simultaneously to facilitate cytochorme *c* release.

In order to determine the possible mechanism involved, numerous electron micrographs of cells in different treatment groups as determined by fluorescence

confocal microscopy were recorded, , and scored with the numbers of mitochondrial profiles within the mitochondrial morphologies identified in Chapter II—normal, normal/vesicular, vesicular, vesicular/swollen, and swollen. The results are displayed graphically in Figure III.4, including the number of cells and the total number of mitochondria scored in each case. As expected, control cells that have not been treated with H_2O_2 display only normal mitochondrial profiles with a very small number of swollen mitochondria that may result from the specimen preparation procedure (Figure III.4a). Cells treated with H_2O_2 that have released cytochrome *c* display 87% swollen mitochondrial profiles (Figure III-4b). When pre-treated with zVAD-fmk, a general caspase inhibitor, cytochrome *c* release is not prevented, nor is mitochondrial swelling after H_2O_2 treatment, which confirms our previous observation that cytochrome *c* release is caspase independent (Figure III.4c). When pre-treated with CsA, there is a large increase in normal mitochondrial profiles (up to 46%) and a number that exhibit vesicular morphology with a total of 22% falling into the normal/vesicular, vesicular, or vesicular/swollen morphologies when cytochorme *c* is released (Figure III.4d). This vesicular morphology is a dramatic transformation of the mitochondrial inner membrane during the release of cytochrome *c* into a form in which the matrix becomes fragmented into individual vesicular compartments. This same morphology was found in the etoposide treated apoptotic cells in our previous study described in Chapter II that supported the outer membrane pore mechanism for cytochrome *c* release. When the mPTP inhibited by CsA, the same observation of a significant number of vesicular mitochondria suggests that H_2O_2 may induce

cytochrome *c* release through the formation of a large pore in the outer membrane that probably involves the proapoptotic proteins, Bax, Bak, and Bid (references, perhaps Kuwana et al). This might result from DNA fragmentation caused by H_2O_2 activating the p53 pathway as is the case with etoposide treatment(Datta, Babbar et al. 2002; Karpinich, Tafani et al. 2002). Since zVAD, a general caspase inhibitor, inhibited transformation to the vesicular form in etoposide treated cells as described in Chapter II, we investigated the results of inhibiting caspases with zVAD and the mPTP with CsA, hypothesizing that the results would resembles those with zVAD alone in the etoposide apoptosis model. As expected, H_2O_2 treated cells protected by zVAD and CysA together inhibit the vesicular and swollen mitochondrial morphology but did not inhibit cytochrome *c* release as shown in Figure III.4e.

DISCUSSION

Abundant evidence confirms the hypothesis that cytochrome *c* can be released from the mitochondria via both mPTP dependent and mPTP independent mechanisms (Newmeyer and Ferguson-Miller 2003), (Green and Kroemer 2004). Are they functionally coordinated, or distinct processes? mPTP dependent swelling of mitochondria, followed by outer membrane rupture causing the release of apoptogenic proteins has been observed in response to instances such as toxic hepatic injury and ischemia damage in the brain and heart. However, whether this is the primary mechanism is still under debate (Forte and Bernardi 2006). Many believe mPTP opening is a consequence of apoptosis and this channel is thought to play a role in principally necrosis, not apoptosis; but others support mPTP opening as a critical event in the process of apoptosis (Lemasters, Nieminen et al. 1998; Garrido, Galluzzi et al. 2006; Kinnally and Antonsson 2007). This debate results largely from to lack of adequate methods to probe mPTP activity directly in intact cells. The evidence for its occurrence *in vivo* is largely based on either indirect methods, such as measurements of mitochondrial depolarization, or on pharmacological tools, such as the effects of *in vitro* pore inducers or inhibitors such as CsA (Bernardi, Scorrano et al. 1999).

We have been able to test the involvement of mPTP during cytochorme *c* release by observing and characterizing mitochondrial structure using correlated light and transmission electron microscopy (TEM) at different stages of apoptosis. The swelling of mitochondria that would reflect persistent opening of mPTP is directly testable by TEM. Chapter II reports our previous study of etoposide induced

apoptosis. In that case during or after cytochrome c release, a novel vesicular mitochondrial morphology was found, indicating an inner membrane remodeling. CsA did not inhibit this transformation nor did it inhibit cytochorme *c* release without mitochondrial swelling. Thus, we believe that the vesicular morphology accompanies an mPTP independent mechanism for cytochorme *c* release during etoposide induced apoptosis.

Since apoptosis can be induced by different treatments through different pathways, we tested the H_2O_2 initiated apoptosis system. Contrary to our previous finding that cytochrome *c* release occurs before $\Delta\Psi_m$ loss, $\Delta\Psi_m$ dropped quickly after H_2O_2 treatment. $\Delta\Psi_m$ loss and mPTP opening occurred prior to cytochorme *c* release in this system (Figure III.1). We next studied mitochondrial structure by thin section (80 nm) using TEM. Figure III.2 shows that mitochondrial swelling occurs in a faster and irreversible manner that leads to OM rupture. Our observations suggest that an mPTP dependant mechanism to induce mitochondrial swelling and passive release of mitochondrial proteins by OM rupture may be involved in this system. In order to test this hypothesis, we used CsA to inhibit the opening of mPTP. Our data show inhibition of mPTP only inhibits the immediate drop of $\Delta\Psi_m$, but it doesn't inhibit cytochrome *c* release. Quantitation of mitochondrial morphology by TEM shows a large increase in normal mitochondrial profiles in the CysA protected group as well as a significant number of vesicular mitochondria indicating that a secondary mPTP independent mechanism takes place. This result may explain the observation that the inhibition of mPTP significantly delays mitochondrial swelling but does not inhibit

cytochorme *c* release and cell death in an mPTP dependent manner, such as Ca^{2+} overload and response to ROS (Broekemeier and Pfeiffer 1989; Bernardi, Krauskopf et al. 2006). Note that the mPTP independent apoptosis regulated by Bcl-2 family proteins was not inhibited by CsA (Baines, Kaiser et al. 2005).

Here, we propose that H_2O_2 initiates both the following two mechanisms for cytochorme *c* release, depending upon certain factors and suggest these two mechanisms could be functionally coordinated: **(1) The primary mechanism:** High local ROS induces mitochondrial depolarization, followed by mPTP opening, mitochondrial matrix swelling, and the rupturing of the outer membrane. **(2) The secondary mechanism:** The formation of a large pore in the outer membrane through which proteins can exit. During or after the release of cytochrome *c*, a transformation of the mitochondrial inner membrane was found to a form in which the matrix was fragmented into individual vesicular matrix compartments. This mechanism appears to be the same as that in etoposide induced cell death and may result from a similar cause, DNA fragmentation by H_2O_2.

In summary, mitochondrial swelling occurs in different stages under different mechanisms. In the mPTP dependant mechanism, it occurs early in the program and is the immediate cause of cell death, while in the mPTP independent mechanism, it occurs later and is the consequence of cell death.

METHODS

1. Culture conditions and the induction of apoptosis

HeLa cells expressing cytochrome *c*-4CYS were grown and maintained at 37° C in Dulbecco's modified Eagles's medium (DMEM, Gibco) supplemented with 10% FBS, 2mM L-glutamine, 200 mg/ml penicillin, and 100 mg/ml streptomycin sulfate in a humidified atmosphere of 5% CO_2/95% air. Cells were subcultured 1:10 by incubating them in 0.25% trypsin (Gibco) when they were confluent and re-suspending cells in growth medium.

Apoptosis was induced with H_2O_2 at different concentrations and incubation times: 200μM H_2O_2 for 2min to 1.5 hour; 100 μM H_2O_2 for 4 hours; 50μM H_2O_2 for 8 hours. When indicated zVAD-fmk (100 μM, Sigma) was added hours before the apoptotic stimulus to inhibit caspase activity. TMRE (50 nM, Sigma) was added to monitor the $\Delta\Psi_m$, and when indicated Cyclosporin A (CsA, 0.1 μM, Sigma) was used to inhibit opening of the mitochondrial transition pore (mPTP).

2.Cytochrome *c* labeling with biarsenical ligands

The staining media were prepared by the addition of a premixed DMSO stock solution to give a final concentration of 2.5 μM of FlAsH (or ReAsh)-1,2-ethanedithiol $(EDT)_2$ and 10 μM EDT (Fluka) in DMEM. Cells were incubated at 37° C in an incubator for 1 hour and were then rinsed in glucose-containing Hanks' buffered saline solution (HBSS, Gibco) and incubated for 10 min at room temperature

in HBSS containing 62.5 μM EDT. Cells were washed three times with HBSS and returned to the incubator for at least 12 hours before treatment.

3.Confocal microscopy

For time-lapse analysis, cells were grown in 35 mm microwell dishes containing a glass coverslip with an etched grid (MatTek Corp. Ashland, MA). Images were acquired using a Leica TCS SP2 inverted confocal microscope. FlAsH and Calcein were excited using the 488nm line from an Ar/Kr laser attenuated to 35%. TMRE was excited using the 543nm line from an Ar/Kr laser attenuated to 34%. ReAsh was excited using the 633nm line from an Ar/HeNe laser. The detector slits of the confocal microscope were adjusted to detect FlAsH emission between 497-553 nm, ReAsh emission between 647-706 nm, TMRE emission between 555-620 nm and Calcein emission between 497-553 nm.

4.Single cell analysis of mitochondrial structure by correlated confocal and electron microscopy.

By growing HeLa cells in special Petri dishes containing an etched grid (MatTek Corp. Ashland, MA), we can monitor cytochrome *c* release and $\Delta\Psi_m$ simultaneously by confocal microscopy and subsequently fix and embed the identical cells for examination by electron microscopy and by electron tomography. After confocal imaging, cells were fixed immediately by an 1 hour incubation on ice in a 2.5% paraformaldehyde – 2.5% glutaraldehyde – 0.1 M sodium cacodylate pH 7.4

buffer. After washing three times in ice-cold 0.1 M sodium cacodylate buffer containing 3 μM calcium chloride for 3 minutes, the primary fixed cells were then incubated with 1% osmium tetroxide – 0.8% potassium ferrocyanide – 3 μM calcium chloride in 0.1 M sodium cacodylate for 60 minutes on ice. After washing with distilled water 3 times for 3 minutes, fixed cells were stained and stabilized in ice-cold 2% uranyl acetate for 30 min on ice and dehydrated in an ice-cold ethanol series of 20, 50, 70, 90% successively on ice for 3minutes each. The cells were then dehydrated at room temperature 3 times for 3 minutes each in 100% ethanol and infiltrated in well-mixed 50% ethanol, 50% Durcupan ACM resin (Fluka) for 60 minutes with agitation at room temperature followed by 100% Durcupan ACM twice for 1 hour with agitation after which the samples were placed in an oven and allowed to polymerize at 60-80° C for at least 48 hours. The glass coverslip was peeled away from the bottom using a razor blade and the selected area was cut out and glued to a block for sectioning. Thin sections (approximately 80nm) were collected and pre-stained with 2% uranyl acetate and Sato lead before examination in an FEI Tecnai 12 TEM

FIGURES & LEGEND

Figure III.1: 200 µM H_2O_2 causes $\Delta\Psi_m$ drop, induces mPTP opening and mitochondrial swelling

HeLa cells transfected with Cyt. *c*-4CYS were grown in Petri dishes with a glass coverslip containing an etched grid and then stained with ReAsH and TMRE. Apoptosis was initiated with 200 µM H_2O_2.

(a) Respectively ReAsh (Cyt. *c*-4CYS) in red, TMRE (ΔΨm) in yellow, Calcein (mPTP indicator) in green at the start of the experiment

(b) Confocal images of the same field of cells recorded every 4 minutes following treatment with 200 µM H_2O_2.

(c) Morphology Analysis by TEM shows mitochondrial swelling was induced by different concentrations of H_2O_2 treatment.

(d) Morphology Analysis by TEM shows mitochondrial swelling occurs during H_2O_2 treatment that coincided with the opening of the mPTP.

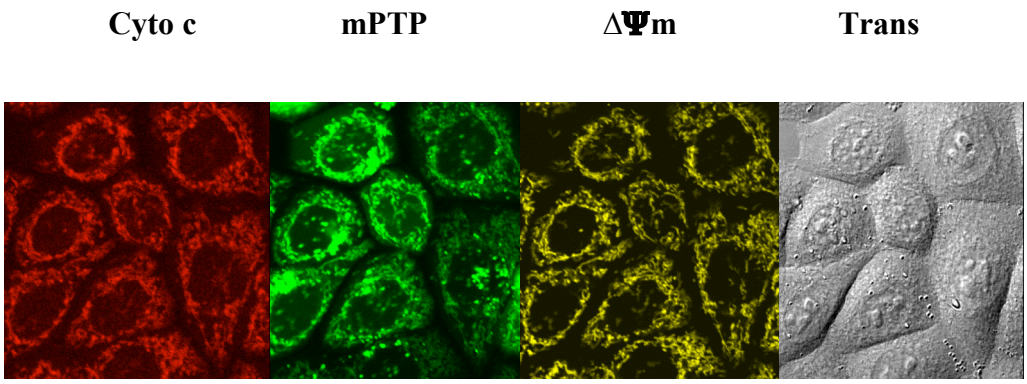

Figure III.1.a

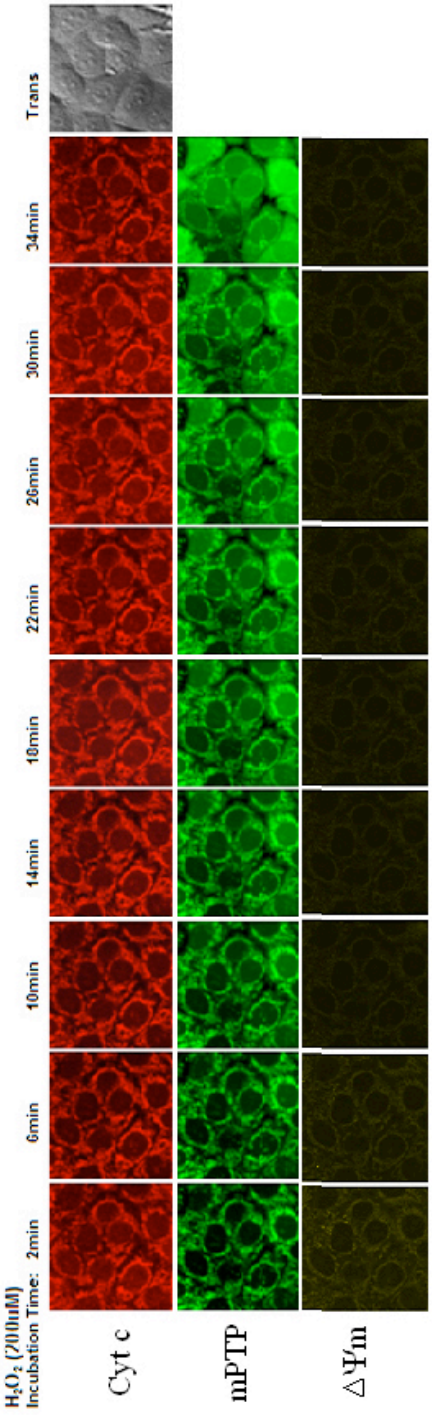

Figure III.1.b Continued

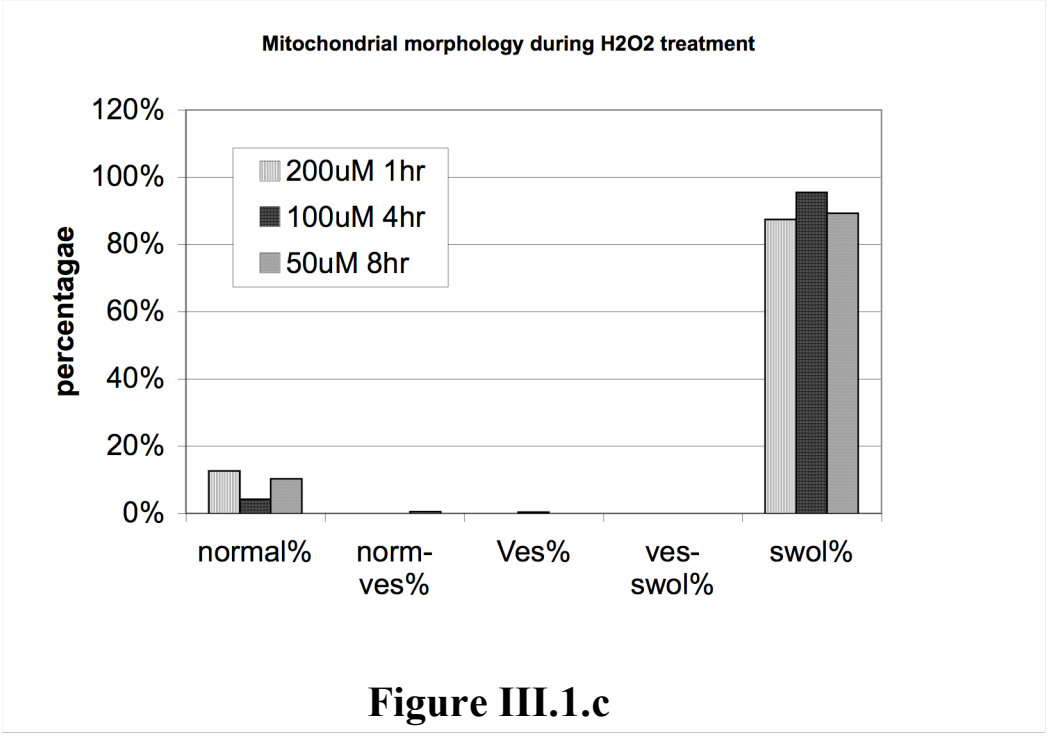

Figure III.1.c

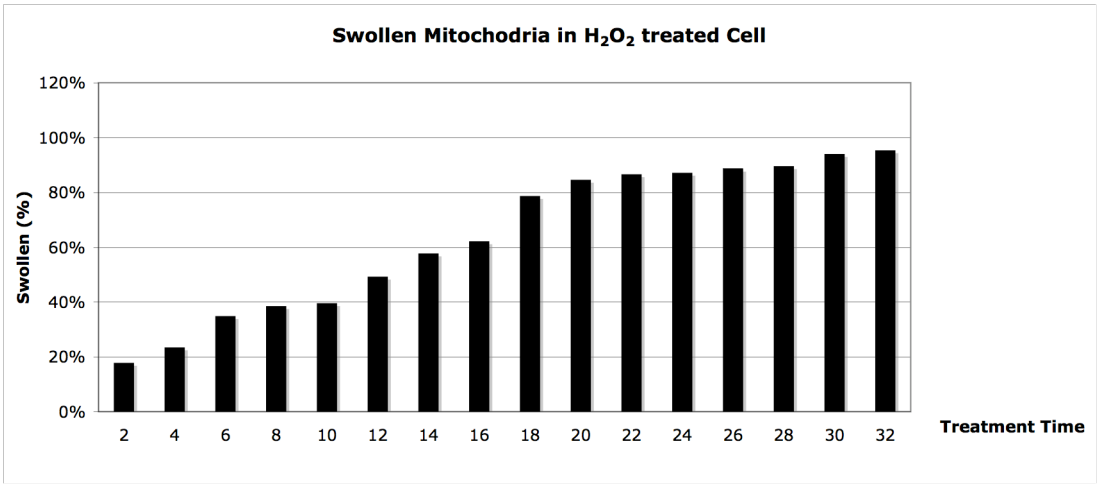

Figure III.1.d

Figure III.1 Continued

Figure III.2: H_2O_2 induces mitochondrial matrix swelling and outer membraneru rupture releasing cytochrome c

.

HeLa cells transfected with Cyt. *c*-4CYS and stained with ReAsH to monitor Cyt. *c*-4CYS (red), TMRE to monitor $\Delta\Psi_m$ (yellow), and Calcein-AM to monotor mPTP opening (green) were selected by confocal microscopy before preparation for TEM of the same fields of cells.

(a) Group treated with 200μM H_2O_2 for 2 min, have lost $\Delta\Psi_m$, have opened mPTP, but have not released Cyt. *c*. The TEM shows some partially swollen mitochondria (arrows) as well as many normal mitochondria. The arrows point to the swollen mitochondria that have expanded matrix space, few cristae and less dense staining of the matrix ; the inset at lower left is a low magnification image of the complete field of 3 cells. Scale bar is 1000nm

(b) Group treated with 200μM H_2O_2 for 1.5 hours, have released Cyt. *c*. These cells display only swollen mitochondria in TEM, and some circular vacuoles (arrows) that we believe are the inner membrane protrusions that ruptured outer membranes in grossly swollen mitochondria. The inset at lower left shows a low magnification image of this field of 3 cells.Scale bars is 1000nm.

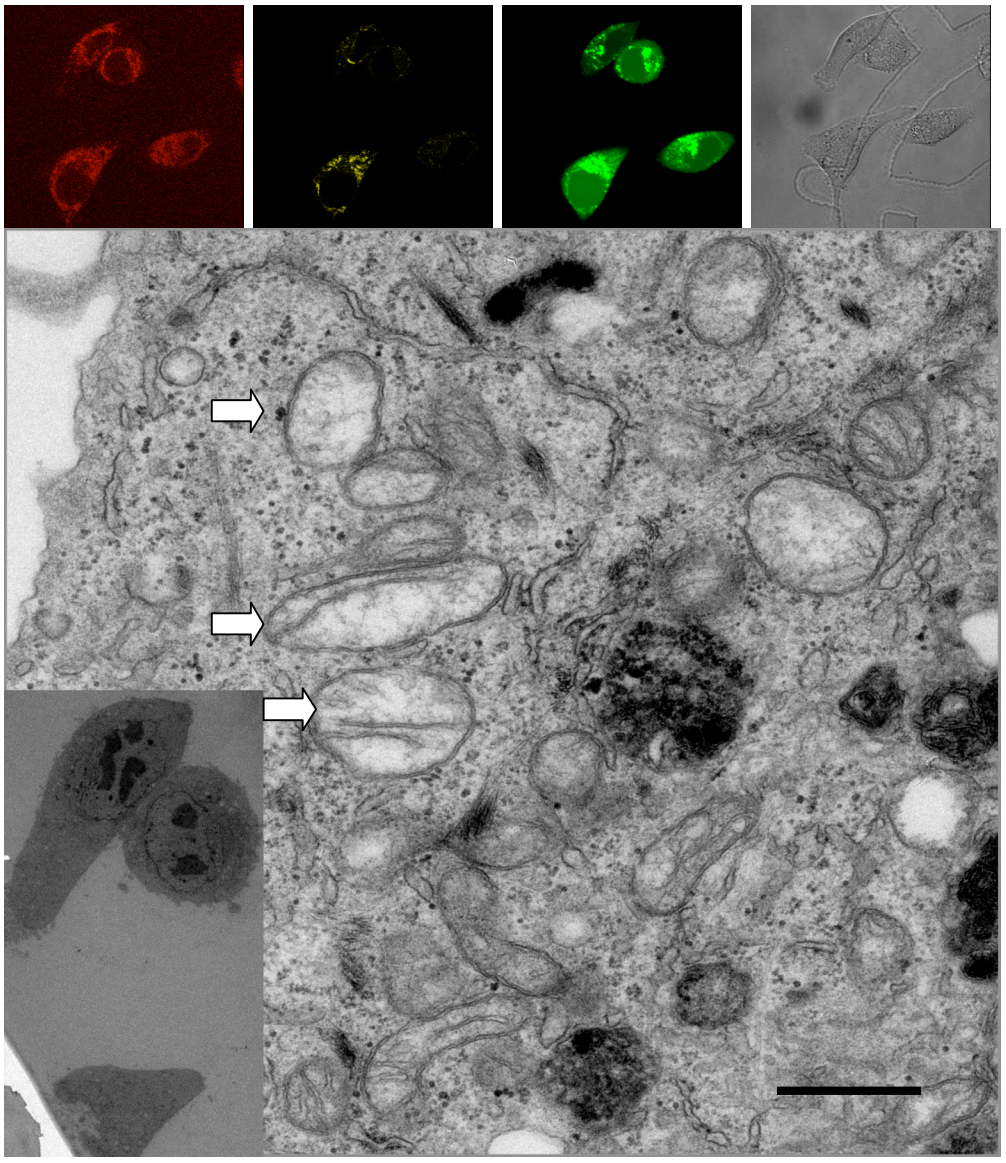

Figure III.2.a

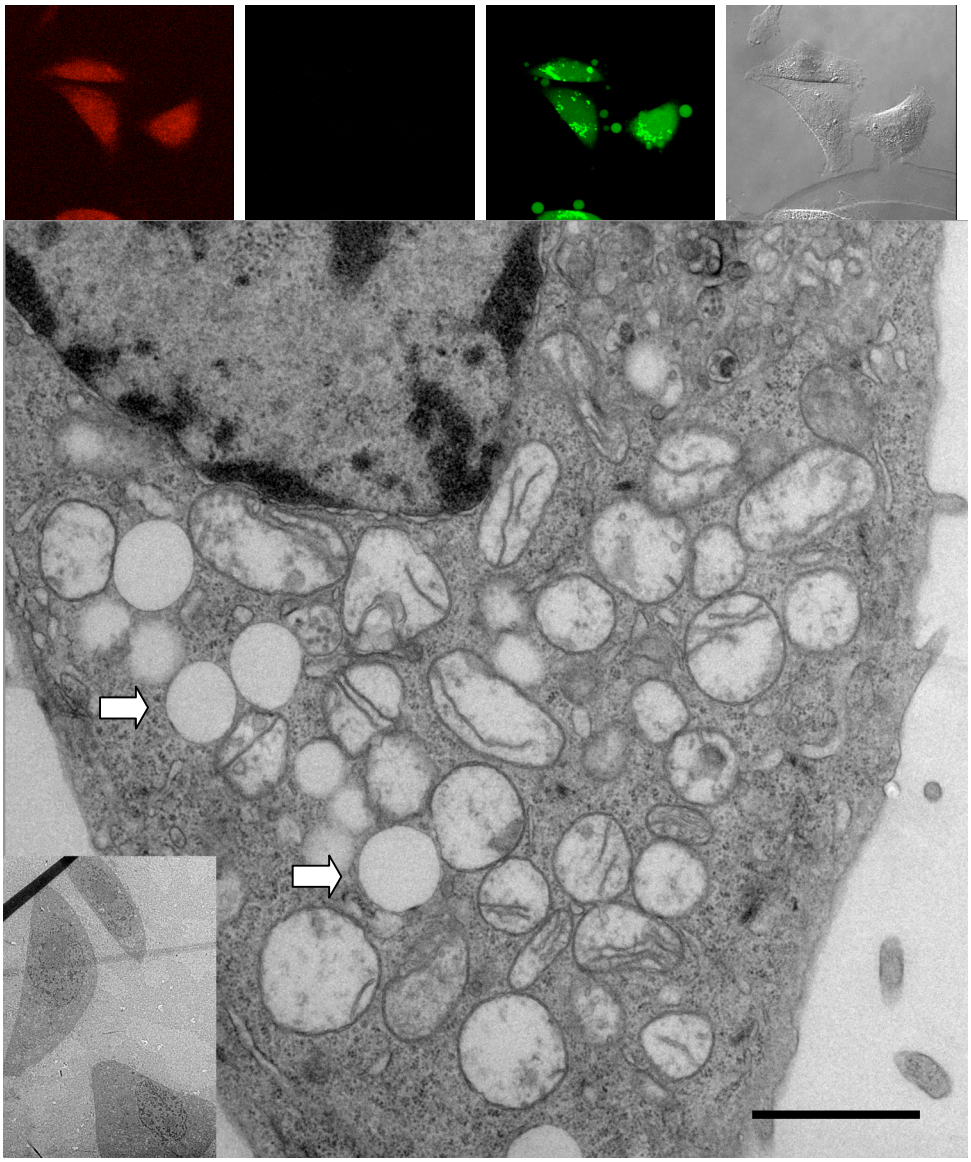

Figure III.2.b Continued

Figure III.3: CsA inhibiting mPTP prevents immediate loss of $\Delta\Psi_m$, but it doesn't prevent cytochrome *c* release.

(a) Flow cytometry analysis of TMRE fluorescence to monitor $\Delta\Psi_m$ changes following treatment with 200 μM H_2O_2 for 1 hr. A sample with no TMRE staining is used as the "**No Label"** control. All other samples were stained with 50nM TMRE. Untreated and FCCP treated cells are used as positive and negative controls respectively. Cyclosporine A (CsA), an mPTP inhibitor, inhibited $\Delta\Psi_m$ loss.

(b) Confocal images show CsA could not inhibit cytochrome *c* release in cells incubated with 200 μM H_2O_2 for 1hour. Cells were stained with FlAsH (green) to show distribution of Cyt.*c*-4CYS and with TMRE (red) to show mitochondria with $\Delta\Psi_m$.

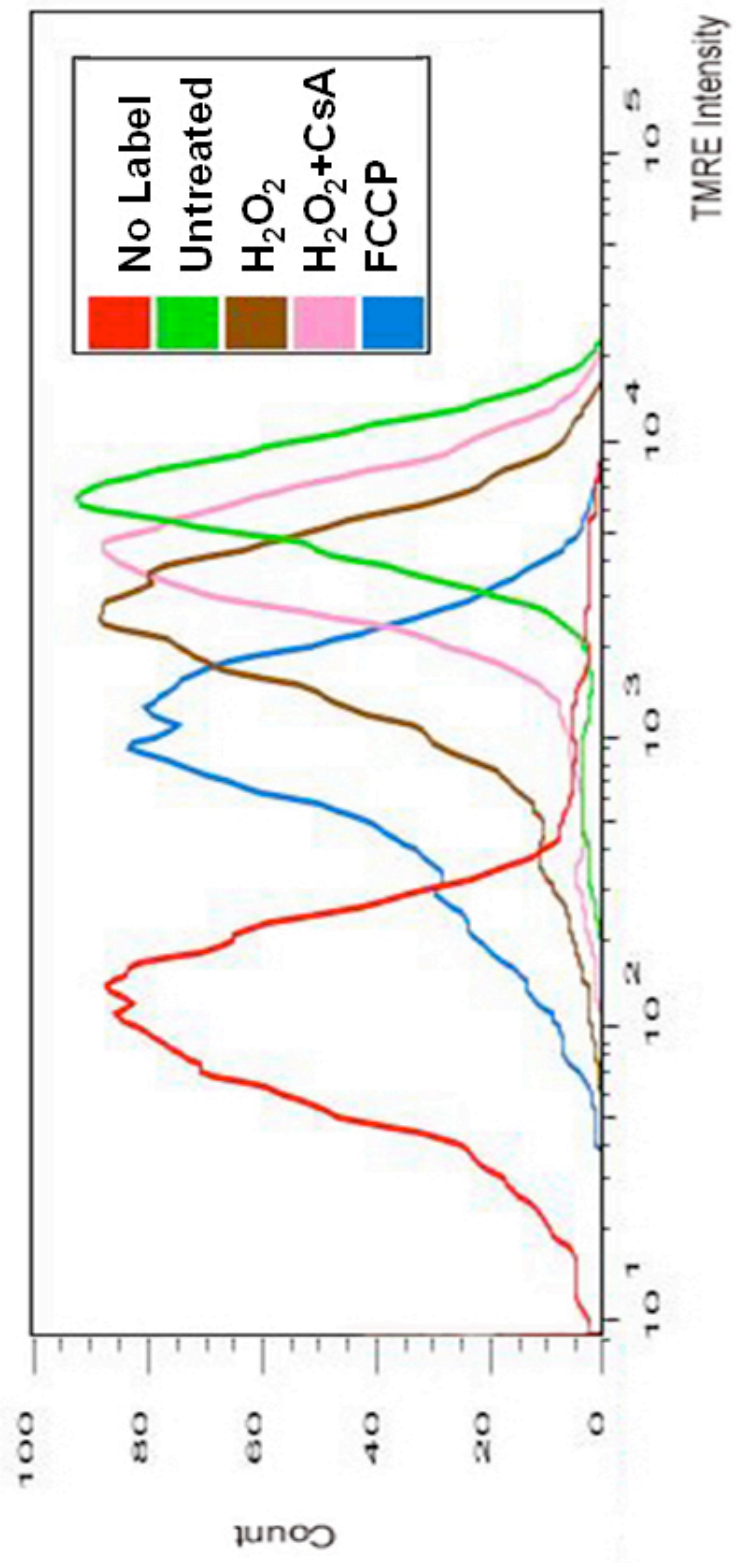

Figure III.3.a

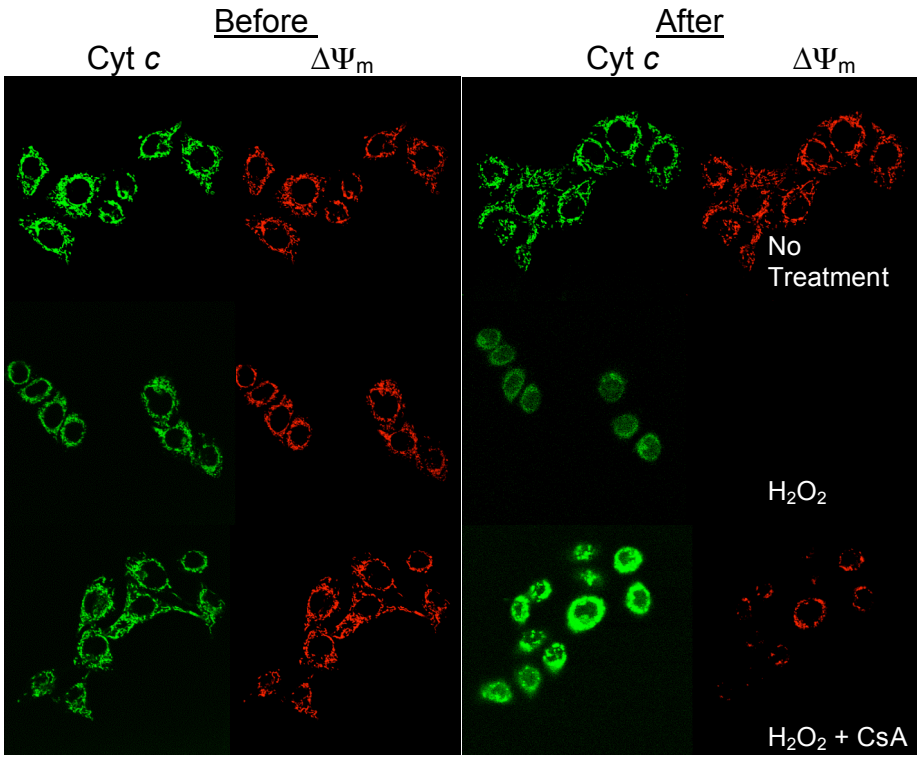

Figure III.3.b Continued

Figure III.4: Morphology Analysis reveals that two mechanisms for cytochrome c release exist in the same cell.

Bar graphs show the percentages of mitochondria observed within each of the five morphologies – Normal, Normal/Vesicular, Vesicular, Vesicular/Swollen, and Swollen – for cells under different treatments. Cells were selected based upon FlAsH and TMRE staining of HeLa cells transfected with Cyt. *c*-4CYS (see Fig. 2 for examples). Following preparation for electron microscopy, electron micrographs of each cell were collected and all of the mitochondria within a thin section of each cell were classified in a double-blind fashion. Cell death was induced by 200μM H_2O_2 treatment for 1 hour. The number of cells / number of mitochondria analyzed are indicated at the top of each graph.

(a) Control cells show normal mitochondrial morphology.

(b) mitochondria swell during H_2O_2 induced cell death.

(c) zVAD, a general caspase inhibitor, didn't prevent mitochondrial swelling.

(d) Cyclosporin A (CsA), an mPTP inhibitor, inhibited mitochondrial swelling, but induced formation of vesicular mitochondrial structure which indicates an outer membrane pore mechanism for cytochorme *c* release.

(e) zVAD and CsA together prevented mitochondrial swelling and inhibited transformation to the mitochondrial vesicular structure, but did not prevent release of cytochrome *c*.

(f) Vesicular mitochondrial structure is found in CsA treated cells following addition of 200μM H_2O_2. Scale bar is 100nm.

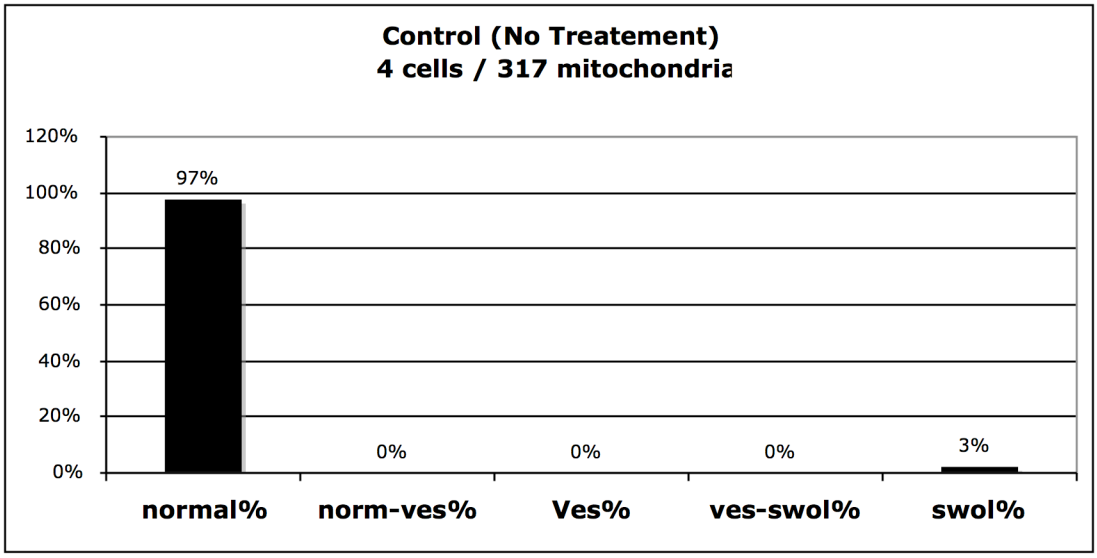

Figure III.4.a

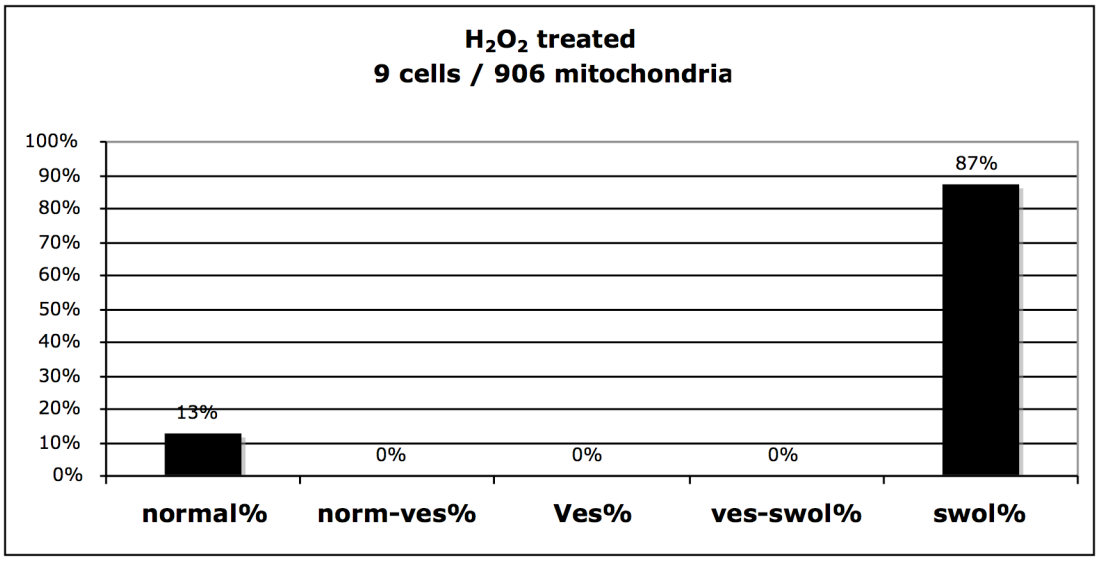

Figure III.4.b

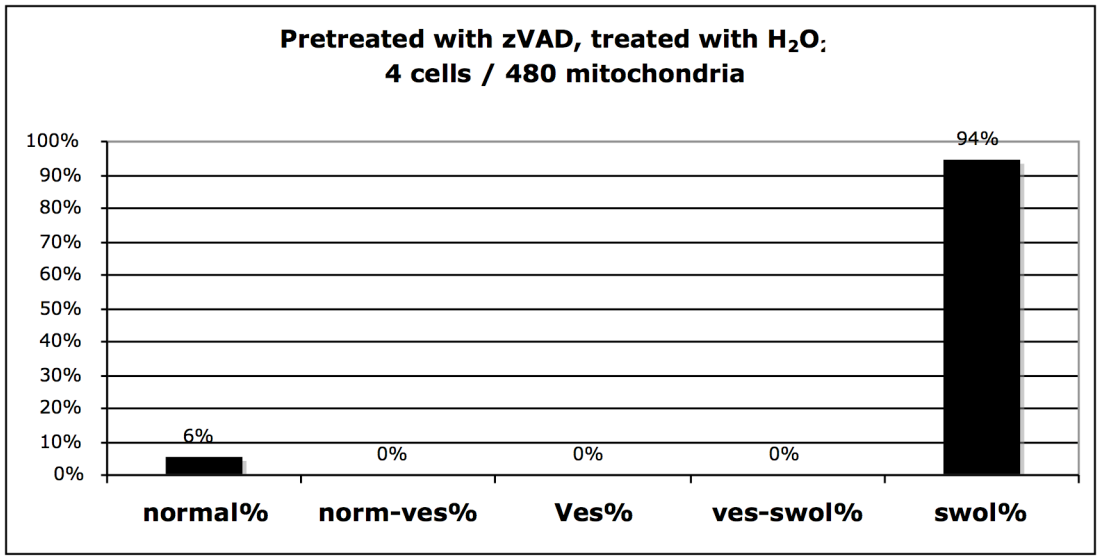

Figure III.4.c

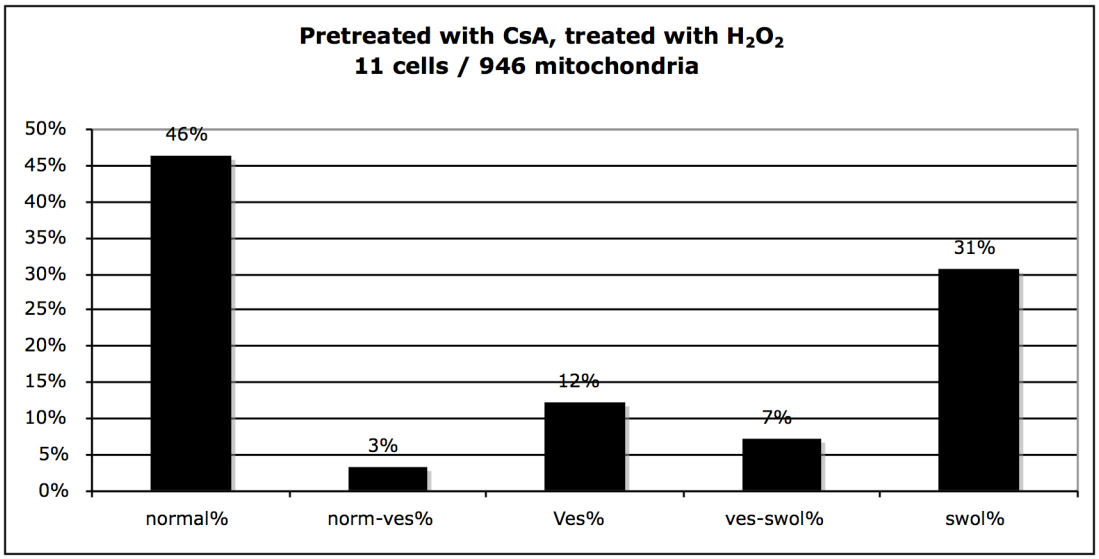

Figure III.4.d

Figure III.4 Continued

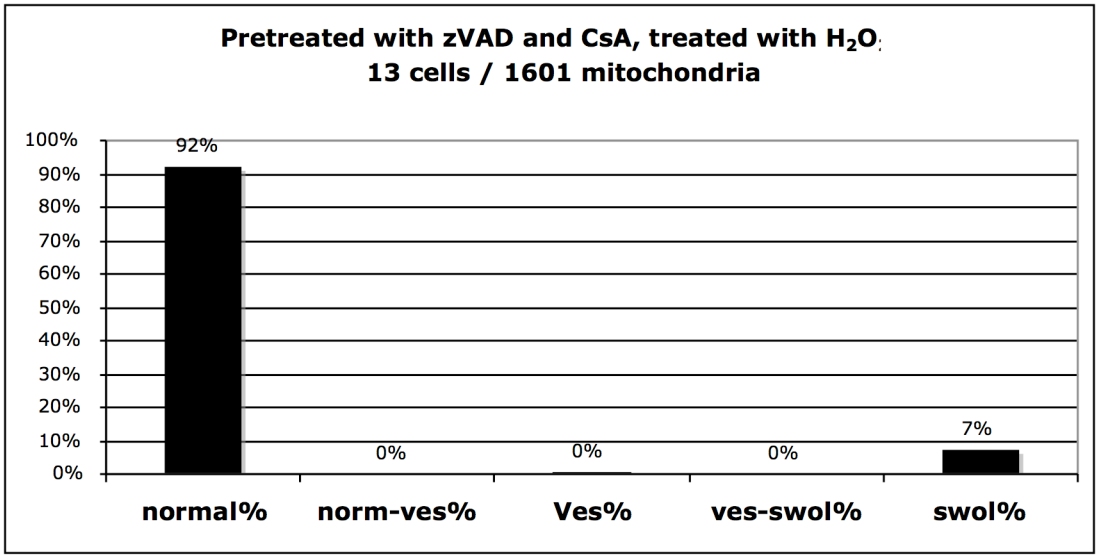

Figure III.4.e

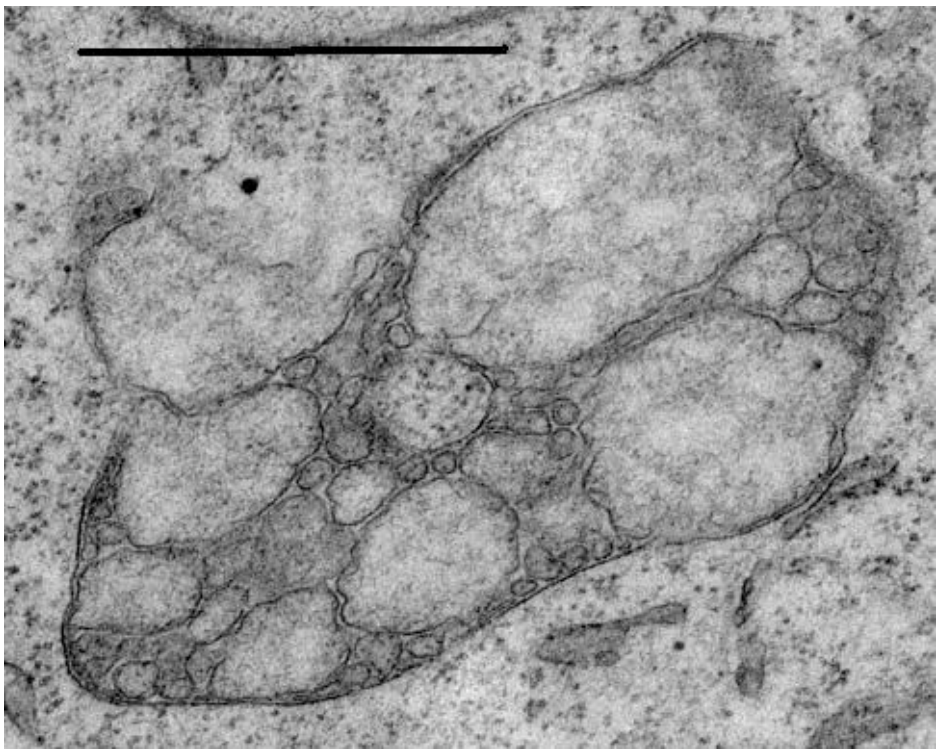

Figure III.4.f

Figure III.4 Continued

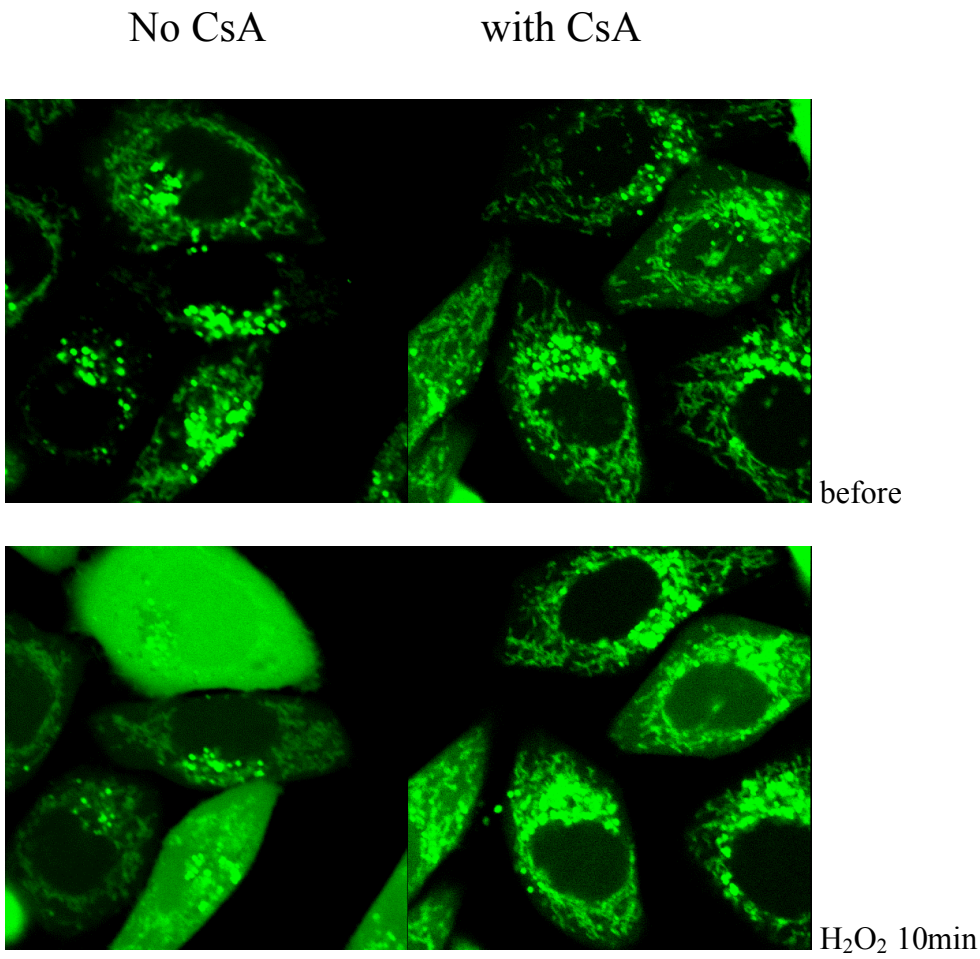

Figure III.5 Cyclosporin A (CsA, 0.1μM) inhibits mPTP opening in response to H_2O_2

HeLa cells were treated with H_2O_2 (200 μM) for 10 minutes. mPTP opening was determined by monitoring the fluorescence of calcein trapped in mitochondria. Confocal images revealed the mPTP opened within 10 minutes while CsA inhibited mPTP opening.

ACKNOWLEDGEMENT

This chapter, in full, is being prepared for future publication. This work was done with the help of Phoung (Kathy) Tran, Tong Xu, Doug Green and Terrence Frey, who are also co-authors on the paper. I would like to acknowledge Phuong (Kathy) Tran for her great assistance and Tong Xu for her excellent advice and assistance with flow cytometry. This project was supported by Blasker Science and Technology Grant from the San Diego Foundation to TGF, and by NIH Grants AI40646, AI52735, and CA69381 to DRG.

.

IV

Electron Microscopy/Tomography Study of Mitochondrial Fusion

Abstract

'In vitro fusion assay' employing temperature sensitive mutants of identified fusion proteins and different incubations conditions can separate mitochondrial fusion events to different stages. We have studied mitochondrial fusion in samples from these different stages by Electron Microscopy/Tomography using samples provided by Dr. Jodi Nunnari's group. Mitochondrial outer membranes fuse first and align the separate inner membranes together. The Inner membranes fuse starting at many contact sites and the complete fusion of inner membranes forms the cristae with crista junctions. The 3D tomogram of a mitochondrion undergoing fusion reveals a structure similar to the vesicular mitochondria morphology discussed in Chapter II, suggesting inner membrane fusion may be the reverse of the vesicular transformation observed during during mitochondrial fragmentation.

Introduction

Mitochondria are complex and dynamic organelles that constantly undergo fission and fusion. These opposing events function in cells to create a connected, functional, and responsive mitochondrial compartment (Meeusen, Devay et al. 2006). Disruption of fusion causes extensive fragmentation of the tubular network of mitochondria (Olichon, Baricault et al. 2003). Conversely, disruption of fission generates elongated, interconnected morphology (Yoon, Krueger et al. 2003). In addition to the regulation of mitochondrial morphology, it is now clear that mitochondrial dynamics play additional roles in mitochondrial function (Chan 2006).

Genetic approaches in flies and yeast have identified proteins that are required for mitochondrial fission and fusion. Remarkably, among these are several highly conserved dynamin-related proteins (DRPs), which are large, self-assembling GTPases that regulate membrane dynamics in a variety of cellular processes (Hoppins, Lackner et al. 2007). Among them, Dnm 1 (Drp1 in mammals) is essential for fission. Fission of mitochondrial membranes is accomplished as Dnm1 becomes concentrated in the outer membrane, where it complexes with the adapter Mdv1 and the integral outer membrane protein Fis 1 (Bleazard, McCaffery et al. 1999; Sesaki and Jensen 1999). The two essential dynamin-related GTPases required for mitochondrial fusion are Fzo1 (Mfn1 and 2 in mammals) and Mgm1 (OPA1 in mammals) (Meeusen, Devay et al. 2006).

In order to study the mitochondrial fusion, Meeusen, et al. performed a novel '*in vitro* fusion assay' to separate outer and inner membrane fusion events into two

experimental stages: Stage 1 included mitochondrial centrifugation, incubation, and re-suspension, and Stage 2 included the addition of exogenous NTPs and an energy regeneration system. Through this manipulation, Stage 1, which lacks an exogenous energy source, supports only outer membrane fusion; Stage 2, with an essential energy regeneration system and GTP provides the essential energetic requirements for inner membrane fusion. Stage 1 conditions generate a fusion intermediate comprised of two adjacent, tightly adhered but un-fused inner membrane compartments that are encircled by a fused and continuous outer mitochondrial membrane. Uncoupling these two stages indicates that outer and inner membrane fusion processes are mechanistically distinct and separable events (Meeusen, McCaffery et al. 2004).

The inter-membrane space DRP, Mgm1, is the only known inner membrane GTPase that plays a role in fusion (Meeusen and Nunnari 2005). It has recently been shown that Mgm1/OPA1 plays a role in the structural maintenance of ATP synthase and cristae morphology (Olichon, Baricault et al. 2003; Amutha, Gordon et al. 2004). Mgm1/OPA1's role in cristae maintenance provides a mechanistic explanation for how Mgm1/OPA1 could be involved in inner membrane fusion. Reducing the levels of OPA1 by siRNA upsets the balance between mitochondrial fusion and fission and leads to mitochondrial fragmentation (Arnoult, Grodet et al. 2005) and disruption of normal cristae structure that in at least one study led to vesicular mitochondria (Griparic et al. 2004; insert reference here).

During apoptosis, the mitochondria undergo extensive fragmentation. The mechanism responsible for this extensive fission is not well understood. In Chapter II

we discussed the vesicular mitochondrial morphology that was found during apoptosis in HeLa cells. An elegant and simple mechanism for inner membrane fission was proposed in Chapter II, requiring the elongation of cristae junctions within individual lamellar cristae to a point where they meet and fuse around the periphery of lamellar cristae (Figure II.7), and we presented evidence in support of this mechanism (Figure II.6. This fragments the matrix into separate vesicular matrix compartments without compromising the integrity of the matrix. To test the hypothesis that the vesicular mitochondrial morphology observed in Chapter II may be related to the extensive mitochondrial fission during apoptosis, we collaborated with Dr. Jodi Nunnari from the University of California at Davis to study manipulated fusion samples from isolated yeast cells. Fission is the reverse topological process of fusion. By observing the mitochondrial fusion samples at different stages, we expected to observe similar transition structures.

RESULTS

1. Mitochondrial outer membranes fuse and align the separate inner membranes.

We examined Stage 1 mitochondria by TEM and EM tomography. TEM shows that these mitochondria have a completely fused outer membrane encapsulating a boundary of separate, but aligned and associated, inner membranes (Figure IV.1). In Figure IV.1a it appears that three separate mitochondria are fusing into one, and the gaps between the three matrix compartments are obvious. Figure IV.1b shows a fusion mitochondrion with at least three tightly aligned inner membranes, indicating that at least three mitochondria were brought together. The distance of the gap between the separate inner membranes may suggest different fusion timing. In Figures IV.1c and IV.1d, EM tomography confirms that there is no fusion between the separate inner membranes and that the outer membrane encapsulates individual matrix compartments formed by the inner membranes.

2. Mitochondrial inner membrane fusion starts with many contact sites. Complete fusion of the inner membrane may form cristae with crista junctions.

Electron Microscopy/Tomography reveals the contact sites between separate inner membranes of the Stage 2 mitochondria that may begin the fusion process. After the alignment of two individual inner membranes, the separate membranes begin to fuse through formation of many contact sites (Figure IV.2). Figure IV.3 shows a fusion mitochondrion containing two compartments defined by inner boundary membranes (rendered white and turquoise in Figure IV.3c); each contains several

cristae, and all are contained within the already fused outer membrane. However, the inner membranes have very tight interfaces with many contact sites (Figures IV.2c,d). Note the green and red cristae within the white inner boundary membrane in Figure 3c and d; they form about 50% of a hemisphere that is cut off by the inner boundary membrane. These may be the remnants of the interface between the matrix compartment of a third fused mitochondrion and the white compartment that were recently fused with the formation of the cristae and cristae junctions (CJ's). Note that the discrete CJ's made by the green cristae with the white inner boundary membrane and the elongated CJ made by the red cristae form most of a semicircle on the inner boundary membrane in Figure 3d similar to the elongated CJ's of the mitochondria described in Chapter II that are in the process of transformation to the vesicular morphology.

DISCUSSION

The goal of this project is to determine whether the fusion mechanism is the reverse of the fission model proposed in Chapter II that was based upon the vesicular transformation observed during apoptosis. In Chapter II, we proposed a schematic topological model by which normal mitochondria transform to vesicular mitochondria by the elongation of cristae junctions until the nearest neighbors within each lammelar crista fuse together, followed by continued elongation of the fused crista junctions around the perimeter of the lamellar cristae (Figure II.7, Chapter II). The transition from normal mitochondria to the vesicular form effectively fragments the matrix into separate vesicular matrix compartments. All that remains to complete fragmentation of the mitochondria is outer membrane fission.

Two similar structural stages were found as we studied the different fusion stages of mitochondria. The Stage 1 mitochondrion (Figure IV.2) is similar to the vesicular mitochondria (Figure II.4c, Chapter II) in that both contain individual matrix compartments within a complete outer membrane. The Stage 2 mitochondrion (Figure IV.3) has similar elongated cristae junctions when compared with a mitochondrion that was treated with etoposide and exhibited 'normal' morphology in thin section TEM but has elongated cristae junctions shown by tomogram (see Group 3 tomogram in Figure II.6.b, Chapter II). Both observations suggest that the transformation of the vesicular structure may be the reverse of the fusion process consistent with our hypothesis that the vesicular mitochondrial structure observed during apoptosis reveals the mechanism of mitochondrial inner membrane fission.

METHOD

1. Electron Microscopy and Tomography

Sample blocks were prepared in Dr. Nunnari's lab. For TEM the thin sections (approximately 80nm) were collected and pre-stained with 2% uranyl acetate and Sato lead before examination in an FEI Tecnai 12 TEM

For EM tomography single-tilt series 3-D reconstructions were obtained from semi-thick samples (approximately 300 nm) in a tilt-series every 2° from -60° to +60° on an FEI Tecnai 12 TEM. The IMOD software suite was used to process the images in each tilt series (Boulder Laboratory for 3-Dimensional Electron Microscopy of Cells, University of Colorado, Boulder). X-Voxtrace software enabled volume segmentation of tomographic data using manual tracing followed by rendering using Synu (National Center for Microscopy and Imaging Resources, UCSD).

FIGURES & LEGENDS

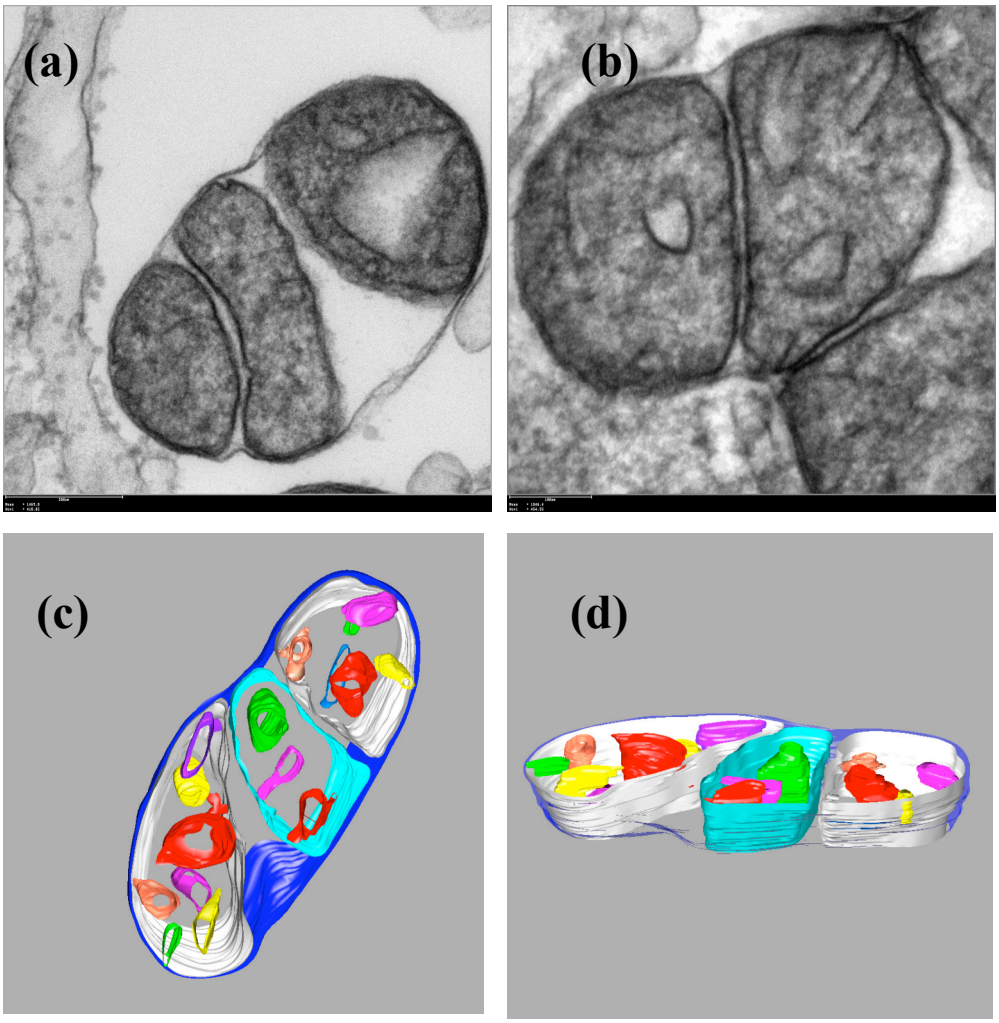

Figure IV.1. EM/ Tomography analysis of Stage 1 mitochondria.

(a) Shows outer membrane fusion of two yeast mitochondria in an *in vitro* mitochondrial fusion system;

(b) Shows the separate, but tightly aligned and opposing inner membranes from Stage 1 mitochondria.

(c,d) Tomogram of Stage 1 mitochondria reveals three domains in which separate inner boundary membranes (rendered in white, turquoise, and white) contain multiple cristae.

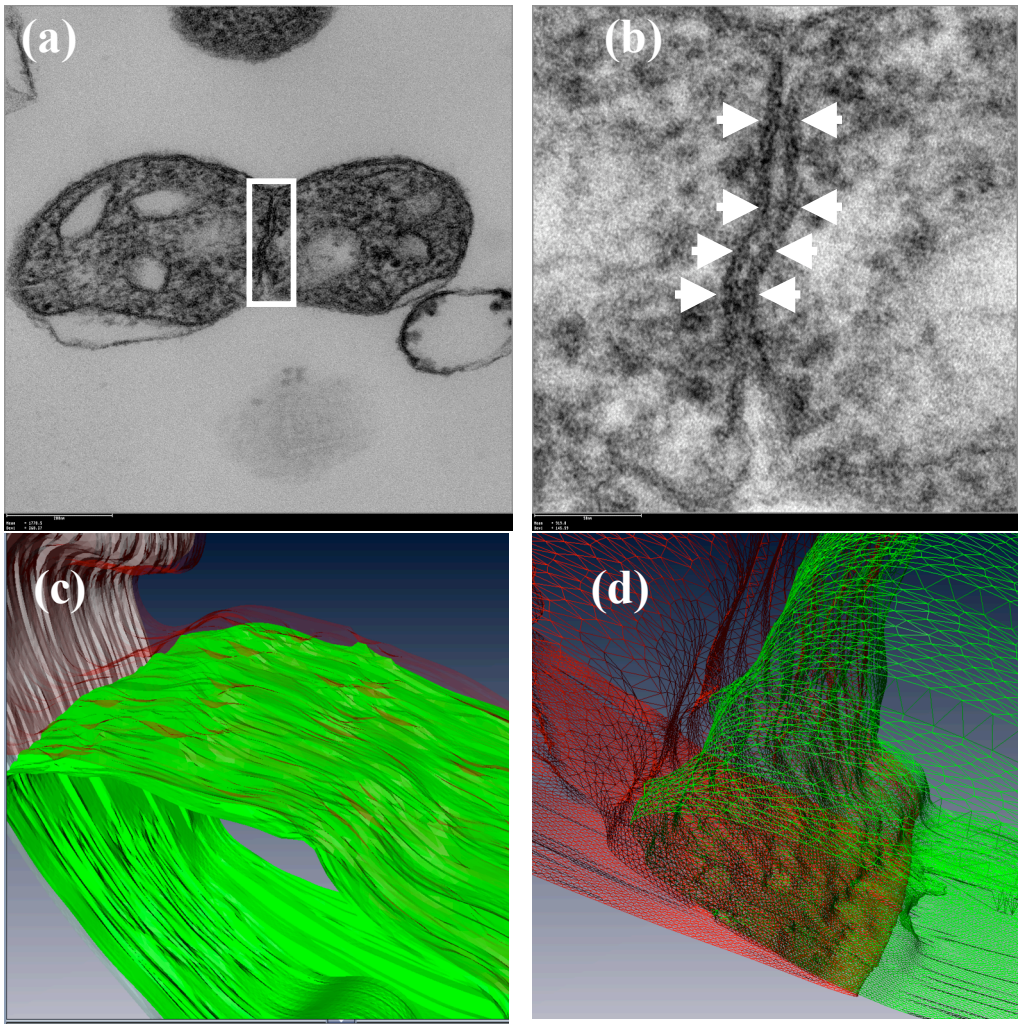

Figure IV.2. Inner membranes fused through many contact sites.

(a) Outer and inner membrane fusion of two stage 2 mitochondria.

(b) Zoom-in view of square area in (a) showing inner membranes beginning to fuse through many contact sites (Arrows)

(c) Tomogram of two inner membranes fusing through many contact sites. Translucent red and opaque green indicate different inner membranes.

(d) Contact Sites at the interface of the two inner membranes rendered as mesh networks in red and green

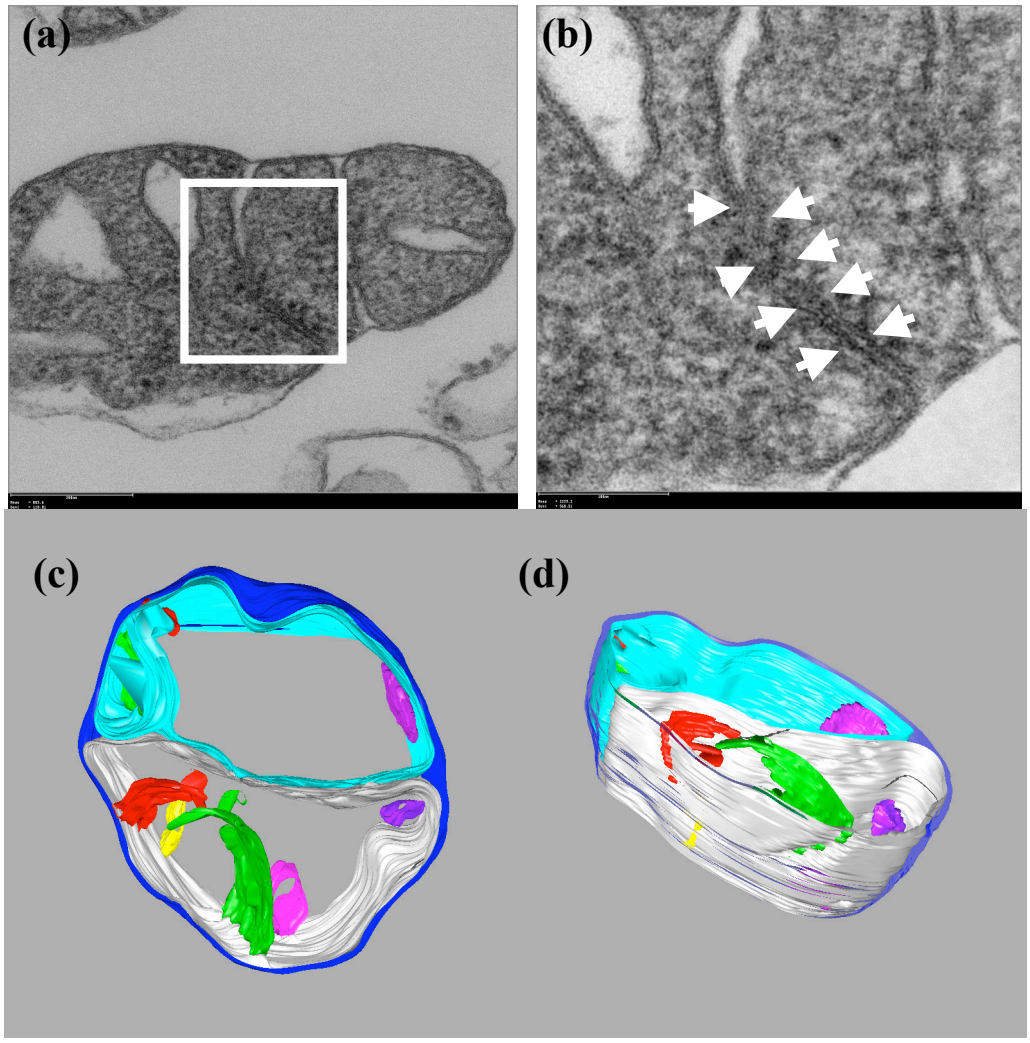

Figure IV.3. Inner membranes continue to fuse and form cristae.

(a) Stage2 mitochondrion shows inner membrane fusion beginning at the interface between separate inner membranes.

(b) Zoom-in view of the square area of (a) showing partial fusion of inner membrane (Arrow)

(c,d) Tomogram of a Stage 2 mitochondrion. **(d)** Fused inner membranes begin to form the elongated cristae junctions and cristae. Note the elongated CJ's of the red and green cristae in (d) that form a hemisphere and may be the remnants of a third mitochondrial matrix compartment that has nearly completed the fusion process.

ACKNOWLEDGEMENT

The project in this chapter was in collaboration with Dr. Jodi Nunnari and was also supported by Blasker Science and Technology Grant from the San Diego Foundation to TGF.

V.

Conclusion

Mitochondria play a critical role in apoptosis with the release of proteins such as cytochrome c, from the inter-membrane space. Two mechanisms have been proposed by which cytochrome *c* could exit mitochondria. First, outer membrane rupture following matrix swelling might occur following mPTP opening in the inner membrane collapsing the $\Delta\Psi_m$. The second mechanism is transport of cytochrome *c* across a specific Bcl-2 regulated pore in the outer membrane. Using correlated four dimensional fluorescence microscopy and Electron Microscopy/ Tomography, we studied the ultrastructure of the identical cells at different apoptotic stages. Our data reveal different mitochondrial morphologies that may reflect different mechanisms for apoptosis. These two mechanisms could be separate or/and coordinate under different stimulations. Study of these morphologies provides evidence and new observations for apoptosis research. Structures observed during the formation of vesicular mitochondria observed in mitochondria undergoing the second mechanism provide important clues to the mechanism of inner membrane fusion and fission.

REFERENCES

Agsteribbe, E. and M. Hartog (1987). "Processing of precursor RNAs from mitochondria of Neurospora crassa." Nucleic Acids Res **15**(18): 7249-63.

Akao, M., B. O'Rourke, et al. (2003). "Mechanistically distinct steps in the mitochondrial death pathway triggered by oxidative stress in cardiac myocytes." Circ Res **92**(2): 186-94.

Akao, M., Y. Teshima, et al. (2002). "Antiapoptotic effect of nicorandil mediated by mitochondrial atp-sensitive potassium channels in cultured cardiac myocytes." J Am Coll Cardiol **40**(4): 803-10.

Aktas, O., T. Prozorovski, et al. (2006). "Death ligands and autoimmune demyelination." Neuroscientist **12**(4): 305-16.

Alexander, C., M. Votruba, et al. (2000). "OPA1, encoding a dynamin-related GTPase, is mutated in autosomal dominant optic atrophy linked to chromosome 3q28." Nat Genet **26**(2): 211-5.

Algeciras-Schimnich, A., L. Shen, et al. (2002). "Molecular ordering of the initial signaling events of CD95." Mol Cell Biol **22**(1): 207-20.

Amutha, B., D. M. Gordon, et al. (2004). "A novel role of Mgm1p, a dynamin-related GTPase, in ATP synthase assembly and cristae formation/maintenance." Biochem J **381**(Pt 1): 19-23.

Anderson, S., A. T. Bankier, et al. (1981). "Sequence and organization of the human mitochondrial genome." Nature **290**(5806): 457-65.

Andersson, S. G., O. Karlberg, et al. (2003). "On the origin of mitochondria: a genomics perspective." Philos Trans R Soc Lond B Biol Sci **358**(1429): 165-77; discussion 177-9.

Arnoult, D., B. Gaume, et al. (2003). "Mitochondrial release of AIF and EndoG requires caspase activation downstream of Bax/Bak-mediated permeabilization." Embo J **22**(17): 4385-99.

Arnoult, D., A. Grodet, et al. (2005). "Release of OPA1 during apoptosis participates in the rapid and complete release of cytochrome c and subsequent mitochondrial fragmentation." J Biol Chem **280**(42): 35742-50.

Arnoult, D., M. Karbowski, et al. (2003). "Caspase inhibition prevents the mitochondrial release of apoptosis-inducing factor." Cell Death Differ **10**(7): 845-9.

Arnoult, D., P. Parone, et al. (2002). "Mitochondrial release of apoptosis-inducing factor occurs downstream of cytochrome c release in response to several proapoptotic stimuli." J Cell Biol **159**(6): 923-9.

Arnoult, D., F. Petit, et al. (2003). "Mitochondria in HIV-1-induced apoptosis." Biochem Biophys Res Commun **304**(3): 561-74.

Asin-Cayuela, J. and C. M. Gustafsson (2007). "Mitochondrial transcription and its regulation in mammalian cells." Trends Biochem Sci **32**(3): 111-7.

Baines, C. P., R. A. Kaiser, et al. (2005). "Loss of cyclophilin D reveals a critical role for mitochondrial permeability transition in cell death." Nature **434**(7033): 658-62.

Baines, C. P., R. A. Kaiser, et al. (2007). "Voltage-dependent anion channels are dispensable for mitochondrial-dependent cell death." Nat Cell Biol **9**(5): 550-5.

Basso, E., L. Fante, et al. (2005). "Properties of the permeability transition pore in mitochondria devoid of Cyclophilin D." J Biol Chem **280**(19): 18558-61.

Berg, J. M., J. L. Tymoczko, et al. "Biochemistry 5th Edition."

Bernardi, P. and G. F. Azzone (1981). "Cytochrome c as an electron shuttle between the outer and inner mitochondrial membranes." J Biol Chem **256**(14): 7187-92.

Bernardi, P., K. M. Broekemeier, et al. (1994). "Recent progress on regulation of the mitochondrial permeability transition pore; a cyclosporin-sensitive pore in the

inner mitochondrial membrane. [Review] [61 refs]." Journal of Bioenergetics & Biomembranes **26**(5): 509-17.

Bernardi, P., A. Krauskopf, et al. (2006). "The mitochondrial permeability transition from in vitro artifact to disease target." Febs J **273**(10): 2077-99.

Bernardi, P., L. Scorrano, et al. (1999). "Mitochondria and cell death. Mechanistic aspects and methodological issues." Eur J Biochem **264**(3): 687-701.

Bleazard, W., J. M. McCaffery, et al. (1999). "The dynamin-related GTPase Dnm1 regulates mitochondrial fission in yeast." Nat Cell Biol **1**(5): 298-304.

Boekema, E. J. and H. P. Braun (2007). "Supramolecular structure of the mitochondrial oxidative phosphorylation system." J Biol Chem **282**(1): 1-4.

Boldin, M. P., T. M. Goncharov, et al. (1996). "Involvement of MACH, a novel MORT1/FADD-interacting protease, in Fas/APO-1- and TNF receptor-induced cell death." Cell **85**(6): 803-15.

Brady, N. R., S. P. Elmore, et al. (2004). "Coordinated behavior of mitochondria in both space and time: a reactive oxygen species-activated wave of mitochondrial depolarization." Biophys J **87**(3): 2022-34.

Broekemeier, K. M. and D. R. Pfeiffer (1989). "Cyclosporin A-sensitive and insensitive mechanisms produce the permeability transition in mitochondria." Biochem Biophys Res Commun **163**(1): 561-6.

Brustovetsky, N. and M. Klingenberg (1996). "Mitochondrial ADP/ATP carrier can be reversibly converted into a large channel by Ca2+." Biochemistry **35**(26): 8483-8.

Chai, J., C. Du, et al. (2000). "Structural and biochemical basis of apoptotic activation by Smac/DIABLO." Nature **406**(6798): 855-62.

Chan, D. C. (2006). "Mitochondrial Fusion and Fission in Mammals." Annu Rev Cell Dev Biol.

Chinnaiyan, A. M., K. O'Rourke, et al. (1995). "FADD, a novel death domain-containing protein, interacts with the death domain of Fas and initiates apoptosis." Cell **81**(4): 505-12.

Christianson, T. W. and D. A. Clayton (1988). "A tridecamer DNA sequence supports human mitochondrial RNA 3'-end formation in vitro." Mol Cell Biol **8**(10): 4502-9.

Cipolat, S., T. Rudka, et al. (2006). "Mitochondrial Rhomboid PARL Regulates Cytochrome c Release during Apoptosis via OPA1-Dependent Cristae Remodeling." Cell **126**(1): 163-75.

Clayton, D. A. (1984). "Transcription of the mammalian mitochondrial genome." Annu Rev Biochem **53**: 573-94.

Crompton, M., S. Virji, et al. (1998). "Cyclophilin-D binds strongly to complexes of the voltage-dependent anion channel and the adenine nucleotide translocase to form the permeability transition pore." Eur J Biochem **258**(2): 729-35.

Datta, K., P. Babbar, et al. (2002). "p53 dependent apoptosis in glioma cell lines in response to hydrogen peroxide induced oxidative stress." Int J Biochem Cell Biol **34**(2): 148-57.

Davies, K. J. (1995). "Oxidative stress: the paradox of aerobic life." Biochem Soc Symp **61**: 1-31.

Delettre, C., G. Lenaers, et al. (2000). "Nuclear gene OPA1, encoding a mitochondrial dynamin-related protein, is mutated in dominant optic atrophy." Nature Genetics **26**(2): 207-10.

Du, C., M. Fang, et al. (2000). "Smac, a mitochondrial protein that promotes cytochrome c-dependent caspase activation by eliminating IAP inhibition." Cell **102**(1): 33-42.

Estaquier, J. and D. Arnoult (2007). "Inhibiting Drp1-mediated mitochondrial fission selectively prevents the release of cytochrome c during apoptosis." Cell Death Differ **14**(6): 1086-94.

Finkel, T. and N. J. Holbrook (2000). "Oxidants, oxidative stress and the biology of ageing." Nature **408**(6809): 239-47.

Forte, M. and P. Bernardi (2006). "The permeability transition and BCL-2 family proteins in apoptosis: co-conspirators or independent agents?" Cell Death Differ **13**(8): 1287-90.

Frey, T., C. Renken, et al. (2002). "Insight into mitochondrial structure and function from electron tomography." Biochim Biophys Acta **1555**(1-3): 196-203.

Frey, T. G. and C. A. Mannella (2000). "The internal structure of mitochondria." Trends Biochem Sci **25**(7): 319-24.

Frey, T. G., G. A. Perkins, et al. (2006). "Electron Tomography of Membrane-Bound Cellular Organelles." Annu Rev Biophys Biomol Struct.

Frezza, C., S. Cipolat, et al. (2006). "OPA1 Controls Apoptotic Cristae Remodeling Independently from Mitochondrial Fusion." Cell **126**(1): 177-89.

Gaietta, G., T. J. Deerinck, et al. (2002). "Multicolor and electron microscopic imaging of connexin trafficking." Science **296**(5567): 503-7.

Garrido, C., L. Galluzzi, et al. (2006). "Mechanisms of cytochrome c release from mitochondria." Cell Death Differ **13**(9): 1423-33.

Gilkerson, R. W., J. M. Selker, et al. (2003). "The cristal membrane of mitochondria is the principal site of oxidative phosphorylation." FEBS Lett **546**(2-3): 355-8.

Goldstein, J. C., C. Munoz-Pinedo, et al. (2005). "Cytochrome c is released in a single step during apoptosis." Cell Death Differ **12**(5): 453-62.

Goldstein, J. C., N. J. Waterhouse, et al. (2000). "The coordinate release of cytochrome c during apoptosis is rapid, complete and kinetically invariant." Nat Cell Biol **2**(3): 156-62.

Gray, M. W., G. Burger, et al. (1999). "Mitochondrial evolution." Science **283**(5407): 1476-81.

Green, D. R. and G. I. Evan (2002). "A matter of life and death." Cancer Cell **1**(1): 19-30.

Green, D. R. and G. Kroemer (2004). "The pathophysiology of mitochondrial cell death." Science **305**(5684): 626-9.

Green, D. R. and J. C. Reed (1998). "Mitochondria and apoptosis." Science **281**(5381): 1309-12.

Griparic, L., N. N. van der Wel, et al. (2004). "Loss of the intermembrane space protein Mgm1/OPA1 induces swelling and localized constrictions along the lengths of mitochondria." J Biol Chem **279**(18): 18792-8.

Heath-Engel, H. M. and G. C. Shore (2006). "Mitochondrial membrane dynamics, cristae remodelling and apoptosis." Biochim Biophys Acta.

Hegde, R., S. M. Srinivasula, et al. (2002). "Identification of Omi/HtrA2 as a mitochondrial apoptotic serine protease that disrupts inhibitor of apoptosis protein-caspase interaction." J Biol Chem **277**(1): 432-8.

Herrmann, J. M., W. Neupert, et al. (1997). "Insertion into the mitochondrial inner membrane of a polytopic protein, the nuclear-encoded Oxa1p." Embo J **16**(9): 2217-26.

Hirata, H., A. Takahashi, et al. (1998). "Caspases are activated in a branched protease cascade and control distinct downstream processes in Fas-induced apoptosis." J Exp Med **187**(4): 587-600.

Hoppins, S., L. Lackner, et al. (2007). "The Machines that Divide and Fuse Mitochondria." Annu Rev Biochem.

Hsu, H., J. Xiong, et al. (1995). "The TNF receptor 1-associated protein TRADD signals cell death and NF-kappa B activation." Cell **81**(4): 495-504.

Huser, J. and L. A. Blatter (1999). "Fluctuations in mitochondrial membrane potential caused by repetitive gating of the permeability transition pore." Biochem J **343 Pt 2**: 311-7.

Irwin, W. A., N. Bergamin, et al. (2003). "Mitochondrial dysfunction and apoptosis in myopathic mice with collagen VI deficiency." Nat Genet **35**(4): 367-71.

Itoh, N. and S. Nagata (1993). "A novel protein domain required for apoptosis. Mutational analysis of human Fas antigen." J Biol Chem **268**(15): 10932-7.

Jakobs, S. (2006). "High resolution imaging of live mitochondria." Biochim Biophys Acta **1763**(5-6): 561-75.

Joza, N., S. A. Susin, et al. (2001). "Essential role of the mitochondrial apoptosis-inducing factor in programmed cell death." Nature **410**(6828): 549-54.

Karbowski, M., D. Arnoult, et al. (2004). "Quantitation of mitochondrial dynamics by photolabeling of individual organelles shows that mitochondrial fusion is blocked during the Bax activation phase of apoptosis." J Cell Biol **164**(4): 493-9.

Karpinich, N. O., M. Tafani, et al. (2002). "The course of etoposide-induced apoptosis from damage to DNA and p53 activation to mitochondrial release of cytochrome c." J Biol Chem **277**(19): 16547-52.

Kerr, J. F., A. H. Wyllie, et al. (1972). "Apoptosis: a basic biological phenomenon with wide-ranging implications in tissue kinetics." Br J Cancer **26**(4): 239-57.

Kinnally, K. W. and B. Antonsson (2007). "A tale of two mitochondrial channels, MAC and PTP, in apoptosis." Apoptosis **12**(5): 857-68.

Koehler, C. M. (2000). "Protein translocation pathways of the mitochondrion." FEBS Lett **476**(1-2): 27-31.

Kokoszka, J. E., K. G. Waymire, et al. (2004). "The ADP/ATP translocator is not essential for the mitochondrial permeability transition pore." Nature **427**(6973): 461-5.

Kroemer, G., L. Galluzzi, et al. (2007). "Mitochondrial membrane permeabilization in cell death." Physiol Rev **87**(1): 99-163.

Kroemer, G. and J. C. Reed (2000). "Mitochondrial control of cell death." Nat Med **6**(5): 513-9.

Kuwana, T., M. R. Mackey, et al. (2002). "Bid, Bax, and lipids cooperate to form supramolecular openings in the outer mitochondrial membrane." Cell **111**(3): 331-42.

Lane, N. (2006). "Mitochondrial disease: powerhouse of disease." Nature **440**(7084): 600-2.

Lee, Y. J., S. Y. Jeong, et al. (2004). "Roles of the mammalian mitochondrial fission and fusion mediators Fis1, Drp1, and Opa1 in apoptosis." Mol Biol Cell **15**(11): 5001-11.

Lemasters, J. J., A. L. Nieminen, et al. (1998). "The mitochondrial permeability transition in cell death: a common mechanism in necrosis, apoptosis and autophagy." Biochim Biophys Acta **1366**(1-2): 177-96.

Li, H., H. Zhu, et al. (1998). "Cleavage of BID by caspase 8 mediates the mitochondrial damage in the Fas pathway of apoptosis." Cell **94**(4): 491-501.

Li, L. Y., X. Luo, et al. (2001). "Endonuclease G is an apoptotic DNase when released from mitochondria." Nature **412**(6842): 95-9.

Liu, X., C. N. Kim, et al. (1996). "Induction of apoptotic program in cell-free extracts: requirement for dATP and cytochrome c." Cell **86**(1): 147-57.

Loew, L. M. (1996). "Determination of mitochondrial membrane potential in single living cells using confocal microscope images." *SPIE* **2678**: 80-87.

Luo, X., I. Budihardjo, et al. (1998). "Bid, a Bcl2 interacting protein, mediates cytochrome c release from mitochondria in response to activation of cell surface death receptors." Cell **94**(4): 481-90.

MacKenzie, J. A. and R. M. Payne (2007). "Mitochondrial protein import and human health and disease." Biochim Biophys Acta **1772**(5): 509-23.

Malka, F., O. Guillery, et al. (2005). "Separate fusion of outer and inner mitochondrial membranes." EMBO Rep **6**(9): 853-9.

Mannella, C. A., M. Marko, et al. (1994). "The internal compartmentation of rat-liver mitochondria: tomographic study using the high-voltage transmission electron microscope." *Microscopy Research and Technique* **27**(4): 278-83.

Mannella, C. A., D. R. Pfeiffer, et al. (2001). "Topology of the mitochondrial inner membrane: dynamics and bioenergetic implications." IUBMB Life **52**(3-5): 93-100.

Manor, J. C., T. Frey, et al. (2006). "Membrane remodeling and diffusion of cytochrome c from a geometrically idealized mitochondrial crista." International Conference on Bioinformatics and Computational Biology **(in press)**.

Meeusen, S., R. Devay, et al. (2006). "Mitochondrial Inner-Membrane Fusion and Crista Maintenance Requires the Dynamin-Related GTPase Mgm1." Cell **127**(2): 383-95.

Meeusen, S., J. M. McCaffery, et al. (2004). "Mitochondrial fusion intermediates revealed in vitro." Science **305**(5691): 1747-52.

Meeusen, S. L. and J. Nunnari (2005). "How mitochondria fuse." Curr Opin Cell Biol **17**(4): 389-94.

Montoya, J., T. Christianson, et al. (1982). "Identification of initiation sites for heavy-strand and light-strand transcription in human mitochondrial DNA." Proc Natl Acad Sci U S A **79**(23): 7195-9.

Munoz-Pinedo, C., A. Guio-Carrion, et al. (2006). "Different mitochondrial intermembrane space proteins are released during apoptosis in a manner that is coordinately initiated but can vary in duration." Proc Natl Acad Sci U S A **103**(31): 11573-11578.

Muzio, M., A. M. Chinnaiyan, et al. (1996). "FLICE, a novel FADD-homologous ICE/CED-3-like protease, is recruited to the CD95 (Fas/APO-1) death--inducing signaling complex." Cell **85**(6): 817-27.

Nakagawa, T., S. Shimizu, et al. (2005). "Cyclophilin D-dependent mitochondrial permeability transition regulates some necrotic but not apoptotic cell death." Nature **434**(7033): 652-8.

Newmeyer, D. D. and S. Ferguson-Miller (2003). "Mitochondria: releasing power for life and unleashing the machineries of death." Cell **112**(4): 481-90.

Nicastro, D., A. S. Frangakis, et al. (2000). "Cryo-electron tomography of *Neurospora mitochondria*." J Struct Biol **129**(1): 48-56.

Nisoli, E., E. Clementi, et al. (2004). "Mitochondrial biogenesis as a cellular signaling framework." Biochem Pharmacol **67**(1): 1-15.

Nunnari, J., W. F. Marshall, et al. (1997). "Mitochondrial transmission during mating in Saccharomyces cerevisiae is determined by mitochondrial fusion and fission and the intramitochondrial segregation of mitochondrial DNA." Mol Biol Cell **8**(7): 1233-42.

Ojala, D., J. Montoya, et al. (1981). "tRNA punctuation model of RNA processing in human mitochondria." Nature **290**(5806): 470-4.

Olichon, A., L. Baricault, et al. (2003). "Loss of OPA1 perturbates the mitochondrial inner membrane structure and integrity, leading to cytochrome c release and apoptosis." J Biol Chem **278**(10): 7743-6.

Olichon, A., E. Guillou, et al. (2006). "Mitochondrial dynamics and disease, OPA1." Biochim Biophys Acta.

Palade, G. E. (1952). "The fine structure of mitochondria." Anat Rec **114**(3): 427-51.

Parone, P. A., D. I. James, et al. (2006). "Inhibiting the mitochondrial fission machinery does not prevent bax/bak-dependent apoptosis." Mol Cell Biol **26**(20): 7397-408.

Pavlov, E. V., M. Priault, et al. (2001). "A novel, high conductance channel of mitochondria linked to apoptosis in mammalian cells and Bax expression in yeast." J Cell Biol **155**(5): 725-31.

Perkins, G., C. Renken, et al. (1997). "Electron tomography of neuronal mitochondria: three-dimensional structure and organization of cristae and membrane contacts." J Struct Biol **119**(3): 260-72.

Perkins, G., J. Song, et al. (1998). "Electron Tomography of Mitochondria from Brown Adipocytes Reveals Crista Junctions." J Bioenergetics and Biomembranes **30**(5): 431-442.

Perkins, G. A., C. W. Renken, et al. (2001). "Electron tomography of mitochondria after the arrest of protein import associated with Tom 19 depletion." *Eur. J. Cell Biol.* **80**: 139-150.

Petronilli, V., G. Miotto, et al. (1999). "Transient and long-lasting openings of the mitochondrial permeability transition pore can be monitored directly in intact cells by changes in mitochondrial calcein fluorescence." Biophys J **76**(2): 725-34.

Pfanner, N. and A. Geissler (2001). "Versatility of the mitochondrial protein import machinery." Nat Rev Mol Cell Biol **2**(5): 339-49.

Rapaport, D. (2005). "How does the TOM complex mediate insertion of precursor proteins into the mitochondrial outer membrane?" J Cell Biol **171**(3): 419-23.

Ricci, J. E., R. A. Gottlieb, et al. (2003). "Caspase-mediated loss of mitochondrial function and generation of reactive oxygen species during apoptosis." J Cell Biol **160**(1): 65-75.

Ricci, J. E., C. Munoz-Pinedo, et al. (2004). "Disruption of mitochondrial function during apoptosis is mediated by caspase cleavage of the p75 subunit of complex I of the electron transport chain." Cell **117**(6): 773-86.

Schapira, A. H. (2006). "Mitochondrial disease." Lancet **368**(9529): 70-82.

Scheffler, I. E. (1999). Mitochondria. New York, John Wiley and Sons.

Schinzel, A. C., O. Takeuchi, et al. (2005). "Cyclophilin D is a component of mitochondrial permeability transition and mediates neuronal cell death after focal cerebral ischemia." Proc Natl Acad Sci U S A **102**(34): 12005-10.

Scorrano, L., M. Ashiya, et al. (2002). "A distinct pathway remodels mitochondrial cristae and mobilizes cytochrome c during apoptosis." Dev Cell **2**(1): 55-67.

Sesaki, H. and R. E. Jensen (1999). "Division versus fusion: Dnm1p and Fzo1p antagonistically regulate mitochondrial shape." J Cell Biol **147**(4): 699-706.

Shadel, G. S. and D. A. Clayton (1997). "Mitochondrial DNA maintenance in vertebrates." Annu Rev Biochem **66**: 409-35.

Shaw, J. M. and J. Nunnari (2002). "Mitochondrial dynamics and division in budding yeast." Trends Cell Biol **12**(4): 178-84.

Shiozaki, E. N. and Y. Shi (2004). "Caspases, IAPs and Smac/DIABLO: mechanisms from structural biology." Trends Biochem Sci **29**(9): 486-94.

Sies, H. (1997). "Oxidative stress: oxidants and antioxidants." Exp Physiol **82**(2): 291-5.

Sjostrand, F. S. (1953). "Electron microscopy of mitochondria and cytoplasmic double membranes." Nature **171**(4340): 30-2.

Skulachev, V. P. (1996). "Why are mitochondria involved in apoptosis? Permeability transition pores and apoptosis as selective mechanisms to eliminate superoxide-producing mitochondria and cell." FEBS Lett **397**(1): 7-10.

Slee, E. A., M. T. Harte, et al. (1999). "Ordering the cytochrome c-initiated caspase cascade: hierarchical activation of caspases-2, -3, -6, -7, -8, and -10 in a caspase-9-dependent manner." J Cell Biol **144**(2): 281-92.

Stark, R. and M. Roden (2007). "ESCI Award 2006. Mitochondrial function and endocrine diseases." Eur J Clin Invest **37**(4): 236-48.

Susin, S. A., H. K. Lorenzo, et al. (1999). "Molecular characterization of mitochondrial apoptosis-inducing factor." Nature **397**(6718): 441-6.

Taanman, J. W. (1999). "The mitochondrial genome: structure, transcription, translation and replication." Biochim Biophys Acta **1410**(2): 103-23.

Tang, X. Q., J. Q. Feng, et al. (2005). "Protection of oxidative preconditioning against apoptosis induced by H2O2 in PC12 cells: mechanisms via MMP, ROS, and Bcl-2." Brain Res **1057**(1-2): 57-64.

Tartaglia, L. A., T. M. Ayres, et al. (1993). "A novel domain within the 55 kd TNF receptor signals cell death." Cell **74**(5): 845-53.

Truscott, K. N., P. Kovermann, et al. (2001). "A presequence- and voltage-sensitive channel of the mitochondrial preprotein translocase formed by Tim23." Nat Struct Biol **8**(12): 1074-82.

Verhagen, A. M., P. G. Ekert, et al. (2000). "Identification of DIABLO, a mammalian protein that promotes apoptosis by binding to and antagonizing IAP proteins." Cell **102**(1): 43-53.

Voos, W. and K. Rottgers (2002). "Molecular chaperones as essential mediators of mitochondrial biogenesis." Biochim Biophys Acta **1592**(1): 51-62.

Wallace, D. C. (1997). "Mitochondrial DNA in aging and disease." Sci Am **277**(2): 40-7.

Wallace, D. C., G. Singh, et al. (1988). "Mitochondrial DNA mutation associated with Leber's hereditary optic neuropathy." Science **242**(4884): 1427-30.

Weiss, J. N., P. Korge, et al. (2003). "Role of the mitochondrial permeability transition in myocardial disease." Circ Res **93**(4): 292-301.

Yoon, Y., E. W. Krueger, et al. (2003). "The mitochondrial protein hFis1 regulates mitochondrial fission in mammalian cells through an interaction with the dynamin-like protein DLP1." Mol Cell Biol **23**(15): 5409-20.

Zorov, D. B., C. R. Filburn, et al. (2000). "Reactive oxygen species (ROS)-induced ROS release: a new phenomenon accompanying induction of the mitochondrial permeability transition in cardiac myocytes." J Exp Med **192**(7): 1001-14.

Zou, H., Y. Li, et al. (1999). "An APAF-1.cytochrome c multimeric complex is a functional apoptosome that activates procaspase-9." J Biol Chem **274**(17): 11549-56.